International Max-Planck Research School on Astrophysics
Max-Planck-Institut für Extraterrestrische Physik

Gamma-Ray Bursts:

A Population Study

Arne Rau

Vollständiger Abdruck der von der Fakultät für Physik der Technischen Universität München zur Erlangung des akademischen Grades eines

Doktors der Naturwissenschaften

genehmigten Dissertation.

Vorsitzender: Univ.-Prof. Dr. M. Lindner
Prüfer der Dissertation:
1. Hon.-Prof. Dr. G. Hasinger
2. Univ.-Prof. Dr. F. v. Feilitzsch

Die Dissertation wurde am 31. Oktober 2005 bei der Technischen Universität München eingereicht und durch die Fakultät für Physik am 14. Dezember 2005 angenommen.

Contents

Zusammenfassung

In der vorliegenden Arbeit erhält der interessierte Leser Einblick in drei separate Aspekte der Beobachtungen von Gammastrahlungsblitzen (engl: *Gamma-ray Bursts* = GRBs). Der Reihenfolge der beobachtbaren Strahlungskomponenten dieser kosmologischen Explosionen nach, werden die Gamma- und Nachglühemission (engl: *afterglow emission*) sowie die Charakteristiken der Muttergalaxien (engl: *host galaxies*) untersucht. Die Arbeit basiert auf vier Publikationen im renomierten referierten Zeitschrift *Astronomy & Astrophysics*.

Im ersten Teil wird die prompte Gammaemission, entstehend in internen Schocks in ultrarelativistischen, kollimierten Materieausströmungen (engl: *jets*), untersucht. Dazu werden die GRBs, welche mit dem Anti-Koinzidenz Schild (SPI-ACS) des Spektrometers SPI des Satelliten *INTEGRAL* entdeckt wurden, verwendet. Es wird gezeigt, dass SPI-ACS erfolgreich als omnidirektionaler GRB-Detektor bei Energien oberhalb von 80 keV arbeitet. 236 GRB-Kandidaten wurden während der ersten 26.5 Monate der Mission entdeckt und ihre Eigenschaften sind im ersten SPI-ACS GRB-Katalog zusammengefasst. Durch gleichzeitige Beobachtungen mit anderen Gammastrahlungsdetektoren, welche im Interplanetaren Netzwerk (engl: *Interplanetary Network* = IPN) zusammengefasst sind, konnte der GRB-Ursprung für 179 Ereignisse bestätigt werden.

Neben der bereits bekannten bimodalen Verteilung der GRB-Dauer (lange (>2 s) und kurze Ereignisse (<2 s)), wurde eine weitere Gruppe mit sehr kurzer Dauer (<0.25 s) entdeckt. Anhand verschiedener Untersuchungen, zB.: $\log N$–$\log C_{max}$ und $<V/V_{max}>$, zeige ich, dass der Ursprung dieser sehr kurzen Population (ca. 40 % der Gesamtereignisse) deutlich von dem der regulären GRBs abweicht. Die sehr kurzen Ereignisse zeigen eine homogenen Verteilung im Euklidischen Raum, während Ereignisse länger als 0.25 s eine deutliche Abweichung von der Homogenität aufzeigen. Letzteres entspricht den bereits bekannten Ergebnissen des *CGRO* Instruments BATSE. Zeitgleich zu den sehr kurzen Ereignissen in SPI-ACS fand ich Saturierungen in einzelnen oder benachbarten Germaniumkristallen des Spektrometers. Dieses deutet auf den Ursprung eines grossen Teils der Ereignisse durch hochernergetische Kosmische Strahlung hin. Vernachlässigt man die sehr kurzen Ereignisse, so erscheint die Population der kurzen GRBs eher als eine Fortsetzung der langen GRBs zu kurzen Dauern, als eine separate Population.

Im zweiten Teil der Arbeit wird der Fokus von der hochenergetischen Gammastrahlung auf die Phase des Nachglühens und die Untersuchung der Muttergalaxien im optischen und nah-infraroten Wellenlängenbereich gelegt. Dieses wird an einem Beispiel, dem optischen dunklen GRB/XRF 030528 durchgeführt (XRF = engl: *X-ray Flash*). Ich demonstriere, dass Nachglühen, welche bei optischen Wellenlängen aufgrund interstellarer Absorp-

tion nicht sichtbar sind, durch Beobachtungen im Nah-Infraroten entdeckt werden können. Leider waren die Beobachtungen von GRB/XRF 030528 nicht ausreichend, um neben der eigentlichen Entdeckung eine akkurate Lichtkurve zu erhalten oder um die Entfernung mit Hilfe photometrischer Rotverschiebung zu bestimmen. Aus diesem Grund beantragte und erhielt ich Beobachtungszeit am *Very Large Telescope* der Europäischen Südsternwarte in Chile, um die Muttergalaxie spektroskopisch zu untersuchen. Basierend auf den prominenten Sauerstoff- und Wasserstoff-Emissionslinien im Spektrum, konnte eine Rotverschiebung von z=0.782$\pm$0.001 abgeleitet werden. Die Linienleuchtkräfte und -verhältniss zeigen, dass die Muttergalaxie eine sehr aktive Phase der Sternentstehung durchlebt sowie eine sub-solare Metallizität aufweist. Diese Beobachtungen stimmen mit den anderer GRB-Muttergalaxien und den theoretischen Vorläufermodellen von langen GRBs überein. Mit einer Sternenmasse von $\sim 10^{10}\,M_{\odot}$ ist die Muttergalaxie von GRB/XRF 030528 eine der massereichsten GRB-Muttergalaxien bei $z\sim$0.8.

Mit Hilfe der bekannten Entfernung können die Eigenschaften der prompten Gammastrahlung im Ruhesystem berechnet werden. Demzufolge wird GRB/XRF 030528, im Gegensatz zur Klassifizierung im Beobachtersystem als XRF, als ein röntgenreicher Ausbruch (engl: *X-ray Rich Burst* = XRR) eingeordnet. Das zeigt, dass die generell verwendete Unterteilung in GRBs, XRRs und XRFs im Beobachtersystem bestenfalls als eine technische Klassifizierung gesehen werden kann, ohne repräsentativ für die physikalischen Eigenschaften der Ereignisse zu sein. Auf Grund der immer deutlicher werdenden Indizien, dass GRBs, XRRs und XRFs eine kontinuierliche Verteilung in den intrinsischen und beobachtbaren Eigenschaften bilden, wird eine strenge Unterteilung generell in Frage gestellt. Stattdessen können die beobachteten Unterschiede durchaus durch stetige Verteilungen des Lorentzfaktors der Ausströmungen, des Kontrastes zwischen den Lorentzfaktoren miteinander wechselwirkender Dichteschalen, des Blickwinkels hinsichtlich der Achse der Ausströmungen oder der Rotverschiebung, erklärt werden.

Im abschliessenden Teil meiner Arbeit beschreibe ich eine Himmelsdurchmusterung nach langsam-variablen optischen Quellen, wie zB. “verwaiste” Nachglühen von GRBs (engl: *orphan afterglows*). Eine natürliche Konsequenz der Kollimierung der ultra-relativistischen Ausströmungen von GRBs ist, dass nur für solche Ereignisse die prompte Gammastrahlung detektiert werden kann, für welche sich der Beobachter innerhalb der Öffnungswinkels der Ausströmung befindet. GRBs, die nicht direkt auf den Beobachter gerichtet sind, können jedoch durch ihre “verwaisten” Nachglühen entdeckt werden, da erwartet wird, dass die späte Emission in einen grösseren Raumwinkel abgestrahlt wird (bis hin zu isotroper Abstrahlung).

Die beschriebene Himmelsdurchmusterung wurde mit dem Wide Field Imager am ESO/MPG 2.2 m Teleskop in La Silla (Chile) durchgeführt. Ca. 12 Quadratgrad wurden in bis zu 25 Nächten mit einer Grenzhelligkeit von R=23 beobachtet. Vier zuvor unbekannte variable Quellen konnten entdeckt werden, von denen ich drei als einen Kataklysmischen Variablen, einen Flarestern und eine Zwergnova identifizieren konnte. Der vierte Veränderliche wurde in einer Beobachtungsnacht als helles Objekt nahe einer konstanten, schwächeren Quelle entdeckt. Die beobachtete räumliche Assoziation legt einen aussergalaktischen Ursprung nahe. Leider konnte der Abfall der Lichtkurve des Variablen, aufgrund fehlender Beobachtungen, nicht bestimmt werden, womit eine Unterscheidung zwischen einem Flarestern, einer Su-

pernova oder eines möglichen GRB Nachglühens nicht möglich war. Diesbezügliche spektroskopische Nachbeobachtungen wurden für die ESO Periode 77 vorgeschlagen.
Es ist theoritisch vorhergesagt, dass die ultra-relativistischen Ausströmungen der GRBs von Materie mit kleinerem Lorentzfaktor und grösserem Öffnungswinkel begleitet werden. Beobachter, welche nur geringfügig auserhalb der prompte Gammastrahlung liegen können somit sogenannte “on-axis” verwaiste Nachglühen detektieren. Deren Beobachtung kann Aufschluss über das Öffnungswinkelverhältnis der Regionen, aus der die Gammastrahlung sowie das optische Nachglühen entsteht, geben. Ich habe Monte-Carlo Simulationen durchgeführt, um zu zeigen, dass die durchgeführte Himmelsdurchmusterung keine ausreichende Himmelsüberdeckung besass, um das Öffnungswinkelverhältnis akkurat genug bestimmen zu können. Es werden zukünftige Himmelsdurchmusterungen mit grösserer Überdeckung vorgeschlagen, die die Möglichkeit haben, die Kollimierung von GRBs mit grosser Genauigkeit zu ermitteln.

Chapter 1
Introduction

One of the most exciting fields of modern astrophysics was born with the serendipitous discovery of Gamma-ray bursts (GRBs) by the american *Vela* satellites more than three decades ago (Klebesadel et al. 1973). Following the detection of the first long-lasting X-ray and optical afterglows at the end of the last century (Costa et al. 1997, van Paradijs 1997) and the unequivocal evidence of their connection with stellar scale events at cosmological distances (Metzger et al. 1997a), GRB research became multi-disciplinary and related to a variety of astrophysical branches. Covering the full extent of our present-day observational and theoretical knowledge on GRBs is beyond the scope of this introduction and could certainly fill the pages of a full PhD thesis by it's own. Instead, I will mention in this chapter only briefly the most important moments, observational facts and empirical laws in GRB science and will focus more on the individual aspects approached by the population study presented in the main part of this PhD thesis. I would like to refer the further interested reader to the many excellent review articles written during the last years for more comprehensive discussions of the history, progress and problems in the field (e.g., Dermer 2002; Woosley et al. 2002; Djorgovski et al. 2003; Ghisellini 2003; Waxmann 2003; Zhang & Meszaros 2004).

1.1 The early years

Before the era of space based satellites hardly anybody had thought about the possible existence of gamma-ray bursts (but see Colgate 1968) and it was only by chance that the first events were discovered. Originally designed to insure the Limited Nuclear Test Ban Treaty signed by the US, Great Britain and the Soviet Union in 1963, the system of american *Vela* satellites detected nearly two dozen brief flashes of gamma-rays in the years 1967-1973 which were incompatible with having planetary, terrestrial or solar origin (Strong et al. 1974). These events showed a variety of light curve shapes with durations ranging from hundreds of milliseconds to several minutes (e.g., Fig. 1.1). During these short times the detected GRBs were the brightest objects on the gamma-ray sky and, as it turned out many years later, reached luminosities comparable to the integrated luminosities of a few hundred thousand galaxies in the same time interval.

The next milestone was set with the launch of the *Compton Gamma-Ray Observatory* (CGRO) in 1991, with the *Burst and Transient Experiment* (BATSE) on board (Fishman et al. 1985). Before the satellite was safely de-orbited into the Pacific Ocean in 2000, BATSE had detected more than 3000 bursts with a typical location accuracy of a few degrees. The resulting sky-map provided firm evidence for an isotropic distribution of GRBs on the sky even at

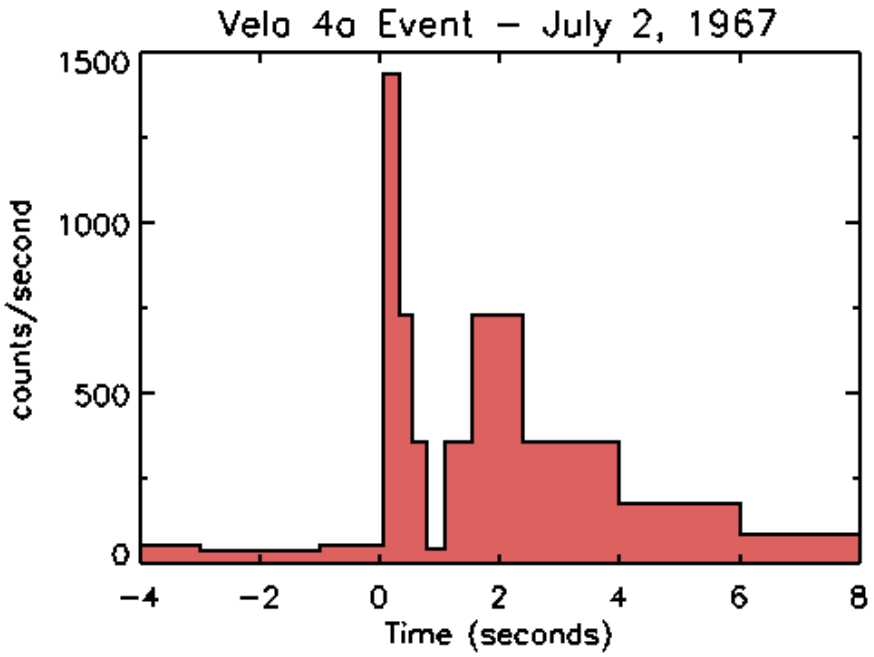

Figure 1.1. The first known gamma-ray burst, detected by the *Vela 4a* satellite on July 2nd, 1967 (Klebesadel et al. 1973). The count rate of the satellite gamma-ray detector abruptly increased indicating a sudden flash of gamma-ray photons. The event was also detected by *Vela 4b* and a planetary, terrestrial or solar origin could be excluded by a triangulation using the arrival times at the two satellites.

the faintest intensities (Meegan et al. 1992). In addition, the distribution of the bursts over their peak flux (log$N$-log$P$) showed a distinct lack of faint bursts compared to a homogenous distribution in an Euclidian space (Fishman et al. 1994).
From the properties of the observed gamma-ray photons two classes of bursts were identified. A population with short durations (typically below 2 s) and hard gamma-ray colours and a population of long-duration bursts (above 2 s) with softer spectrum were found (Fig. 1.2; Kouveliotou et al. 1993). Systematic analysis of the high energy spectra indicated that most GRBs from both classes could be reasonably well described by a smoothly-joining broken power law, known as Band-function[1], with a slope of -1 ± 1 below the peak of the energy spectrum, E_p, and of -2^{+1}_{-2} at energies above E_p. The distribution of E_p found by BATSE was lognormal and centered around $\sim$250 keV. Lately, the *High Energy Transient Explorer* (HETE-2) extended the range of E_p to the low energy regime with the detection of X-ray flashes (XRFs) and X-ray rich bursts (XRRs) (Lamb et al. 2004). These objects resemble "normal" GRBs in many respects but have significantly lower peak energies[2].
Among the transient γ-ray sources, some where found to be repetitively bursting. These so-called soft gamma-ray repeaters (SGRs) constitute a small separat class of objects (4 sources

[1]The Band-function consists of a power law continuum at low energies with an exponential cutoff, $N_E(E) \propto E^{\alpha}$ exp (-E/E_p), and a steeper power law, $N_E(E) \propto E^{\beta}$, with $\alpha > \beta$ above E_p (Band et al. 1993).

[2]X-ray flashes and X-ray rich bursts are defined as having $\log[S_X(2-30\,\mathrm{keV})/S_\gamma(30-400\,\mathrm{keV})] > 0.0$ and –0.5 respectively

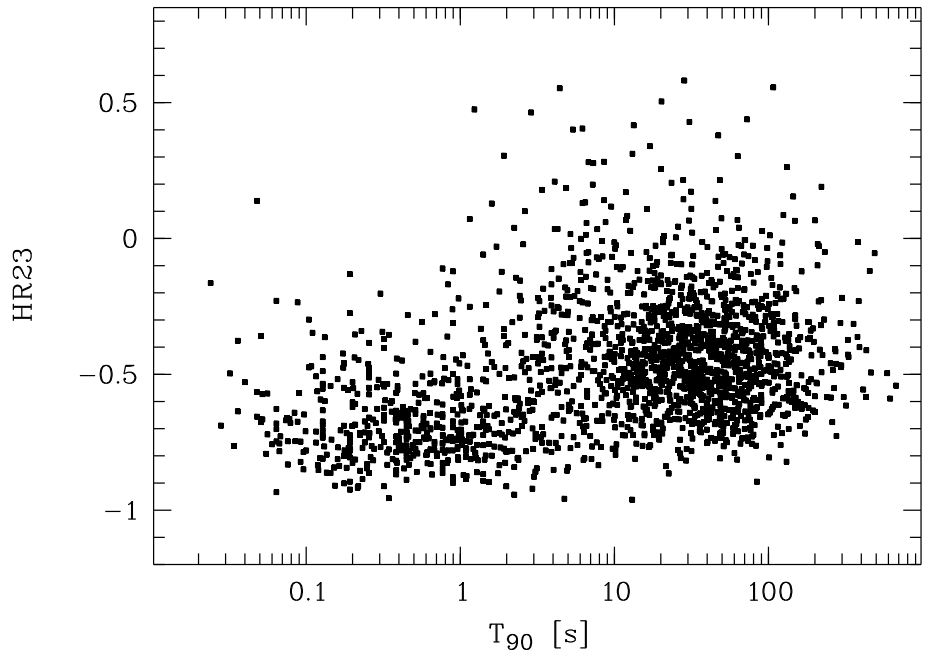

Figure 1.2. Spectral hardness distribution of 1973 BATSE bursts as a function of the duration measured in T_{90}, the time interval over which a burst emits from 5% of its total measured counts to 95%. The hardness ratio $HR23$ is defined as (2–3)/(2+3) where "2" stands for the flux in the 50–100 keV band and "3" for that in the 100–300 keV band, respectively. The two classes, short/hard and long/soft, are clearly distinguishable.

known so far), all located near the Galactic Plane or in the nearby Large Magellanic Cloud. SGRs are thought to be magnetars; strongly magnetized neutron stars with emissions powered by dissipation of magnetic energy (Duncan & Thompson 1992). Besides their repetition they differ from "classical" GRBs in the softness of their spectra (typical bremsstrahlung temperatures of 30 keV as opposed to 300 keV for gamma ray bursts) together with the very short durations of their outbursts (0.1-1 s).

1.2 The afterglow era

Until the mid-90's more than one hundred different GRB progenitor models had been published in refereed journals (Nemiroff 1994). The two mainly discussed scenarios placed the GRB either in the Galactic Halo or at cosmological distances. While the isotropy and the paucity of faint bursts had already suggested a cosmological origin for at least a significant fraction of the events, the final proof came with the discovery of the first long-wavelength counterpart. Shortly after the launch of the Italian-Dutch *BeppoSAX* satallite in 1996, the Wide-Field Cameras on board provided an arcmin localization for a GRB from Feb 27, 1997. Prompt optical follow-up observations lead to the discovery of its optical afterglow (van Paradijs et al. 1997) and at the same time the soft X-ray Narrow-Field Instrument of *BeppoSAX* detected its X-ray counterpart (Costa et al. 1997). Further ground-based observa-

tions noted an underlying galaxy in the vicinity of the optical transient (Metzger et al. 1997b, van Paradijs et al. 1997). Despite this discovery, the final establishment of the distance scale had to wait until the first successful redshift measurements for the GRBs 970505 (z=0.8349; Metzger et al. 1997a) and 971214 (z=3.42; Kulkarni et al. 1998). Over the last years more than one hundred afterglows of long-duration GRBs have been detected and a redshift distribution ranging from z=0.008 to z=6.29 has been established (Fig. 1.3). With the distance scale for long-duration GRBs now being settled, their cosmological distances make them the most luminous objects in the Universe.

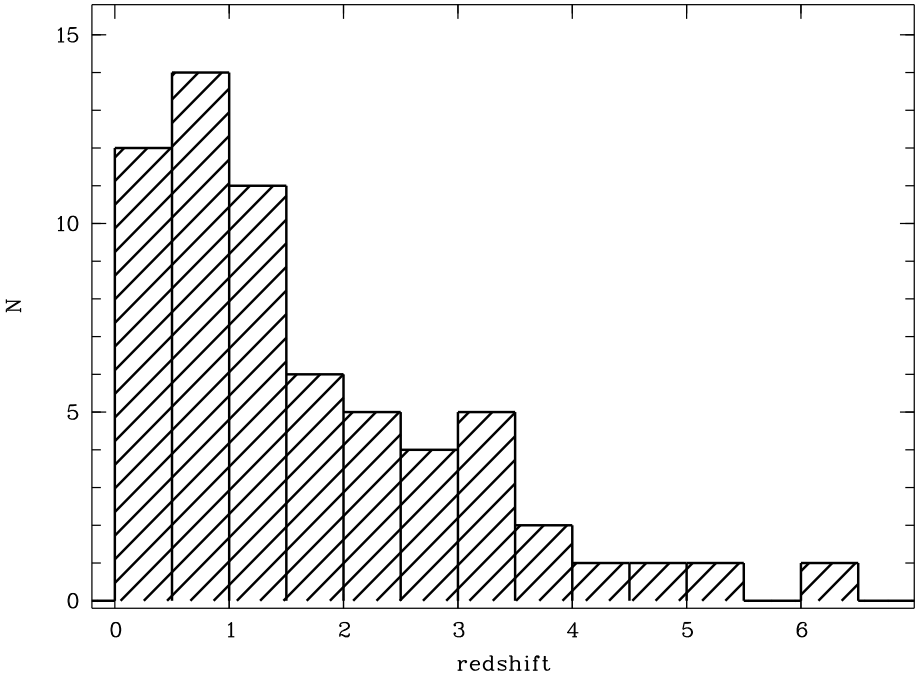

Figure 1.3. Observed redshift distribution of GRBs (as of Oct 13, 2005). Note that the distribution has an observational bias. The redshifts are obtained from metal absorption lines in the afterglow light (see Sect. 1.2) or from emission lines of the underlying host galaxies (see Sect. 1.5). For high redshift bursts the prominent absorption lines (except Lyα) move from the observer frame optical band into the near-infrared band and the host galaxies are in many cases to faint for infrared spectroscopy. Rapid simultaneous multi-band photometry for a photometric redshift determination is required but not commonly availible so far.

Until recently our knowledge of GRB afterglows was restricted to the long-duration population only. Only a small number of rapid and accurate localizations of short bursts had been available so far but no afterglow had been found. This has changed now with the localizations of a small number of short bursts with NASA's *Swift* and *HETE-2* satellites and the detections of the first X-ray, optical and radio afterglows (Kennea et al. 2005; Price et al. 2005a; Soderberg et al. 2005a). For three events candidate host galaxies at z=0.16 (Price et al. 2005b), z=0.226 (Prochaska et al. 2005a) and z=0.258 (Prochaska et al. 2005b) were identified.

1.3 The theory of gamma-ray burst emission

The basic scenario for the understanding of GRBs is the dissipative fireball model which was already proposed before the detection of the first afterglows (Cavallo & Rees 1978; Goodman 1986; Paczynski & Rhoads 1993; Mezsaros & Rees 1993). In this model a huge amount of energy is deposited in a very small volume, constrained to be as small as 60 km by the observed variability timescales (Bhat et al. 1992). This implies enourmous gamma-ray photon densities which in turn leeds to an exceedingly high optical depth to pair-production at the explosion site (so-called "compactness problem"). This is in contradiction with the observed optically thin gamma-ray spectra. In order to explain the observations the emitting regions had to have ultra-relativistic bulk motions with Lorentz factors of $\Gamma \sim 10^{2-3}$. Observational verification for this came with the detection of abrupt quenching of the scintillation behaviour of the radio afterglow of GRB 970508 a few days after the burst (Frail et al. 1997). During this time the afterglow emitting region must have grown with superluminal speed, thus minimizing the scintillation.

A consequence of the high Lorentz factors is that the ejecta must be relatively depleted of baryons. If not, the expansion of the fireball should lead to a conversion of most of its internal energy into kinetic energy of the entrained baryons, rather than into photon luminosity. This would make it energetically very inefficient. In addition, a quasi-thermal spectrum would be expected, in contradiction to the typically observed non-thermal spectrum. These problems where solved with the internal and external fireball shock model (Rees & Meszaros 1992, 1994; see Fig. 1.4). Internal shocks between shells of different Γ are likely to happen in the ultra-relativistic outflow. When these shocks occur after the outflow became optically thin, the kinetic energy of the baryons will be re-converted into non-thermal particle and photon energy. This leads to the observed power-law shaped gamma-ray spectrum.

After producing the prompt emission, the merged shells travel with relativistic velocity further and start to sweep up the local ambient medium (interstellar gas and possibly gas that was previously ejected by the progenitor). This causes a deceleration and sidewards expansion of the outflow and naturally leads to the so-called external shocks (see Fig. 1.4). Relativistic electrons gyrate in random magnetic fields produced in these shocks and radiate synchrotron emission. Under the assumption that the electrons follow a power-law distribution with index p, the resulting emitted photon spectrum follows a power-law with index $-p/2$ at late times (for more details see Sari et al. 1998). As the outflow decelerates the typical Lorentz factor and the peak emission frequency decrease and the entire spectrum shifts towards lower frequencies. This causes the afterglow flux at a specific frequency to decrease following a power law, consistent with the observations.

The observed photon fluxes together with the established cosmological distances of the GRBs imply an enormous energy output. If these energies would be emitted isotropically, they would correspond to luminosities of up to 4×10^{54} erg (Bloom et al. 2001) which is equal to the energy equivalent of one solar mass. An easy way out of this dilemma is a collimated outflow which reduces the energy output by a factor of 10^{2-3} (Rhoads 1997). Observational evidence for a jetted geometry comes from the detection of breaks in the light curves of several GRBs. Initially, the emission of an ultra-relativistic jet with Lorentz factor

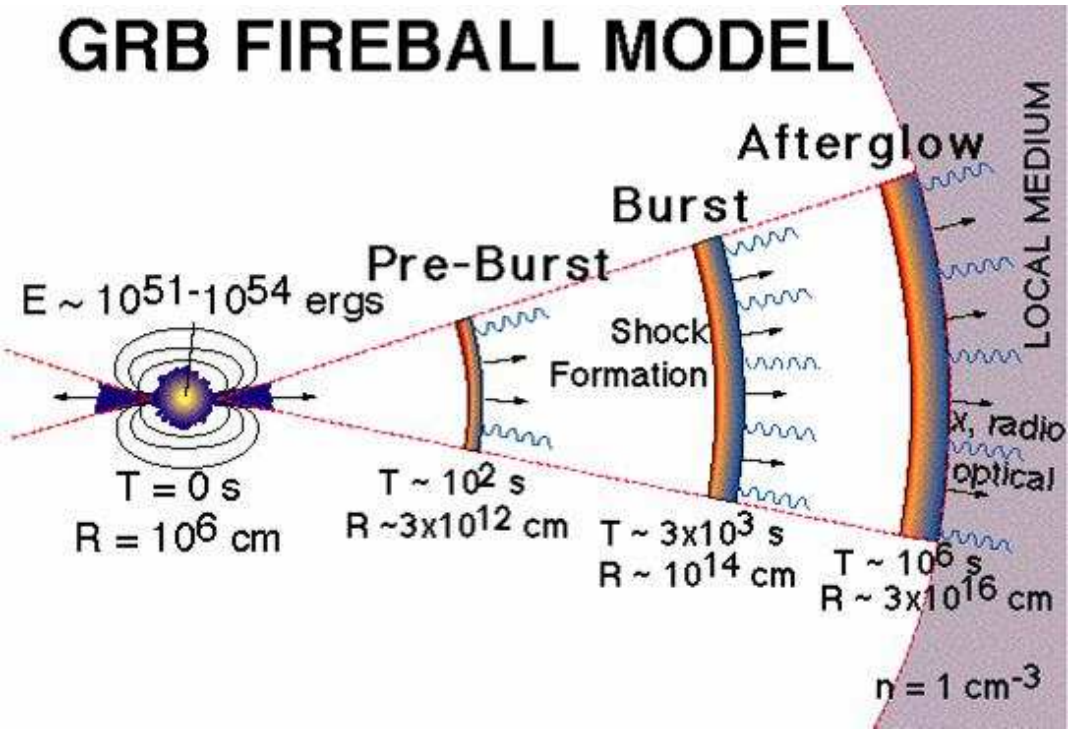

Figure 1.4. Emission regions in the GRB fireball model. An ultra-relativistic outflow emerges from a newly formed spinning black hole. Shocks produced in colliding shells give rise to the gamma-ray emission. When the ejecta plunges into the local medium it decelerates, expands sidewards and produces the observed afterglow from X-ray to radio. The electro-magnetic signals of the sequence of events reach the earth compressed due the extreme velocity of the outflow.

Γ will be beamed into the forward direction within an angle of $1/\Gamma$. As long as this beaming angle is smaller than the geometrical opening angle of the outflow, the observer will receive light only from within the relativistic cone and the dynamical evolution is similar to that of an isotropic explosion. After about a day, the outflow decelerates and the jet opening angle widens to several degrees. When the relativistic beaming angle becomes larger then the jet opening angle, the observer will measure a reduced flux compared to the isotropic case. This jet break is quasi-achromatic and has been observed in a number of GRB light curves. Although this observed effect has been considered now for many years as the best evidence for collimated outflows in GRBs, alternative explanations like e.g., a sudden change in the circumburst density (Panaitescu & Kumar 2001) or a break in the power law distribution of the electrons in the shock (Li & Chevalier 2001) are plausible.
The collimation corrected energy output corresponds to the typical energies emitted in supernova explosions. Compiling a sample of bursts with known redshift and observed jet break times, Frail et al. (2001) found a surprising clustering of the corrected luminosities around 10^{51} erg. This suggested that GRBs are produced by an universal energy reservoir and thus could be seen as some kind of "standard candle". On the other hand, more recent estimates showed that there is still an intrinsic scatter of at least 1–2 orders of magnitude in the beaming corrected luminosity (see also Fig. 1.5).
A further indication for the robustness of the afterglow theory comes from a correlation found

between the rest frame peak energy, $E_p(1+z)$, and the collimation corrected bolometric luminosity (Fig. 1.5, Ghirlanda et al. 2004). The small dispersion in the correlation compared to the scatter around the correlation using the isotropic bolometric energy (Lloyd-Ronning & Ramirez-Ruiz 2002; Amati et al. 2002) supports the theory on which the estimate of the jet opening angle is based. One of the major problems for these analysis is the assignment of breaks in the afterglow light curve with the jet break time for individual bursts. More and more available well sampled light curves reveal a multitude of deviations from a simple power law and several breaks at different times. Also, breaks in the radio band are typically later than in the optical bands. This allows to shift individual points in Fig. 1.5 by a factor of up to one hundred in bolometric luminosity.

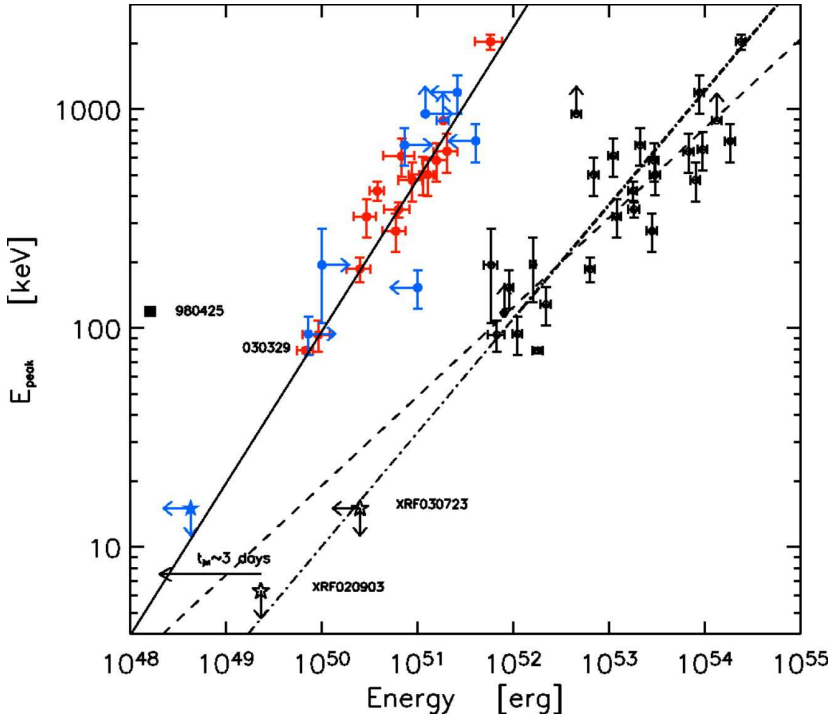

Figure 1.5. Rest frame peak energy vs. bolometric energy (rest frame 1 keV–10 MeV) for GRBs with known redshift. The right part of the diagram shows the relation for the isotropic energy release known as the Amati-Relation (Amati et al. 2002) while the left part shows the collimation corrected luminosities known as the Ghirlanda-Relation. Filled red circles: events with observed jet break in the light curve. Filled blue circles: lower and upper limits. The solid and dashed lines are the best fitting correlations. (From Ghirlanda et al. 2004).

A signature of the jet geometry is also expected to be visible in the polarization of the afterglow light. Different theoretical models predict a variety of net polarization including one or several changes of the polarization angle by 90 degrees. Up to now only for 5 GRBs polarization at optical wavelengths was measured and generally a very low level was found (typical 3% with an exception at 10%; Hjorth et al. 1999; Wijers et al. 1999; Rol et al. 2000; Bersier et al. 2003). The by far most extensive polarization light curve was obtained for GRB 030329, which showed variability patterns deviating from any of the model predictions (Greiner et al. 2003d). In the case of an isotropic fireball the magnetic field is expected

to by highly tangled diminishing the net polarization. The observed low-level of polarization implies that the components of the magnetic field parallel and perpendicular to the shock region differ by at least some percent. This break in the field symmetry is another argument for jetted outflows in GRBs. Further insight into the jet structure is expected to come from the measurements of the polarization of the prompt γ-ray emission. A significant polarization was claimed for the spectacularly bright burst GRB 021206 (Coburn & Boggs 2003), but the results were arraigned by several other groups (Rutledge & Fox 2004; Wigger et al. 2004) and are not conclusive.

1.4 The progenitors

Two popular models emerged out of the multitude of proposed scenarios for the progenitors of GRBs during the last years, both connected to the formation of a rapidly rotating stellar mass black hole. One such setting is the merging of a binary neutron star system or of a neutron star and a black hole (e.g., Eichler et al. 1989; Narayan et al. 1992; Ruffert & Janka 1998). The other popular model corresponds to the final evolutionary stage of a massive star whose core collaps to a black hole and that have sufficient angular momentum to form a disk (Colgate 1968; Woosley 1993, MacFadyen & Woosley 1999). While the merger scenario is still a good candidate for the origin of the short/hard burst population, there is now a general concensus that the long/soft GRBs are intimately connected to the death of massive stars. The first indication came with the spatial association of the low-redshift GRB 980425 (z=0.008) with the SN 1998bw (Galama et al. 1998). Decisive proof was found with the spectroscopic confirmation of supernovae underlying the two low-redshift bursts GRB 030329 (Fig. 1.6, Hjorth et al. 2003, Stanek et al. 2003) and GRB 031203 (Malesani et al. 2004). These so-called hypernovae (Paczynski et al. 1998) are characterized by very large expansion velocities (of the order of 10000-30000 km/s) and ejected mass of radioactive ^{56}Ni (0.4–0.5 $M_\odot$). Re-brightenings in the afterglow light curves of a number of bursts at higher redshifts are highly suggestive for the collapsar scenario as well. Interestingly, an estimate of the rates of GRBs and hypernovae in the Universe shows that they are statistically equal (Podsiadlowski et al. 2004).

The ejected large mass of ^{56}Ni suggests progenitor masses of $>$20–30 $M_\odot$ (Nomoto et al. 2003). In order to enable the relativistic jet jet to escape from the collapsing progenitor, the star has to have lost most of its hydrogen envelope through a stellar wind. In fact, the lack of hydrogen emission lines in the supernova spectra is consistent with the progenitor having been a Wolf-Rayet star. Further observational evidence for this scenario comes from the detection of signatures of stellar winds in the optical afterglow spectra of GRB 021004 (Schaefer et al. 2003; Mirabal et al. 2003) and GRB 030226 (Klose et al. 2004). E.g., in the spectrum of GRB 030226 two absorption line systems with inferred velocity separation of 2400 km/s were found indicating a fast stellar wind in a strong radiation field. Nevertheless, these signatures are not identified for all bursts with sufficient signal-to-noise ratio.

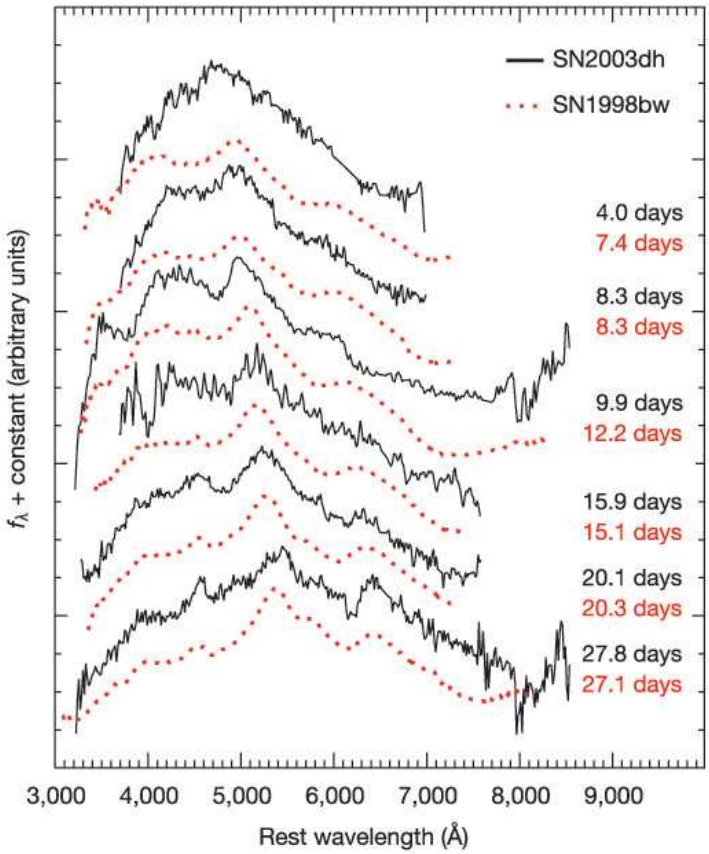

Figure 1.6. Evolution of the optical spectrum of GRB 030329 (solid lines) at z=0.168 (Greiner et al. 2003a) compared to the spectrum of the SN Type Ic 1998bw associated with GRB 980425 (dotted lines). With increasing time (from top to bottom) the afterglow faded away and the supernova signatures emerged and dominated the spectrum. (From Hjorth et al. 2003).

1.5 The host galaxies

For nearly all long-duration GRBs with sub-arcsec localization an underlying host galaxy was found and the current sample consists of more than 30 galaxies with known redshifts in the range of $0.008 \leq z \leq 4.51$ and apparent magnitudes ranging from R=14 to R=30. They appear to be sub-luminous in the near-IR at approximately 8% of L_* in a Schechter luminosity distribution (Fig. 1.7 left; le Floc'h et al. 2003). Although the presently known host sample indicates that bursts can occur in any type of galaxy, the majority of them show dwarf-like morphology. The host galaxies exhibit very blue colors, R-$K \sim 2$–3, comparable to those of faint blue star-forming galaxies at high redshift (Fig. 1.7 right). In fact, the fitting of the spectral energy distribution of 10 hosts with well sampled broadband colors revealed that these galaxies are very similar to young starburst galaxies (Christensen et al. 2004). Unfortunately, the sample of GRB hosts is selected in an inhomogeneous way, such that those with bright optical afterglows are much more likely to be detected. Therefore, hosts with a low level of intrinsic extinction are preferred over highly reddened hosts. This is in agreement with the

very small number of GRBs detections towards luminous dust-enshrouded starbursts such as observed in the deep infrared and sub-millimeter surveys. Indeed, only four hosts are detected as intensively star forming ultra-luminous infrared galaxies (Berger et al. 2003; Tanvir et al. 2004).

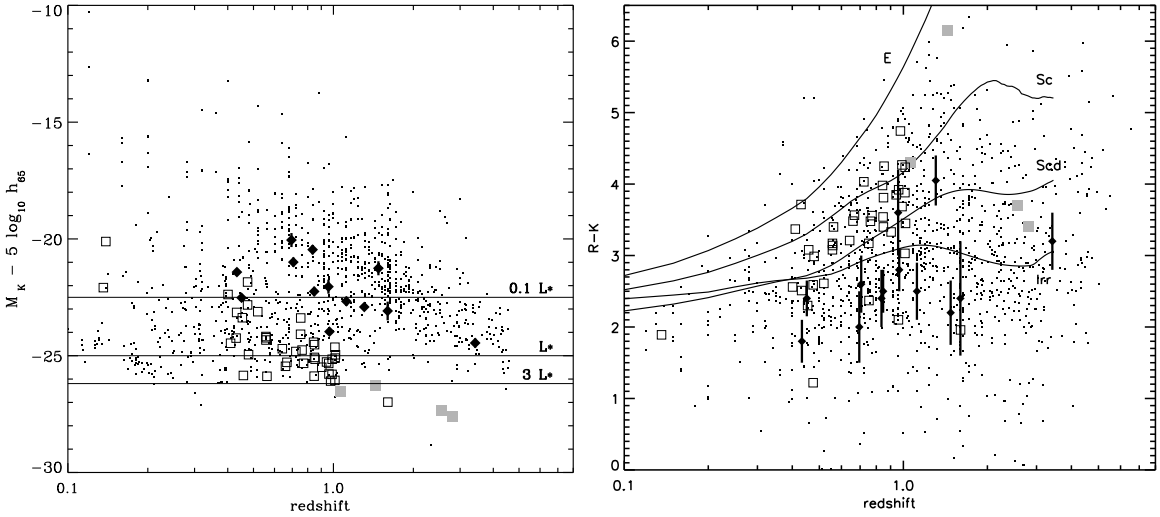

Figure 1.7. Left: Absolute *K*-band magnitudes of a sample of GRB host galaxies with known redshift (filled diamonds) compared to optically/NIR-selected field sources (points) and ISO/SCUBA galaxies (open/filled squares). The majority of the hosts are sub-luminous around 0.1 L_* in the *K*-band. **Right:** Observed $R-K$ colors versus redshift. Solid curves indicate the observed colors of local elliptical (E), spiral (Sc, Scd) and irregular (Irr) galaxies if they were moved back to increasing redshifts. The colors indicate that most of the GRB hosts are consistent with being irregular galaxies (Figure from le Floc'h et al. 2003).

The host galaxies exhibit in general a high effective (per unit mass) star formation rate compared to typical starburst galaxies (Chary et al. 2002, Courty et al. 2004). In addition, there is evidence for higher Lyα emission in GRB host galaxies compared to the observations of other starburst galaxies at similar redshift (Fynbo et al. 2003). This suggests that GRB hosts are valueable probes for the stellar and galaxy formation and evolution in the Universe. The GRB brightness and the transparancy of the Universe for the high-energetic γ-ray emission make them essentially useful at very high redshifts.

The position of the burst in its host galaxy can be used as a further constraint for the GRB progenitor model. In most cases the burst occured within the UV-bright part of the host galaxy (Bloom et al. 2002), suggesting regions of unobscured active star formation. This is not surprising given the short lifetime of the massive progenitor star. A GRB happens essentially instantaneously after the formation of its progenitor and thus will not have left the place of birth. Instead, in the binary merger scenario, the burst could take place well outside its hosting galaxy. The kicks induced by the explosions of two supernovae together with the long merging timescale allow the binary system to travel a considerable distance in its galaxy (several kiloparsec). The lack of afterglows well outside of their hosts is a further support for the collapsar scenario for long-duration GRBs.

1.6 A population study

As introduced in the pages above, the science connected with Gamma-ray bursts stretches over a variety of astrophysical research fields. Involving stellar-scale events located at cosmological distances, GRBs allow to study among many other things the explosion of massive stars, the physics of relativistic ejecta, the inter-stellar and inter-galactic medium and the galaxy structure and evolution in the Universe. This multi-facet nature of GRBs motivated me to investigate three different aspects of Gamma-ray bursts in the present PhD thesis. In the following a brief motivation for each of the three research topics is given. For a more detailed introduction I would like to refer the reader to the respective sections in the individual chapters (2–5).

The prompt emission properties of GRBs with INTEGRAL SPI-ACS
The primarly observed signature of a GRB is typically the prompt gamma-ray emission. With the launch of the *International Gamma-Ray Astrophysics Laboratory* (INTEGRAL), an ESA satellite, in October 2002, a new mission for the detection of the prompt emission was brought into space. One of the instruments is the spectrometer SPI and its anti-coincidence shield SPI-ACS. The SPI-ACS consists of 91 Bismuth Germanate crystals which surround the spectrometer nearly completely and thus provide a quasi-omnidirectional field of fiew of the gamma-ray sky in the $\sim$80 keV to $\sim$10 MeV energy range. Although SPI-ACS does not provide spectral informations and the event localization is based on the method of triangulation using the Interplanetary Network of gamma-ray satellites (Hurley 1997), especially the upper energy range of SPI-ACS makes it a powerful tool for the detection and study of the short/hard burst population.
An important issue is the distinction between cosmological short bursts and other sources of short-time gamma-ray photons, e.g. cosmic-ray events. In chapter 2 I will present and discuss the sample of GRBs detected with SPI-ACS during the first 2 years of the mission and put special emphasis on the origin of the short event population. A statistical analysis of the properties of the whole sample will be given and compared with previous gamma-ray missions.

Dark bursts and X-ray flashes
While for nearly all well-localized GRBs an X-ray afterglow could be detected, a fair fraction of those lacks a detection at longer wavelengths. The reasons for the non-detection of the optical transients of bursts with known X-ray or radio afterglows can be manifold. Probably the most important limitation is introduced directly by the observations, since a slow reaction time, a location in a crowded field, possibly high Galactic foreground extinction, or unfavorable observing conditions, like bright moon and twilight, can easily account for the non-detections of the counterparts. However, this does not provide a valid explanation for all dark bursts. In some cases , e.g. GRB 970828 (Groot et al. 1998; Djorgovski et al. 2001) and GRB 990506 (Taylor et al. 2000) even rapid (less than half a day after the GRB) and deep (R>23) observations did not reveal an afterglow, despite a clearly fading source in the X-ray and/or radio band.
In addition to the observational biases, “dark bursts” may reflect a broad distribution of

physical parameters of the GRB itself or of its environment (e.g. a high density ambient medium). The Lyman alpha suppression at high redshift ($z>5$) could easily account for the lack of optical detections as well. Nevertheless, observations show that the high-z explanation for "darkness" can not apply in all cases. For example, GRB 970828 and GRB 000210 revealed underlying host galaxies at positions coincident with those of the X-ray and radio afterglows (Djorgovski et al. 2001; Piro et al. 2002) for which spectra indicate redshifts of z=0.958 and z=0.8463, respectively.
I studied the origin of the population of observed "dark burst" based on an example event from May 28, 2003 (Chapter 3). This event was also characterized by a very soft observed prompt emission spectrum and was classified as an X-ray flash (see Sect. 1.1) accordingly. Similar to the "dark bursts", the origin of X-ray flashes is widely discussed. A variety of theoretical models has been proposed to explain the observed peak energies of XRFs, among them a high baryon loading in the GRB jets, which can result in bulk Lorentz factors much smaller than those expected in GRBs (Dermer et al. 1999; Huang et al. 2002), or a low contrast between the bulk Lorentz factors of the colliding relativistic shells (Barraud et al. 2005). Other possible models include bursts which are seen slightly outside the jet opening angle (Yamazaki et al. 2002) or high-redshift events for which the intrinsic spectrum is moved to lower energies in the observer frame (Heise et al. 2001).
The first step towards the discrimination between the individual models is the assignment of the distance scale to the explosion site of XRFs. A number of XRFs have been localized to arcminute accuracy in the past but only for two could accurate distances be obtained so far, XRF 020903 at z=0.251 (Soderberg et al. 2004) and XRF 030429 at z=2.66 (Jakobsson et al. 2005). In two more cases, XRF 011030 and XRF 020427, host galaxies with typical properties of GRB hosts have been detected and photometric evidence suggests the redshifts to be $z<3.5$ (Bloom et al. 2003) and $z<2.3$ (van Dokkum & Bloom 2003), respectively. For XRF 030723 a firm upper limit of z=2.3 could be placed from the absence of Lyα absorption and prominent lines in the afterglow spectrum as well as from a light curve bump associated with possible underlying supernova (Fynbo et al. 2004). In Chapter 4 I present the redshift of the XRF studied in Chapter 3 and discuss its implications for the origin of X-ray flashes.

Constraining the collimation of GRBs using orphan afterglows
The standard model of GRBs suggests ultra-relativistic outflows in the form of narrowly collimated jets with opening angles of the order of several degrees (see Section 1.3). A natural consequence of the collimation is that the prompt gamma-ray emission will only be detected if the viewing angle of the observer is equal to or smaller than the opening angle of the jet. This implies that only for a fraction of all bursts in the Universe γ-ray photons will reach the Earth and the total GRB rate will be higher than the observed rate by a factor of roughly 50-500. Nevertheless, GRBs which are not pointed directly at the observer can in principle be discovered through their more isotropic afterglow radiation at longer wavelengths. These so-called orphan afterglows were identified as powerful tools to study the initial opening angle of the jets and to place a constraint on the collimation of the optical afterglow emission (Rhoads 1997).
In 1999, a photometric survey, dedicated to the search for orphan afterglows, was performed using the Wide Field Imager at the MPG/ESO 2.2 m telescope in La Silla, Chile. The large

amount of imaging data required the development of a specialized data reduction pipeline to which part of my PhD time was dedicated. In Chapter 5 the reader will find the detailed description of the pipeline, and the analysis and results of the complete survey. The candidate transients will be described and the results will be discussed in the context of the collimation of GRBs.

Chapter 2
The 1st INTEGRAL SPI-ACS gamma-ray burst catalogue

A. Rau, A. von Kienlin, K. Hurley & G.G. Lichti
Astronomy & Astrophysics, 438, 1175 (2005)

Abstract: We present the sample of gamma-ray bursts detected with the anti-coincidence shield ACS of the spectrometer SPI on-board INTEGRAL for the first 26.5 months of mission operation (up to Jan. 2005). SPI-ACS works as a nearly omnidirectional gamma-ray burst detector above $\sim$80 keV but lacks spatial and spectral information. In this catalogue, the properties derived from the 50 ms light curves (e.g., T_{90}, C_{max}, C_{int}, variability, V/V_{max}) are given for each candidate burst in the sample. A strong excess of very short events with durations $<$0.25 s is found. This population is shown to be significantly different from the short- and long-duration burst sample by means of the intensity distribution and V/V_{max} test and is certainly connected with cosmic ray hits in the detector. A rate of 0.3 true gamma-ray bursts per day is observed.

2.1 Introduction

Although discovered more than three decades ago (Klebesadel et al. 1973), the phenomenon of cosmic gamma-ray bursts (GRB) is still challenging, with many open questions to solve. Therefore, the detection and investigation of GRBs is one of the important scientific objectives of ESA's *International Gamma-Ray Astrophysics Laboratory* (INTEGRAL) mission (Winkler et al. 2003). INTEGRAL contributes to GRB science in two ways. (i) For bursts which occur in the field of view (FoV) of the spectrometer SPI (Vedrenne et al. 2003) and of the imager IBIS (Ubertini et al. 2003), INTEGRAL provides accurate positions ($\sim$2 arcmin) for rapid ground- and space-based follow-up observations. In addition, high-energy spectra in the 20 keV–8 MeV range are recorded (see Mereghetti et al. 2004 for a recent summary). (ii) The anti-coincidence system of SPI (SPI-ACS) acts as a nearly omnidirectional GRB detector in the $\sim$80 keV to $\sim$10 MeV energy range (von Kienlin et al. 2003).
It has long been known that there are two distinct classes of GRBs which differ observationally in duration and spectral properties (Mazets et al. 1981; Norris et al. 1984; Dezalay et al. 1992; Hurley 1992; Kouveliotou et al. 1993; Norris et al. 2000). This was quantified using data from the Burst and Transient Source Experiment (BATSE) detectors (Fishman et al. 1989) on-board NASA's *Compton Gamma-ray Observatory* (CGRO). The sample of more than one thousand bursts included in the 4th BATSE catalogue displayed a clear bimodal

duration distribution, with one group having short durations ($<$2 s) and the other longer durations (seconds to minutes) (Kouveliotou et al. 1993). Statistically, the peak energy of the Band spectrum for short bursts (Band et al. 1993), E_p, is higher (typically $\sim$100–1000 keV) than that of the long-duration events (typically $\sim$70–500 keV) (Fishman & Meegan 1995). The sensitivity of the anti-coincidence system of SPI to the short/ hard burst population is nearly unprecedented, which raised expectations before the launch of the mission that new insights into the distribution of short bursts would be achieved.
In this paper we present the 1st catalogue of gamma-ray bursts detected by SPI-ACS. We describe the instrumentation and data (Sect. 2.2), the sample selection criterion (Sect.2.3) and the sample analysis (Sect.2.4). In Sect.2.5 the duration- and intensity distributions of the sample are discussed.

2.2 Instrumentation & data

The anti-coincidence system[1] of SPI consists of 91 Bismuth Germanate (BGO) crystals with a total mass of 512 kg. The thickness of the individual crystals ranges from 16 to 50 mm. They are positioned in two rings (the upper and lower collimator ring) whose axes are along the viewing direction of the spectrometer, between the coded mask and the detector plane of SPI; in addition, there are side-shield and rear-shield assemblies (Fig.2.1). Incoming γ-rays are converted into optical photons with a wavelength of $\sim$480 nm. Each BGO is redundantly monitored by two photomultiplier tubes. In addition to the BGO, a plastic scintillator (PSAC), whose purpose is the reduction of the 511 keV background produced by particle interactions in the passive mask, is located directly below the coded mask.
Since the ACS encloses the SPI, it provides a quasi-omnidirectional field of view with a large ($\sim$0.3 m^2) effective area for the detection of gamma-rays (von Kienlin et al. 2003a). Unfortunately, the electronics does not allow for good spatial resolution; the burst data consist only of the total event rate from all the crystals (for more details see Lichti et al. 2000) with a time resolution of 50 ms. In addition, however, each BGO crystal is read out every 96 s with an integration time of 1 s, which in principle allows a rough position estimate for long and bright events.
The SPI-ACS data do not include spectral information because the energy of the gamma-rays is not measured. The only information which is avaiable is that the energy of the interacting photon must be above the threshold energy of $\sim$80 keV. Due to the different properties of the individual crystals, their associated photomultipliers, and the redundancy concept (signals from two different crystals are fed to the same front-end electronics) this energy threshold can only be estimated very coarsely.
As a veto shield the SPI-ACS has no upper limit to the energy range (von Kienlin et al. 2003b). Therefore, the physical properties of individual events (e.g., peak flux, fluence) cannot be estimated directly from the data. A conversion from detector counts to photons cm^{-2} s^{-1} is possible only for bursts whose arrival directions and spectra (e.g., the Band function parameters - Band et al. 1993) are accurately known from other gamma-ray instruments. For

[1] developed at the Max-Planck Institute for extraterrestrial Physics, Garching, Germany

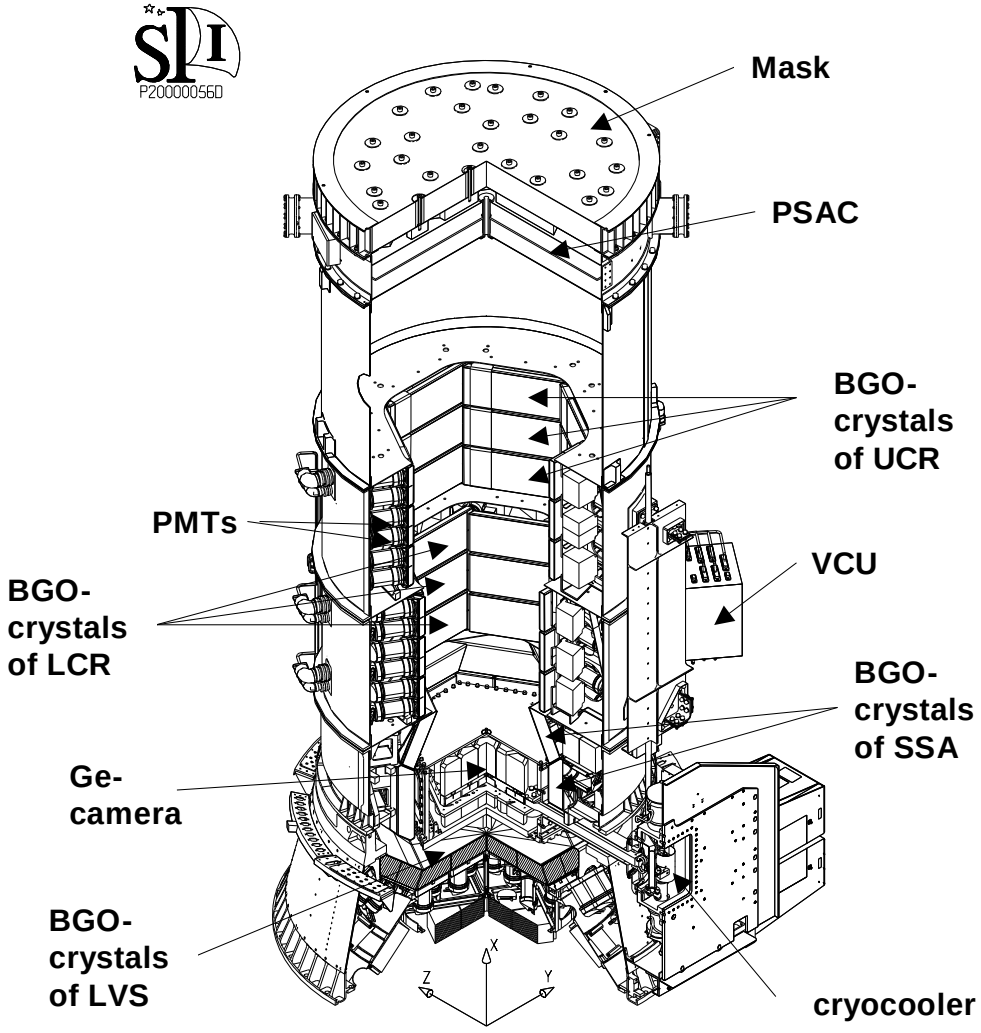

Figure 2.1. Spectrometer SPI and SPI-ACS. The SPI-ACS consists of the plastic scintillator (PSAC) and the BGO crystals of the upper (UCR) and lower collimator rings (LCR) plus the side-shield assembly (SSA) and lower veto shield (LVS). The crystals are monitored by the photomultiplier tubes (PMT) and the events are processed in the veto control unit (VCU).

these bursts the effective area of the detector can be modelled by simulations of the photon transport in the instrument as a function of the incident angle and energy. While the number of GRBs for which this method can be applied is very small, it was especially useful for the determination of the SPI-ACS spectral parameters for the giant flare from SGR 1806-20 on Dec. 27 2004 (Mereghetti et al. 2005).
SPI-ACS is part of the INTEGRAL Burst Alert System (IBAS; Mereghetti et al. 2004). A software trigger algorithm searches for an excess in the overall count rate with eight different time binnings (0.05, 0.1, 0.2, 0.4, 0.8, 1, 2, & 5 s) with respect to a running average background. The trigger thresholds depend on the time binning and are set to 9, 6, 9, 6, 9, 6, 9 & 6σ, respectively. For each trigger an ASCII light curve (5 s pre-trigger to 100 s post-trigger) and the spacecraft ephemeris are stored and made publicly available[2]. It was originally planned to distribute transient detections automatically. However, due to the large number of spurious triggers produced by solar flares, cosmic rays and radiation belt passages, SPI-ACS alerts are now sent only manually to the interested community. During the early mission phase many spurious triggers were produced by rate increases in single 50 ms time bins ($\sim$15 trigger per hour). A software solution was found to remove these events from the data stream.
Since December 2002 SPI-ACS has been an important member of the 3rd Interplanetary Network (IPN) of gamma-ray burst detectors, which provides burst localizations using the triangulation method (Hurley 1997). Thus the lack of spatial resolution of the ACS can at least partly be compensated for. By studying triangulations of a number of bursts with precisely known localizations together with Konus/*Wind* and/or Helicon/*Coronas-F* instruments the absolute timing of the instrument was adjusted and verified to an uncertainty of 25 ms (Rau et al. 2004).

2.3 Sample selection

A sophisticated statistical analysis of the GRB events in the SPI-ACS overall count rate requires a thorough and robust sample selection. Generally, the best method to distinguish gamma-ray bursts from other events occurring in the data stream is their localization in celestial coordinates. Likewise, detections of the events by other missions with gamma-ray detectors, e.g. the instruments participating in the IPN, can be used to discriminate between real cosmic events and those with a solar or particle origin. Due to the lack of spatial information in the SPI-ACS data, observations with independent instruments are required in order to apply this localization-based selection criterion.
Due to the different energy ranges, sensitivities, and parts of the sky observed by the various currently active gamma-ray detectors, the above-mentioned method of selection applies only to a sub-sample of the GRBs observed with SPI-ACS. Due to its nearly omnidirectional field of view and sensitivity, a considerable fraction of GRBs is expected to be detected only by SPI-ACS. Thus, in order to study a statistically more significant sample, we defined our selection criteria to be independent of the confirmation by other instruments and based only

[2] http://isdcarc.unige.ch/arc/FTP/ibas/spiacs/

on the SPI-ACS light curve.

The base sample was constructed from all triggered events in the SPI-ACS overall rate light curve. Each trigger in this preliminary sample was subsequently checked for particle or solar origin using the INTEGRAL Radiation Monitor (IREM) and the Geostationary Operational Environmental Satellites (GOES)[3], respectively. Triangulated events with a localization consistent with the position of a Soft Gamma Repeater (SGR) were removed from the sample. A significance threshold was then applied to each event with a possible cosmic origin, such that a trigger was included in the sample of GRB candidates when its significance S above the background B exceeded S=12σ in any time interval during the event. Here, 1σ corresponds to $1.57\times\sqrt{B}$, where the factor 1.57 takes into account the measured deviation of the background from a Poissonian distribution (von Kienlin et al. 2003b, Ryde et al. 2003). The conservative threshold of S=12σ has been chosen in order to minimize the contamination by weak events of non-GRB origin. Examples of candidate GRBs from the final sample are shown in Fig. 2.2.

Based on the selection criteria described above, a total of 374 candidate GRBs were detected between Oct. 27, 2002 and Jan. 12, 2005. In addition, 14 GRBs with a significance below the selection threshold, but confirmed by other gamma-ray missions, were detected. From the total sample of 388, a cosmic origin for 179 has been confirmed. Most of these events were detected by Konus/*Wind* and/or *Ulysses*. Unfortunately, the *Ulysses* GRB experiment had to be turned off in December 2003 due to the diminishing output of the radioisotope thermoelectric generator.

A summary of the currently active missions and the confirming detections of SPI-ACS candidate GRBs is presented in Tab. 2.1. The number of events detected by SPI-ACS and HETE-2 is relatively low compared to the total number of GRBs detected by HETE-2 during the INTEGRAL mission time. This is not surprising; it is the result of the low sensitivity of SPI-ACS to X-ray flashes and X-ray rich bursts, which constitute approximately 2/3 of the HETE-2 GRB sample (Lamb et al. 2005). These events are characterized by an E_p<80 keV and thus have their emission maximum below the SPI-ACS energy range. The number of bursts detected both in the INTEGRAL FoV and SPI-ACS is very low as well, since the effective area of SPI-ACS is a minimum for events irradiating the satellite from that direction.

Taking into account the observation time losses due to radiation belt passages and regular SPI detector annealings, SPI-ACS was actively observing GRBs for a total 21.6 months up to Jan. 12, 2005[4]. This time corresponds to a rate of 216 candidates and 92 confirmed bursts per year selected according to our criteria. For comparison, Lichti et al. (2000) predicted the rate of GRBs prior to the start of INTEGRAL to be $\sim$160 per year at a 10σ level.

[3] http://www.sec.noaa.gov

[4] The INTEGRAL satellite is in a highly elliptical orbit with a period of 72 hours. Due to the high particle flux the instruments are deactivated during the perigee passage and are online only for $\sim$62 hours per orbit. Approximately twice a year, the SPI Germanium detectors need to be heated up and cooled again (annealing) to counter the degradation of the crystal structure by the space environment (cosmic rays, solar wind, etc.)

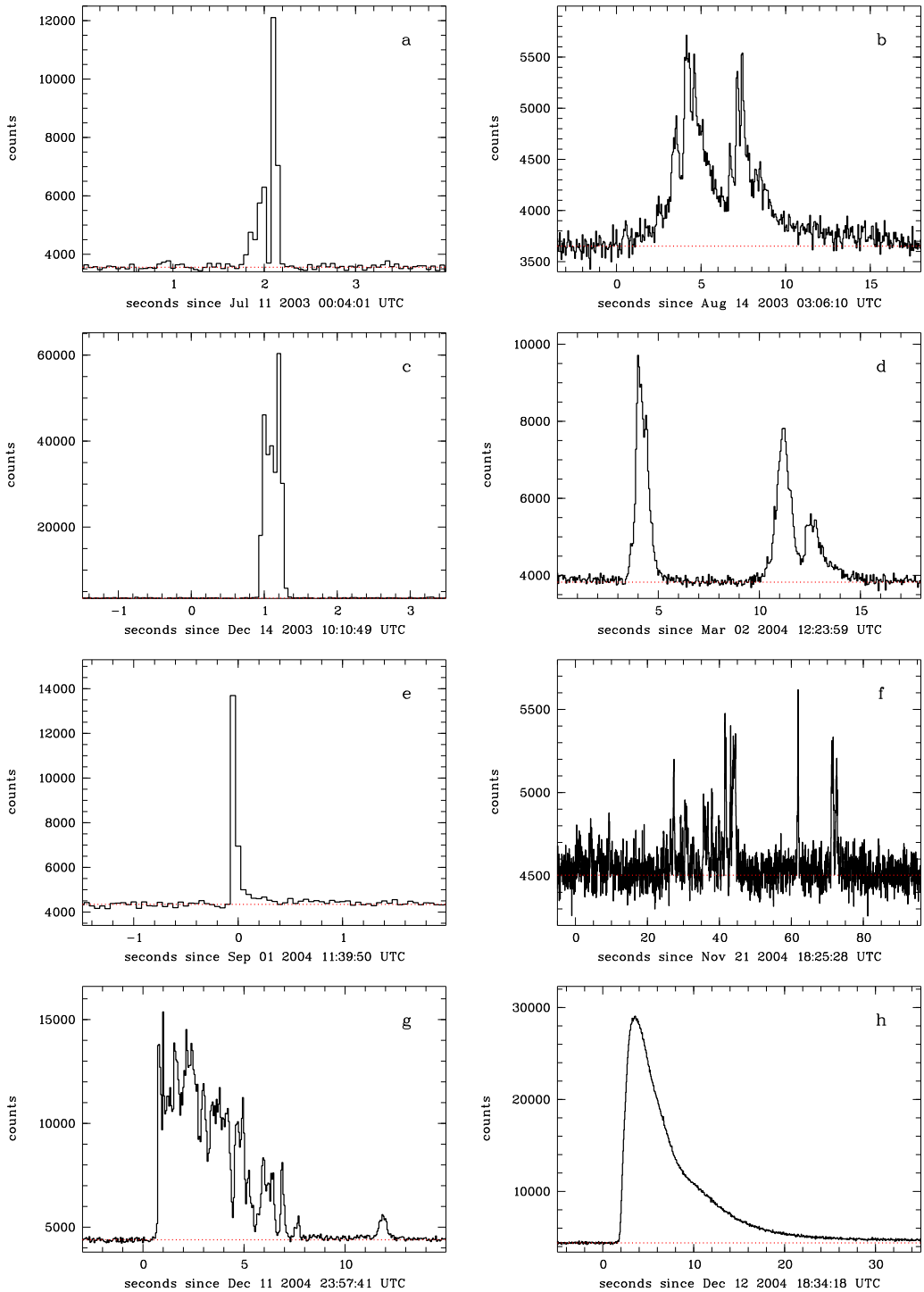

Figure 2.2. SPI/ACS overall count rate light curves with 50 ms time binning for a selection of candidate GRBs from our sample. The horizontal red dotted lines mark the background level. **a)** short GRB 030711. Note that triangulation cannot exclude SGR 0525-66 as the origin (Hurley et al. 2003a); **b)** long GRB 030814 (Hurley et al. 2003b); **c)** bright short GRB 031214 with a very hard ($E_P = 2000 \pm 80$ keV) spectrum (Hurley et al. 2003c, Golenetskii et al. 2003a,2003b); **d)** triple-peaked GRB 040302; **e)** bright unconfirmed event; **f)** multi-peaked GRB 041121; g) structured GRB 041211; h) very bright prototypical FRED (fast rise, exponential decay) GRB 041212.

Table 2.1. Gamma-ray burst detectors and satellites and number of reported simultaneous burst detections with SPI-ACS. (1): single photon counting, (2): 64 ms resolution during flare mode.

Instrument	Energy [keV]	Time Res. [s]	Conf.
Konus/*Wind*	10–10000	0.002–2.39	164
Ulysses	25–150	0.008–2.0	92
Mars Odyssey	30–8000	0.032–0.25	79
HETE-2	6–400	(1)	42
RHESSI	3–20000	(1)	79
INTEGRAL FoV	3–15000	(1)	4
Helicon/*Coronas-F*	10-10000	(2)	3
Swift	15–350	(1)	3
RXTE/ASM	1.5–12	100	2

2.4 Sample analysis

For each candidate GRB in the sample, a linear fit to the background in a time interval before and after the event was performed and the resulting background counts subtracted. Next, a correction for dead time in the detector and electronics ($<$3% for the brightest events in the sample[5]) was applied. The observer frame duration T_{90}, the time interval over which a burst emits from 5% to 95% of its total measured counts, was obtained and integrated burst counts over the whole event as well as the peak counts in the brightest 0.25 s interval were estimated. Due to the lack of spectral response, these detector counts cannot be directly converted into more physical units (fluences and peak fluxes).

For a quantitative evaluation of the uniformity of the SPI-ACS GRB sample we applied the V/V_{max} test (Schmidt 1968). In particular, V/V_{max} compares the volume in which the event was detected to the largest possible volume in which the event would be just at the selection threshold. The ratio of the volumes translates into the ratio of the peak counts, C_p, over the minimum triggering counts, C_{min}, in the same time interval as: $V/V_{max} = (C_p/C_{min})^{-3/2}$. The time intervals used range from the 0.05 s time resolution of SPI-ACS to the T_{90} of the individual events.

In order to estimate the variability of the candidate burst light curves in the sample we used the variability formulation of Reichart et al. (2001), $V_{f=0.45}$. This measure is computed from the variance of the 50 ms binned light curve with respect to a boxcar–smoothed version of itself. Following previous attempts, we used t_{45} as the smoothing time scale; this is the effective time for which the integrated counts of the brightest parts of the event are 45% of the total counts. The deviation of the SPI-ACS background from a Poissonian distribution was taken into account by broadening the distribution by a mean factor of 1.57.

[5]Note that the initial peak of the outburst of SGR1806-20 from Dec. 27 2004, for which the SPI-ACS data were strongly affected by dead time effects, was about 10^2 times stronger than the most luminous GRB in the sample.

All 388 GRBs and candidates in the SPI-ACS sample are listed in Tab. 2.2 (also available online at the CDS) together with the estimated burst properties. A continuously updated on-line version is available[6] including figures and ASCII files of the light curves. The first column of Tab. 2.2 gives the number of the event in this catalogue. The trigger date (YYMMDD) and UTC are listed in the following two columns. The next four columns give the maximum significance of the event above the background, T_{90}, the total integrated counts in the event and the peak counts over 0.25 s. The V/V_{max} statistic and variability measure are shown in columns eight and nine, respectively. The final column lists all other gamma-ray instruments and missions from which detections of the event were reported. Here, "U" stands for *Ulysses*, "K" for Konus/*Wind*, "M" for *Mars Odyssey*, "H" for HETE-2, "R" for RHESSI, "C" for Helicon/*Coronas-F*, "I" for INTEGRAL (SPI/IBIS), "S" for *Swift* and "X" for RXTE/ASM.
The table has numerous events with missing entries. For all GRBs which were confirmed by other instruments but detected by SPI-ACS below the sample selection threshold, only the time, date, significance and common instuments are listed. Furthermore, the variability measure was obtained only for long-duration events with sufficient signal-to-noise ratio.

2.5 Results

2.5.1 Durations

The distribution of the T_{90} durations is shown in Fig. 2.3. For comparison the distribution derived from 1234 GRBs in the 4th BATSE GRB catalogue (Paciesas et al. 1999) was scaled to the elapsed mission time of SPI-ACS and included in the figure.
The distribution of the SPI-ACS burst candidates shows a bimodality similar to what was observed by the BATSE experiment. The long burst population has its maximum at $\sim$30 s and resembles the BATSE results closely. A short duration component is found in the SPI-ACS sample as well, but it deviates significantly from the BATSE sample. While the BATSE short burst logT_{90} distribution can be fit by a Gaussian centered at T_{90}=0.45 s (Horvath 1998) the number of short burst candidates in the SPI-ACS sample rises steeply towards low values of T_{90} and has its maximum at the time resolution of the instrument (0.05 s). Note that number of events with $T_{90}\leq$0.05 s has to be considered as a lower limit as events detected only in a single time bin are rejected already by the software which monitors the telemetry stream (see Sect. 2.2).
A further difference between the two samples is found in the ratios of short to long events. While the 4th BATSE catalogue included $\sim$70% long (T_{90} >2 s) and $\sim$30% short bursts (T_{90} <2 s), around 50% of the total events in the SPI-ACS sample have T_{90}<2 s. Note that the division into short and long bursts is not unambiguously defined, as different class boundaries are generally found when other properties (e.g. fluence, spectral hardness ratios, $<V/V_{max}>$ are included (e.g. Mukherjee et al. 1998, Hakkila et al. 2000). In addition, the SPI-ACS and BATSE burst samples have been compiled using inherently different trigger and instrumental characteristics which imply different definitions for the short and long classes in both

[6] http://www.mpe.mpg.de/gamma/science/grb/1ACSburst.html

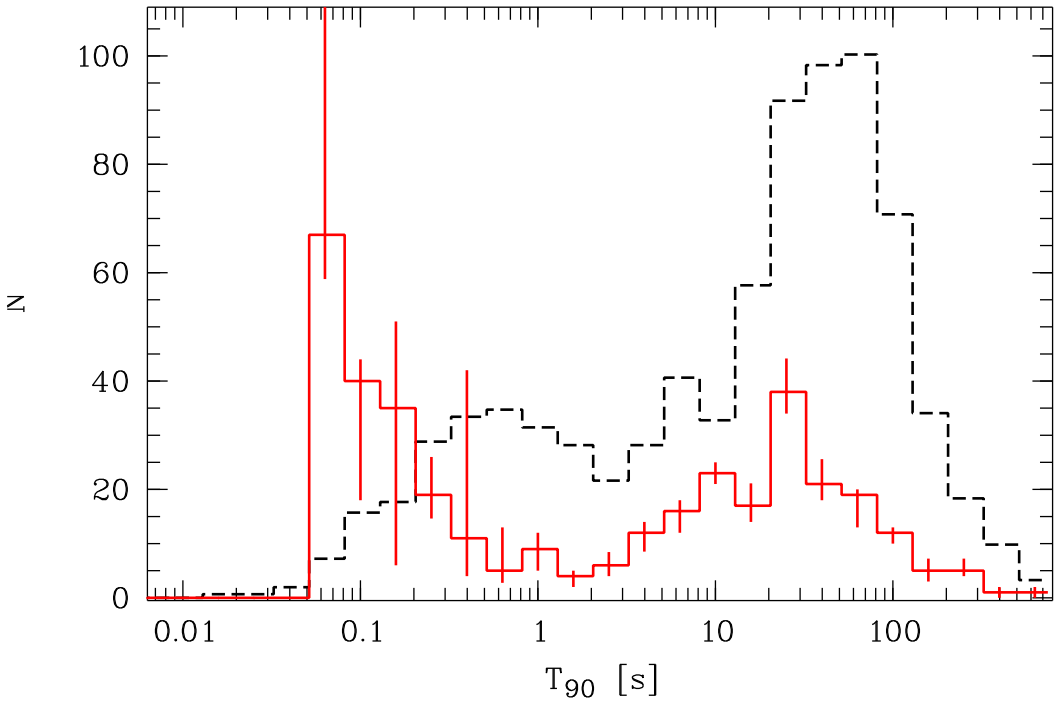

Figure 2.3. Distribution of T_{90} for all SPI-ACS GRB candidates (solid red line) and for 1234 GRBs from the 4th BATSE GRB catalogue (Paciesas et al. 1999; dashed line) scaled to 21.6 months of continuous observation. Note the difference in the distributions of the short events.

instruments.

The total number of detected events in SPI-ACS is of the order of 50% of the BATSE detections, when scaled to a common time interval. On the other hand, BATSE and SPI-ACS are sensitive to different energy bands. The SPI-ACS lower energy threshold of ~ 80 keV reduces the detection capability for bursts with peak energies below that energy. This affects mainly X-ray flashes (E_p<30 keV) and X-ray rich bursts (E_p∼70 keV). For comparison, BATSE could detect events down to E_p<25 keV and was therefore capable of detecting a significant fraction of the X-ray rich burst population.

Fig. 2.3 indicates a slight shift of the long-duration distribution components in SPI-ACS towards lower values of T_{90} compared to the BATSE sample. Again, this could be a result of the lower sensitivity at softer energies for the long (and generally spectrally soft) distribution. In addition, it is typical to find a hard-to-soft evolution during the prompt emission phase. This also leads to shorter durations at higher energies. Finally, measurements of burst properties are instrument dependent, primarily due to siginal-to-noise limitations and temporal binning. This is likely an additional reason for the difference in the observed duration distributions.

The SPI-ACS short-duration population can be fit by a Gaussian with a maximum at the time resolution of 50 ms. This shift with respect to the BATSE result is not of instrumental origin, as the SPI-ACS detectors are very sensitive at the typical peak energies of short GRBs. Also, a significant hard-to-soft evolution is not expected to occur and cause this

offset. The deviations seem to be mainly for events with $T_{90}<0.25$ s. The general lack of spatial information in the data makes it difficult to determine the origin of these events. In Fig. 2.4 we show the duration distribution for the sample of confirmed GRBs. While ∼70% of the long-duration bursts are confirmed, less than 11% (8%) of the GRB candidates with $T_{90}<2$ s (<0.25 s) were detected by other gamma-ray instruments.

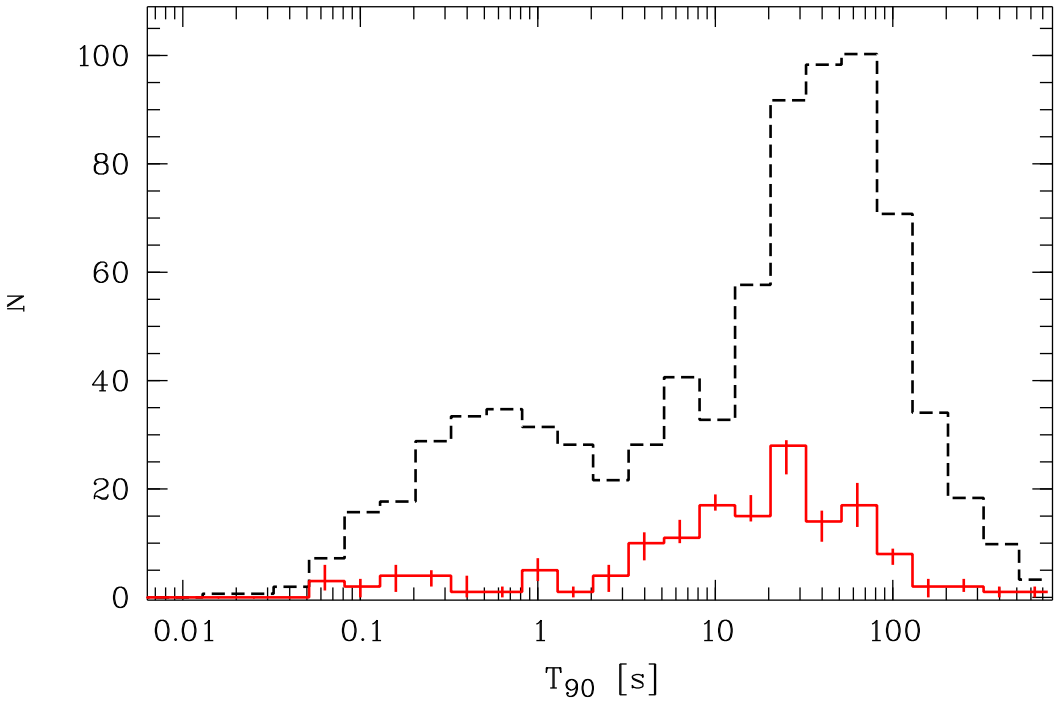

Figure 2.4. Same as Fig. 2.3 except that only the confirmed bursts from the SPI-ACS sample are shown. A comparison with Fig. 2.3 reveals that for most of the long-duration bursts a cosmic origin was confirmed while this is true only for a small fraction of the short events.

Note that we found no evidence of the proposed third (intermediate duration) burst population whose signature was detected in the BATSE sample (Horvath 1998). This population was claimed to to have a softer spectrum than the long-duration GRB sample. Due to the variety of trigger timescales used by SPI-ACS and the lack of spectral information, it is not clear how the temporal sensitivity depends on the spectral hardness and peak flux in the trigger. Thus, it apears difficult to ascertain whether SPI-ACS is indeed insensitive to the intermediate GRBs or whether some intermediate GRBs are included in the sample but for some reason not clearly distinguished from other bursts.

2.5.2 The origin of events with $T_{90}<0.25$ s

There are various possible explanations for the significant excess of unconfirmed 0.05–0.25 s long events in the SPI-ACS sample (an example is shown in Fig. 2.2e). We list them below, and present arguments for and against each of them.

(i) SPI-ACS is observing a real population of short, spectrally very hard GRBs, most of which must have been undetected by BATSE. However, the trigger efficiency of BATSE was quite sensitive to hard photons (Pendleton et al. 1998) and these short hard events would certainly have been seen. Another argument against the idea of observing a real burst population is that several gamma-ray instruments in orbit have the capability to detect such hard events, as demonstrated by the *Mars Odyssey*, Konus/*Wind* and Helicon/*Coronas-F* detection of an event from December 14 2003 (Fig. 2.2c); the number of such confirmations, however, is too low to explain the excess of very short events in this way.

(ii) A small contribution to the short burst population might come from outbursts of Soft Gamma Repeaters. These objects are strongly magnetized neutron stars, ("magnetars" – Duncan & Thompson 1992), which are characterized by brief (typical $\sim$100 ms), very intense (up to 10^{44-45} erg) bursts of hard X-rays and soft gamma-rays. Their light curves resemble those of the short GRBs. Thus, events in the SPI-ACS count rate originating from known SGRs are not easily distinguishable from short GRBs without the localization by triangulation with other instruments. However, the vast majority of these bursts have soft spectra and most of them are not detected by the SPI-ACS.

(iii) The evaporation of primordial black holes through Hawking radiation can lead to a sudden burst of gamma-rays with durations $\sim$100 ms (Halzen et al. 1991). This has been proposed for the BATSE sample of very short bursts by Cline et al. (2003). Our sample of events with $T_{90}<100$ ms is consistent with isotropy in an Euclidean geometry, $<V/V_{max}>\sim0.48$. Recent re-analysis of the BATSE data found a value in agreement with SPI-ACS of $<V/V_{max}>$ = 0.52 ± 0.05 (Cline D., private communication).

(iv) A significant contribution to the short candidates could arise from instrumental effects and/or cosmic ray events. Analyzing the data of very short events together with simultaneous data from the spectrometer SPI revealed that a significant fraction of them are accompanied by the simultaneous saturation of one or several Ge-detectors. An example for an event on Dec. 1, 2003 is shown in Fig. 2.5. At the time of the significant rate increase in SPI-ACS over $\sim$50 ms two neighboring Ge-detectors, #9 and #10, went into a saturation which lasted for $\sim$4 and $\sim$20 s, respectively. The analysis of SPI data from a subset of satellite revolutions shows that a saturation event occurs approximately every four hours and that nearly all of these events have a simultaneous rate increase in SPI-ACS. The opposite approach, an independent search for short events in the SPI-ACS overall count rate, revealed $\sim$15 events per hour at a 4.5σ level. Combining these results shows that approximately every 60th very short SPI-ACS event coincides with a saturation in the Ge detectors.

The saturation of the Ge detectors can be explained by the deposit of a large amount of energy in the crystals. For example, a very energetic cosmic ray particle can traverse a BGO crystal and deposit part of its energy, thus producing the short count rate increase. Depending on the flight direction, the particle can go on to traverse one or several Ge detectors and cause the saturation, or pass through the BGO shield a second time, or not interact with any of the detectors again. The probability of a particle hitting the SPI-ACS and Ge detectors can be estimated from the geometry of the instrument to be $\sim$1/40 of the probability to pass only through the anti-coincidence shield. This is in rough agreement with the rate of SPI-ACS short events that coincide with saturations. Therefore, this simple hypothesis suggests that a

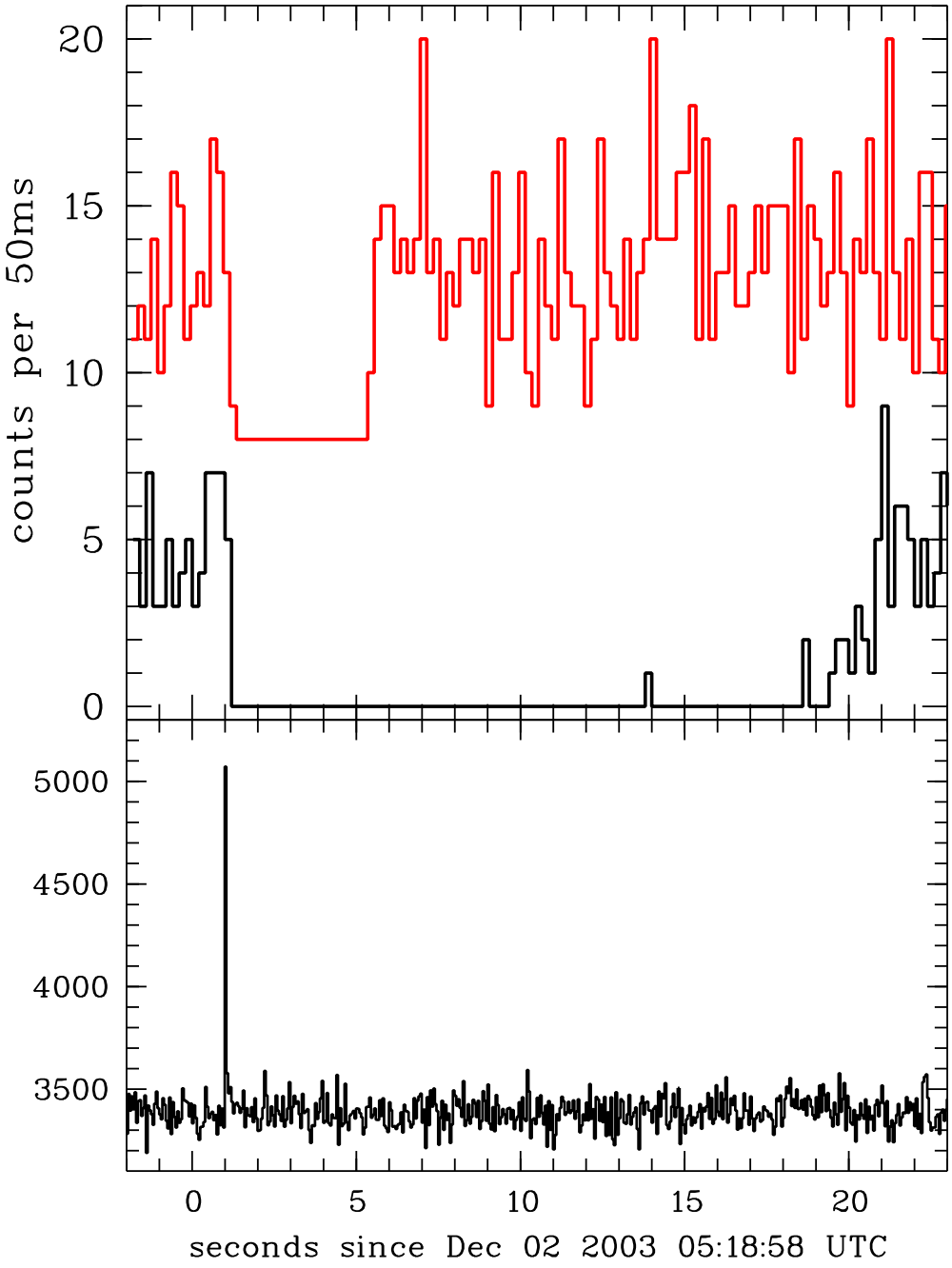

Figure 2.5. Example of a very short event in SPI-ACS (bottom panel) with simultaneous saturation of two SPI Ge detectors (top panel). The SPI-ACS light curve is shown with 50 ms binning and the SPI light curves of detector #9 (red curve) and #10 (black curve) are binned with 200 ms time resolution.

significant fraction of the unconfirmed short burst candidates can originate from cosmic ray particles hitting the instrument.
Most of the saturation events occur in a single Ge-detector. Hits in several detectors are significantly less frequent (Fig. 2.6) but happen either in neighboring detectors or along a line of detectors. If the saturation is caused by a single particle then a particle passing through the coded mask will only deposit energy in one detector as the cross-section for hitting more than one Ge-detector is low. A particle hitting the detector plane from the side can deposit energy (and cause saturation) in several detectors. This is in agreement with the observation that saturation events in more than one detector are always accompanied by a significant rate increase in the SPI-ACS, while a small fraction of the saturation events in single detectors show no corresponding signal in the SPI-ACS overall rate.

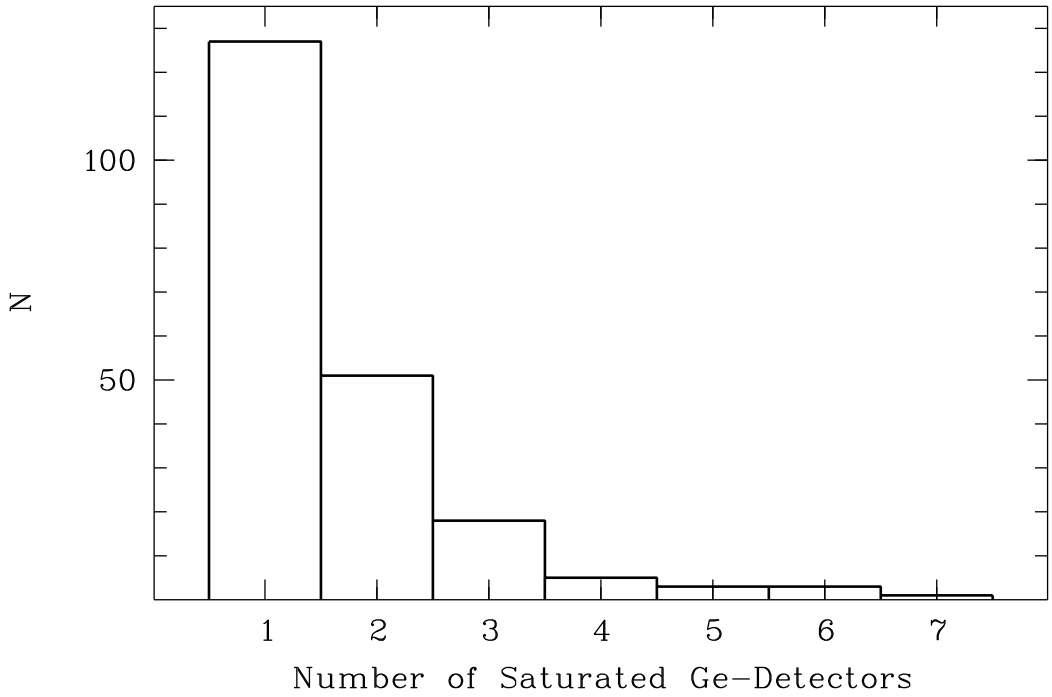

Figure 2.6. Distribution of saturated Ge detectors of SPI for a duration of 15 days (INTEGRAL mission revolutions 137-141). Most saturations occur in a single detector only.

In the case of a particle shower, the number of detectors being hit depends on the width of the distribution of the secondary particles and on the inclination angle. In IBIS/PICsIT strong bursts (2500 counts) up to 170 ms long of particle-induced showers are observed (Segreto 2002). These showers may be produced by cosmic ray hits on the satellite or detector structure. As a consequence of the interaction of the primary particle with matter, high-energy photons and electron-positron pairs are created. These in turn produce a cascade of secondary electrons and photons via bremsstrahlung and pair production. The time profiles of the events observed in PICsIT are rather complex and both straight tracks and closed areas are visible (Segreto 2002). These observations are similar to the detections in SPI and thus support the idea of cosmic rays as a partial origin of the very short SPI-ACS events.

The observed rate increase in SPI-ACS can be produced by the deceleration of a cosmic ray particle in the BGO crystal. This induces a long-lasting (50-150 ms) phosphorescent afterglow energetic enough to cause recurrent triggers in the electronics. BGO was originally selected for SPI-ACS because of its short decay times and very low phosphorescence compared to e.g. CsI(Na) and NaI(Tl). BGO has decay times of 60 ns and 300 ns where the second is by far the more probable (90% vs. 10% for the 60 ns) and an afterglow of 0.005% is expected at 3 ms (Farukhi 1982).
In order to produce a single count in the SPI-ACS rate, a minimum of 80 keV has to be accumulated during an integration time of 600 ns. With a total light yield for BGO of 8000-10000 photons/MeV, this corresponds to $\sim$675 photons. Assuming an exponential decay, the radiation will decrease to 0.005% at 3 μs. Thus the decay is so fast that only a small number of counts ($\sim$3) will be produced. From the afterglow properties the minimum original excitation energy can be estimated. For instance, to have 1000 recurrent triggers (a count rate increase of 1000) in a single crystal, the afterglow must be bright enough to be above the 80 keV threshold for $\sim$3 ms (integration time + dead time). Thus, the 0.005 % afterglow emission at 3 ms corresponds to a $\sim$1.6 GeV initial excitation using the light yield given above. Therefore, particles which deposit $\sim$1.6 GeV or more in a crystal can indeed be the origin of the short event population in the SPI-ACS. Short events showing similar temporal behavior have been discussed for CsI(Na) and CsI(T1) crystals exposed to primary cosmic radiation (Hurley 1978). The same conclusion was reached for the origin, namely cosmic ray nuclei in the iron group. Note that CsI has a significantly more intense afterglow (0.1–1 % at 6 ms).
We performed simulations of particle attenuation in the detectors using *SRIM*[7]. The results showed that heavy cosmic ray nuclei (e.g., Fe) with energies of several GeV per ion can easily produce the observed effects in the SPI-ACS and SPI.

2.5.3 Intensity

The distribution of burst intensities can provide valuable information on the radial distribution of the sources. The integral brightness distribution is expected to follow a power law with a slope of -3/2 for a homogeneous distribution of sources assuming a Euclidean geometry. The lack of spectral resolution limits the analysis for the SPI-ACS sample to detector count units. Fig. 2.7 shows the integral log$N$–logC_{max} distributions for peak counts C_{max} of three sub-samples measured over a timescale of 0.25 s. The solid, dashed and dotted distributions represent the long duration sample ($>$2.5 s), the short bursts (0.25 s$\leq T_{90}<$2.5 s) and the population of very short events ($<$0.25 s), respectively. The deviation from a –3/2 power law (solid line) is visible for each of the sub-samples. Both the long duration and the short duration bursts follow a $\sim$-1.1 slope. The population of very short burst behaves very differently, with a significantly steeper distribution (slope$\sim$-2.3). The turnover at low values of C_{max} corresponds to the selection threshold of the sample.
A deviation from a homogeneous distribution was also found by BATSE (Fishman et al. 1994). Nevertheless, the substitution of peak counts for peak fluxes causes an unknown

[7] http://www.srim.org/

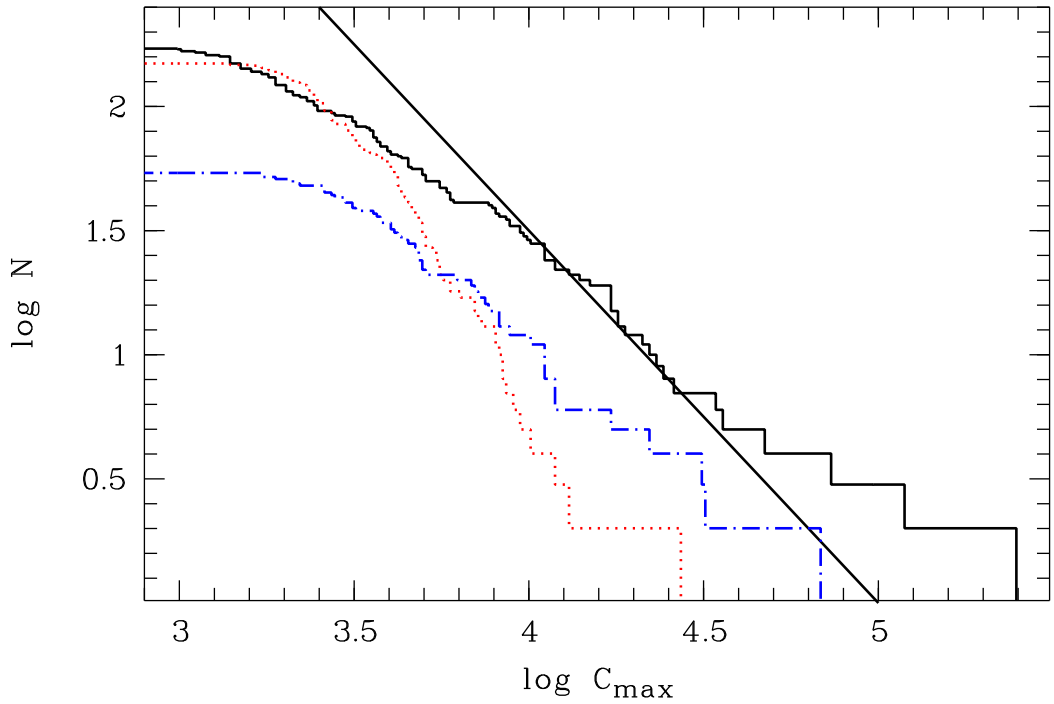

Figure 2.7. log$N$–logC_{max} distribution for three sub-samples, together with the expected power law slope of -3/2 for a homogeneous distribution (solid line). The long duration (T_{90}>2.5 s, solid line) and short duration (0.25 s<T_{90}<2.5 s, blue dash-dotted line) samples follow a similar power law with a slope of ∼-1.1. The very short events (T_{90}<0.25 s, red dotted) have a significantly steeper distribution.

uncertainty in the SPI-ACS results. While in a first-order approach each incoming photon produces one detector count, the uncertain effective area (depending on the incident angle) prevents a direct comparison. Thus, C_{max} depends on the spectral shape of the individual events. Still, a qualitative statement on the behavior of the three sub-samples can be made. Both short- and long duration bursts follow the same slope while the distribution of the very short events differs strongly. This is consistent with the hypothesis that the very short events are not of cosmological origin.
Fig. 2.8 shows the corresponding log$N$–logC_{int} distribution. Here, the integrated detector counts were used as a measure of the fluences. A behavior similar to the sub-samples in the log$N$-logC_{max} distribution is found. The long- and short duration populations evolve similarly while the sample of very short events displays a significantly steeper distribution.

2.5.4 V/V_{max}

Another test for homogeneity is the V/V_{max} test (Schmidt 1968). If the burst population is drawn from a uniform distribution in Euclidean space, the mean value of V/V_{max} will be 0.5. For the individual sub-samples of long, short and very short events we find $<V/V_{max}>$ values of 0.26, 0.31 and 0.48, respectively. As already seen in the intensity distributions, the short and long burst populations behave similarly and show evidence for inhomogeneity.

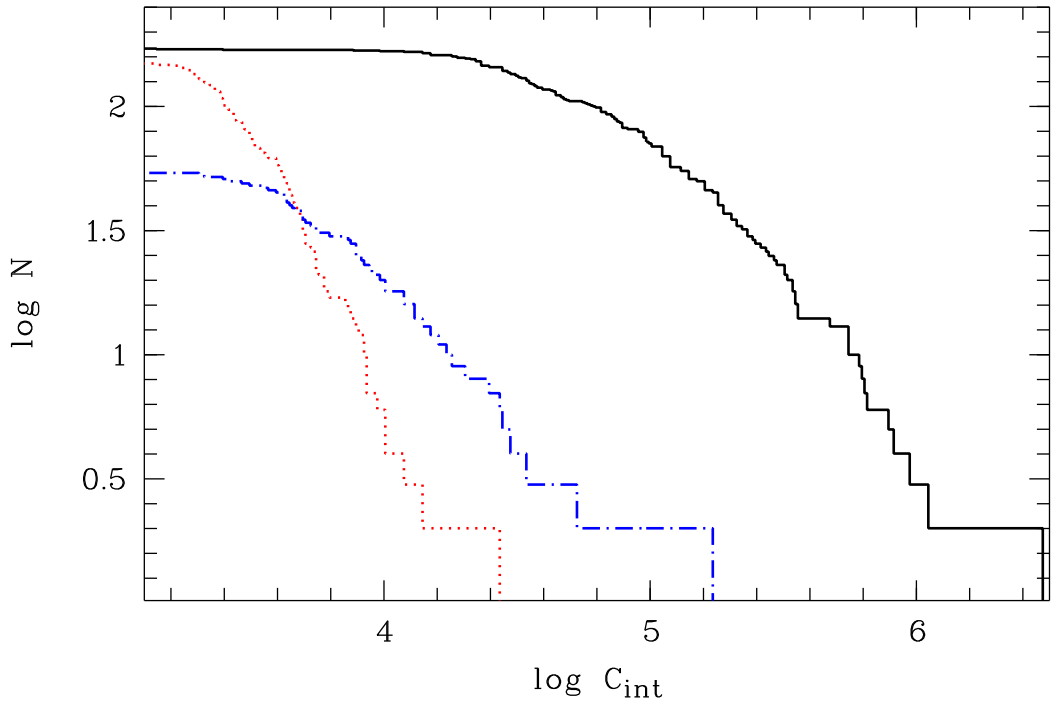

Figure 2.8. Same as Fig. 2.7 for log$N$–logC_{int}.

This is consistent with the BATSE result, namely $<V/V_{max}>\sim$0.34 (Fishman et al. 1994). In contrast, $<V/V_{max}>$ for the very short events is consistent with a homogeneous distribution. Again, this points to a different origin for them compared to the short- and long duration bursts.

2.5.5 Variability

In Fig. 2.9 we show the distribution of the time profile variability of 143 candidate bursts using the measure $V_{f=0.45}$ presented by Reichart et al. (2001). The number of bursts decreases linearly with increasing variability following N=(-74±3)×$V_{f=0.45}$+(33±0.8) for our binning of $\Delta V_{f=0.45}$=0.06. The empirically found correlation between $V_{f=0.45}$ and the isotropic peak luminosity, L_{iso} by Reichart et al. suggests that the majority of the events in the sample are intrinsically faint and only a few bursts have $L_{iso}>10^{53}$ erg.

2.6 Conclusion

The anti-coincidence shield of the INTEGRAL spectrometer SPI is operating successfully as an omnidirectional gamma-ray burst detector above ∼80 keV. The 1st catalogue includes 388 candidate GRBs detected during the first 26.5 months of mission operation. For 179 triggers a cosmic origin could be confirmed by observations with other gamma-ray instruments in space. The sample shows the known duration bimodality with a strong excess at the very

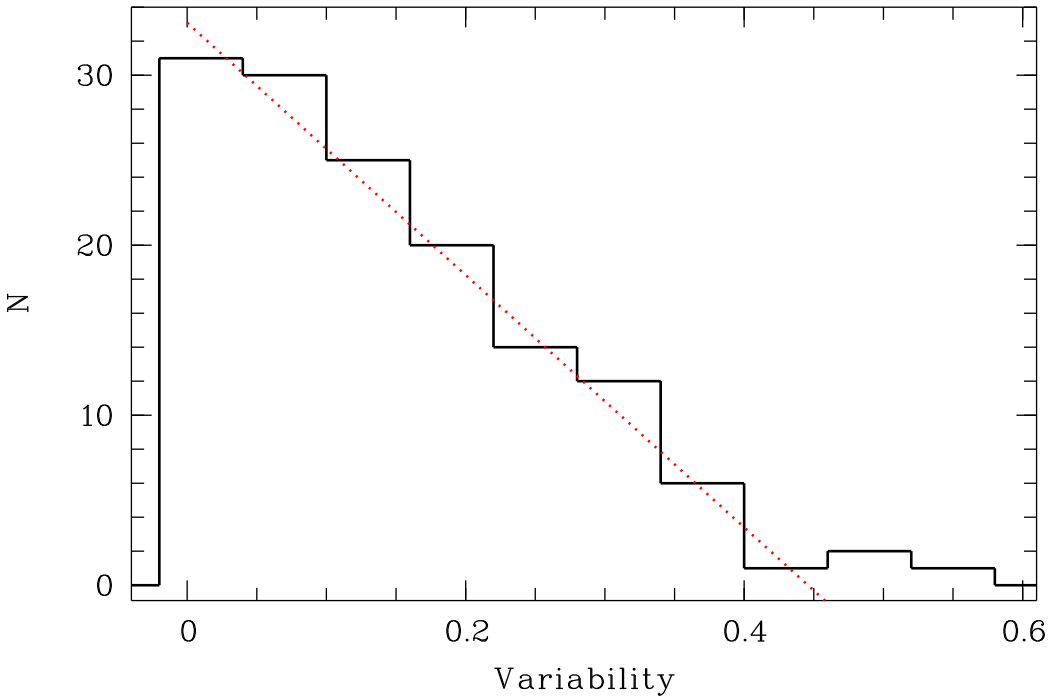

Figure 2.9. Distribution of the variability measure for 143 candidate bursts from the sample (solid line) together with best linear fit (red dotted).

short end of the distribution (<0.25 s). The origin of this population of events (∼40% of the total number) was demonstrated to be significantly different from the normal GRB sample, as shown both by the log$N$–logC_{max} distribution as well as by the V/V_{max} test. Observations of simultaneous saturations in the spectrometer Ge detectors and very short events in the SPI-ACS overall rate suggest a cosmic ray origin for a significant fraction of these events.
The short- and long duration sample includes 236 GRBs, which corresponds to a detection rate of ∼130 GRBs per year of continuous observation (∼1 every three days). The intensity distribution of this sample is consistent with the BATSE results and shows a deviation from a homogenous distribution in Euclidean space.

Acknowledgments: We are grateful for the support from the ISDC shift team, especially to J. Borkowski and M. Beck. We thank the referee, J. Hakkila, for his insightful comments. The SPI-ACS is supported by the German “Ministerium für Bildung and Forschung” through the DLR grant 50.OG.9503.0. KH is grateful for support under the INTEGRAL U.S. Guest Investigator program, NASA grants NAG5-12614 and NNG04GM50G. We are also grateful to V. Pal’shin for assistance in calibrating the ACS timing.

2.7 Appendix A - catalogue table

Table 2.2. SPI-ACS GRB sample. Number of event in catalogue, date, UTC, maximum significance of the event above the background, T_{90}, integrated counts in the event, 0.25 s peak counts, variability and V/V_{max} are given together with the confirmations by other gamma-ray instruments ('U": *Ulysses*, "K": Konus/*Wind*, "M": *Mars-Observer*, "H": *HETE-2*, "R": for *RHESSI*, "C": Helicon/*Coronas-F*, "I": *INTEGRAL* (SPI/IBIS), "S": *Swift* and "X": *RXTE*/ASM. [(1)]: overlapping bursts, thus only limits on integrated counts can be given.

#	Date	UTC	σ	T_{90} [s]	C_{int} [kcnts]	C_{max} [kcnts/0.25 s]	V/V_{max}	$V_{f=0.45}$	Conf.
1	021027	08:33:51	5						UMK
2	021102	15:58:44	30	7.7±0.4	39±2	3.7±0.2	0.25	0.22±0.01	UKR
3	021113	13:37:33	4						UKR
4	021114	21:28:54	17	0.1±0.05	2.7±0.2	2.7±0.2	0.57		
5	021115	00:44:32	14	0.05±0.1	1.7±0.2	1.7±0.2	0.74		
6	021116	08:06:29	35	15±0.8	63±4	2.5±0.2	0.20	0.15±0.01	
7	021117	23:42:18	34	0.25±0.05	7.9±0.4	6.8±0.2	0.21		
8	021121	19:37:20	14	0.05±0.1	2.3±0.2	2.3±0.2	0.74		
9	021125	05:59:14	34	20±2	66±6	3.5±0.2	0.21	0.31±0.01	UK
10	021125	17:58:23	34	19±2	68±5	1.4±0.2	0.21	0.05±0.02	UMKRI
11	021205	03:16:38	41	88±6	190±20	2±0.2	0.15	0.22±0.01	
12	021206	22:49:08	2762	5.7±1	3000±40	250±0.5	0.00	0.18±0.01	UKH
13	021214	19:29:19	38	0.1±0.05	5.9±0.3	5.7±0.2	0.18		
14	021219	07:33:57	4						UKI
15	021222	07:18:51	22	0.05±0.05	3.4±0.2	3.4±0.2	0.40		
16	021223	01:09:55	38	5.2±0.3	39±2	3.1±0.2	0.18	0.12±0.01	
17	021226	14:53:39	60	3.1±0.6	18±1	12±0.2	0.09		MKR
18	030101	20:43:32	42	0.65±0.05	16±0.7	8.2±0.2	0.15	0.01±0.01	UKH
19	030102	15:47:43	25	7.3±0.4	32±2	3±0.2	0.32	0.18±0.01	
20	030102	23:18:59	36	12±0.8	46±3	4.6±0.2	0.19	0.23±0.01	UKR
21	030105	14:34:06	72	0.9±0.05	30±0.9	12±0.2	0.07	0.07±0.01	MKR
22	030107	08:59:41	28	0.15±0.05	5.6±0.3	5.4±0.2	0.27		
23	030109	09:37:37	28	0.7±0.5	5.3±0.5	4.8±0.2	0.27		U
24	030110	09:39:28	18	0.05±0.1	2.6±0.2	2.7±0.2	0.52		K
25	030115	06:24:29	50	66±6	190±10	2.5±0.2	0.12	0.31±0.01	UMKHR
26	030115	08:15:39	15	34±4	37±5	0.98±0.2	0.69		UMKR
27	030116	04:38:36	13	0.2±0.3	2.1±0.2	2.1±0.2	0.85		
28	030117	17:36:14	52	0.05±0.05	8.4±0.2	8.4±0.2	0.11		K
29	030118	03:45:37	31	0.1±0.05	4.4±0.3	4.2±0.2	0.23		
30	030119	08:15:57	14	4.4±0.7	14±2	2±0.2	0.72	0.15±0.01	K
31	030119	10:15:58	15	0.05±0.1	1.7±0.1	1.7±0.2	0.67		
32	030119	16:16:11	39	0.15±0.2	5.9±0.2	5.9±0.2	0.17		
33	030123	20:03:32	12	0.05±0.05	1.9±0.2	1.9±0.2	0.89		
34	030127	12:32:32	95	40±2	210±10	5.5±0.2	0.04	0.08±0.01	UKH
35	030129	11:16:08	35	0.05±0.05	4.9±0.2	4.9±0.2	0.19		
36	030131	07:39:10	4						UK
37	030131	13:55:30	13	0.15±0.2	1.8±0.2	1.8±0.2	0.80		
38	030131	14:42:50	28	0.05±0.05	3.9±0.2	3.9±0.2	0.28		
39	030202	17:21:00	13	62±4	30±7	1.3±0.2	0.83	0.14±0.03	UK
40	030202	22:36:30	15	3±0.05	1.4±0.8	1.7±0.2	0.69		
41	030203	14:00:12	12	0.05±0.05	1.7±0.2	1.7±0.2	0.91		
42	030204	12:45:29	54	15±2	96±5	3.6±0.2	0.10	0.16±0.01	UMKHR
43	030212	08:48:50	59	0.1±0.05	7.3±0.3	7.1±0.2	0.09		
44	030214	14:48:20	12	3±0.5	9.7±1	2±0.2	0.89	0.20±0.01	UR
45	030215	09:48:00	29	0.1±0.2	4.4±0.2	4.4±0.2	0.26		
46	030215	11:13:31	223	34±3	610±20	8.6±0.2	0.01	0.06±0.01	UH
47	030216	16:13:44	15	2.8±0.1	12±1	1.8±0.2	0.66	0.07±0.04	UR
48	030217	02:45:37	207	50±2	360±20	13±0.2	0.01	0.04±0.01	UMHR
49	030217	04:25:41	32	42±4	95±9	1.4±0.2	0.22	0.01±0.01	
50	030217	23:31:42	55	0.15±0.05	12±0.3	12±0.2	0.10		M
51	030218	11:42:37	127	67±1	350±10	12±0.2	0.03	0.31±0.01	U
52	030220	16:12:42	52	53±3	180±10	3.9±0.2	0.11	0.26±0.01	UH

Num	Date	UTC	σ	T_{90} [s]	C_{int} [kcnts]	C_{max} [kcnts/0.25 s]	V/V_{max}	$V_{f=0.45}$	Conf.
53	030222	08:22:23	25	0.15±0.05	4.1±0.3	3.9±0.2	0.32		
54	030222	13:18:49	21	0.15±0.2	3.1±0.2	3.1±0.2	0.42		
55	030222	16:32:47	14	5.3±0.2	15±2	2.4±0.2	0.77	0.32±0.03	MKR
56	030222	19:12:26	17	0.25±0.3	2.6±0.3	2.6±0.2	0.56		
57	030222	22:35:46	16	0.25±0.05	2±0.3	1.7±0.2	0.63		
58	030223	03:53:35	28	0.05±0.05	4.1±0.3	4.1±0.2	0.27		
59	030223	09:45:08	62	15±2	110±7	4±0.2	0.08	0.04±0.01	UK
60	030224	04:16:34	19	0.05±0.1	2±0.1	2±0.2	0.49		
61	030224	07:49:49	7						U
62	030224	11:48:58	46	20±2	95±7	2.1±0.2	0.13		
63	030225	15:02:47	40	45±6	110±10	2.1±0.2	0.16	0.05±0.01	UMKR
64	030226	07:10:10	21	70±4	82±10	1±0.2	0.41	0.08±0.04	M
65	030227	13:11:56	15	10±0.7	23±3	1±0.2	0.67		UK
66	030228	20:26:46	23	26±2	48±5	4.5±0.2	0.37	0.52±0.01	UMKR
67	030302	03:48:03	82	0.1±0.05	10±0.4	10±0.2	0.06		
68	030304	16:15:59	17	0.1±0.2	2.2±0.2	2.2±0.2	0.59		
69	030305	07:50:15	13	0.05±0.05	2±0.2	2.1±0.2	0.86		
70	030307	14:31:57	146	2.7±0.5	100±3	18±0.3	0.02	0.01±0.01	UKHR
71	030308	05:18:24	31	6.5±0.5	36±3	3.5±0.2	0.24	0.13±0.01	UK
72	030310	12:28:01	23	4.1±4	2.5±1	3.2±0.2	0.36		
73	030318	02:46:30	6						K
74	030319	14:03:29	55	0.05±0.05	8.6±0.3	8.6±0.2	0.10		
75	030319	23:33:22	189	0.3±0.1	34±0.7	31±0.3	0.02		
76	030320	10:12:09	278	500±30	560±20	17±0.3	0.01	0.03±0.01	UMKRI
77	030321	15:24:47	20	0.15±0.05	3.1±0.3	3±0.2	0.45		
78	030325	14:15:11	53	1.9±0.3	28±1	8.9±0.2	0.11	0.03±0.01	UMK
79	030325	18:14:13	26	0.1±0.2	3.3±0.2	3.3±0.2	0.30		
80	030326	10:43:42	60	5±0.6	57±3	5.8±0.2	0.09	0.02±0.01	MKR
81	030327	22:37:08	19	46±3	60±7	1.3±0.2	0.49		UM
82	030328	07:27:00	30	110±4	120±10	1.4±0.2	0.25	0.01±0.01	UK
83	030328	16:25:12	28	0.05±0.1	3±0.2	3±0.2	0.27		
84	030329	11:37:25	422	18±2	820±20	36±0.3	0.00	0.10±0.01	H
85	030330	12:40:46	32	0.15±0.2	4.5±0.2	4.5±0.2	0.22		
86	030331	04:05:02	14	0.25±0.05	2.5±0.3	2.2±0.2	0.76		
87	030331	05:38:16	97	33±20	140±8	7.7±0.2	0.04	0.24±0.01	UKR
88	030331	16:28:11	19	0.05±0.05	2.2±0.2	2.3±0.2	0.49		
89	030403	03:37:44	22	5.4±0.5	23±2	2.1±0.2	0.40	0.00±0.01	UKH
90	030403	21:42:13	17	0.15±0.2	2.1±0.2	2.1±0.2	0.55		
91	030405	02:17:27	39	3.9±0.7	34±2	8.1±0.2	0.17	0.20±0.01	UMKH
92	030406	22:42:03	157	63±3	320±20	19±0.3	0.02	0.27±0.01	UMKR
93	030409	13:02:28	19	0.1±0.05	3.2±0.3	3.1±0.2	0.49		
94	030410	00:00:36	14	0.1±0.2	2±0.2	2±0.2	0.75		
95	030410	06:40:28	27	0.15±0.2	4.2±0.2	4.2±0.2	0.29		
96	030410	11:22:12	50	1.5±0.1	17±0.9	10±0.2	0.12	0.05±0.01	KR
97	030413	07:34:35	69	20±1	120±7	5±0.2	0.07	0.32±0.01	UMKHR
98	030414	08:54:32	14	0.05±0.1	1.4±0.1	1.4±0.2	0.78		
99	030414	13:48:24	165	12±2	220±9	11±0.2	0.02	0.03±0.01	UMKR
100	030416	06:05:42	19	0.05±0.05	2.5±0.2	2.5±0.2	0.50		
101	030417	20:04:48	15	0.05±0.1	1.9±0.1	1.9±0.2	0.68		
102	030419	01:12:06	109	38±1	230±10	15±0.2	0.04	0.55±0.01	UKR
103	030419	08:24:03	15	0.15±0.2	2.4±0.2	2.4±0.2	0.67		
104	030421	00:36:32	148	150±4	290±30	14±0.2	0.02	0.22±0.01	UKR
105	030422	07:51:12	24	6.8±1	29±2	2.3±0.2	0.34	0.05±0.02	UMK
106	030422	09:01:22	27	16±2	44±4	2.3±0.2	0.29	0.18±0.01	UMKR
107	030424	20:11:11	32	0.1±0.2	3.6±0.2	3.6±0.2	0.23		
108	030425	11:04:31	14	0.15±0.05	2.3±0.3	2.3±0.2	0.79		
109	030426	08:05:30	88	86±3	240±20	5.1±0.2	0.05	0.12±0.01	
110	030426	23:30:00	45	51±0.5	65±8	3.6±0.2	0.13	0.14±0.01	UMKR
111	030430	08:02:20	27	0.05±0.1	3.3±0.2	3.3±0.2	0.28		
112	030501	01:17:17	27	6.5±0.7	30±2	4.3±0.2	0.29	0.19±0.01	UKR
113	030505	07:38:58	28	37±2	77±8	1.8±0.2	0.27	0.21±0.01	UK
114	030505	09:03:22	27	160±5	160±20	1.4±0.2	0.28		UKR
115	030506	02:04:07	54	23±2	120±7	2.5±0.2	0.10	0.08±0.01	UKHR
116	030507	03:00:57	12	0.15±0.2	1.9±0.2	1.9±0.2	0.92		
117	030509	05:50:23	90	5.5±0.2	69±3	17±0.2	0.05	0.17±0.01	UMK
118	030509	18:15:32	55	0.25±0.05	13±0.5	11±0.2	0.10		

Num	Date	UTC	σ	T_{90} [s]	C_{int} [kcnts]	C_{max} [kcnts/0.25 s]	V/V_{max}	$V_{f=0.45}$	Conf.
119	030510	10:53:41	18	9.4±1	23±3	1.4±0.2	0.50		K
120	030512	09:37:23	40	0.1±0.2	4.4±0.2	4.4±0.2	0.16		
121	030513	10:17:06	20	21±3	34±4	3.2±0.2	0.45	0.33±0.02	U
122	030514	18:22:21	35	28±4	78±9	2.1±0.2	0.20		UMK
123	030518	01:23:45	228	20±1	470±10	11±0.2	0.01	0.17±0.01	UKHR
124	030518	03:12:16	36	19±1	74±5	2.5±0.2	0.19	0.12±0.01	UK
125	030518	21:28:36	16	4.2±0.8	15±1	1.9±0.2	0.61		UK
126	030519	09:32:20	22	3.2±0.3	18±2	3.2±0.2	0.38	0.15±0.01	UKH
127	030522	02:33:47	45	0.1±0.05	5.6±0.3	5.5±0.2	0.13		
128	030522	06:12:28	9						K
129	030523	14:10:52	13	0.05±0.05	2.2±0.2	2.2±0.2	0.81		
130	030523	15:31:02	125	25±2	280±10	9.4±0.2	0.03	0.22±0.01	UMK
131	030524	04:56:05	17	0.1±0.05	2.7±0.3	2.7±0.2	0.57		
132	030524	17:13:30	13	0.15±0.2	1.8±0.2	1.8±0.2	0.80		
133	030524	18:29:30	22	0.05±0.1	3±0.2	3±0.2	0.40		
134	030526	08:59:20	23	0.05±0.1	3.1±0.2	3.1±0.2	0.36		
135	030601	21:31:34	41	130±2	200±20	1.9±0.2	0.16	0.34±0.01	
136	030601	22:11:59	53	18±0.7	97±6	3.7±0.2	0.11	0.17±0.01	UKR
137	030604	12:44:10	12	0.05±0.05	1.8±0.2	1.8±0.2	0.90		
138	030605	02:19:32	74	76±9	180±10	5.5±0.2	0.06	0.16±0.01	UK
139	030605	21:06:24	22	14±1	23±3	4.5±0.2	0.39	0.32±0.01	UK
140	030606	23:47:45	15	16±2	22±3	1.7±0.2	0.66	0.18±0.03	UMK
141	030607	02:19:21	12	0.1±0.05	2±0.2	2±0.2	0.99		K
142	030607	07:07:23	15	0.1±0.05	2.4±0.3	2.4±0.2	0.70		
143	030608	04:30:15	23	0.1±0.05	3.7±0.2	3.7±0.2	0.37		
144	030609	23:27:43	65	28±3	160±10	2.3±0.2	0.08		
145	030610	08:35:42	46	22±2	75±5	3.7±0.2	0.13	0.03±0.01	
146	030614	01:28:40	58	170±20	320±30	2.2±0.2	0.09	0.26±0.01	UKR
147	030614	10:54:54	15	0.05±0.1	2.1±0.1	2.1±0.2	0.68		
148	030615	00:38:54	19	0.15±0.2	3±0.2	3±0.2	0.49		
149	030619	12:29:20	29	0.05±0.1	3.9±0.2	3.9±0.2	0.26		
150	030623	01:55:20	13	69±2	32±6	1.2±0.2	0.85	0.15±0.05	
151	030626	01:46:41	112	37±3	300±10	5.1±0.2	0.03	0.08±0.01	UMKR
152	030629	03:26:39	43	0.15±0.05	9.5±0.4	9±0.2	0.15		KC
153	030705	15:45:00	84	0.15±0.05	10±0.4	9.5±0.2	0.05		
154	030706	00:01:57	41	8.9±0.5	44±3	4.9±0.2	0.16	0.23±0.01	KR
155	030710	23:05:00	20	14±4	31±3	1.5±0.2	0.45	0.02±0.01	UKR
156	030711	00:04:01	91	0.25±0.05	20±0.4	17±0.2	0.05		M
157	030713	10:08:37	13	0.1±0.2	1.9±0.2	1.9±0.2	0.88		
158	030714	22:14:45	25	5.2±0.8	22±2	4.5±0.2	0.33	0.14±0.01	UMKR
159	030715	04:25:51	30	7.4±0.7	37±3	2.7±0.2	0.24	0.04±0.01	UMK
160	030716	11:57:15	19	25±4	44±5	1.8±0.2	0.47	0.13±0.02	UKR
161	030716	17:51:46	17	0.05±0.05	2.3±0.2	2.3±0.2	0.58		
162	030717	20:49:24	44	0.05±0.05	5±0.3	5±0.2	0.14		U
163	030721	23:41:07	197	25±1	340±10	23±0.3	0.01	0.27±0.01	
164	030722	13:31:41	372	15±0.4	640±10	34±0.3	0.01	0.16±0.01	UK
165	030722	21:55:17	17	0.15±0.2	2.4±0.2	2.4±0.2	0.55		
166	030723	09:40:00	27	0.2±0.05	4.6±0.3	4.2±0.2	0.29		
167	030725	11:46:24	51	19±3	90±6	2.8±0.2	0.11		UMKHR
168	030726	01:50:05	24	0.05±0.05	3.7±0.2	3.7±0.2	0.34		
169	030726	06:38:24	253	29±3	620±20	10±0.2	0.01	0.11±0.01	UMKHR
170	030726	12:55:50	12	2±0.2	7.3±1	1.7±0.2	0.89	0.10±0.08	
171	030728	21:07:20	32	0.25±0.2	4.2±0.3	4±0.2	0.23		
172	030729	03:58:00	18	0.05±0.1	2.7±0.3	2.7±0.2	0.52		
173	030731	05:14:31	101	32±4	250±10	3.8±0.2	0.04	0.02±0.01	
174	030731	18:34:46	53	0.9±0.05	10±0.7	7.7±0.2	0.11		
175	030801	16:51:49	119	23±5	210±10	8.1±0.2	0.03	0.03±0.01	UMK
176	030803	03:54:26	16	0.1±0.2	2.3±0.2	2.3±0.2	0.63		
177	030803	15:44:54	17	8.7±2	21±3	1.6±0.2	0.57		KH
178	030804	05:31:09	40	0.05±0.1	4.6±0.2	4.6±0.2	0.16		
179	030804	20:50:33	33	0.05±0.05	4.8±0.3	4.7±0.2	0.22		
180	030806	03:10:06	104	290±40	790±50	3.6±0.2	0.04	0.35±0.01	UMK
181	030808	02:16:05	18	5.9±0.3	19±2	2±0.2	0.51		
182	030808	17:54:14	27	0.05±0.1	3±0.2	3±0.2	0.30		
183	030808	21:00:05	19	0.3±0.05	3.6±0.4	3±0.2	0.47		
184	030810	08:06:34	22	16±3	35±4	2±0.2	0.38		

Num	Date	UTC	σ	T_{90} [s]	C_{int} [kcnts]	C_{max} [kcnts/0.25 s]	V/V_{max}	$V_{f=0.45}$	Conf.
185	030811	18:01:36	13	0.2±0.05	2.9±0.3	2.7±0.2	0.88		
186	030813	10:54:31	16	0.1±0.05	2.7±0.3	2.6±0.2	0.60		
187	030813	21:35:18	17	0.1±0.2	2.5±0.2	2.5±0.2	0.55		
188	030814	03:06:10	103	13±2	140±8	9.4±0.2	0.04	0.11±0.01	UMKH
189	030816	01:14:26	43	0.05±0.05	4.8±0.2	4.8±0.2	0.15		
190	030821	05:31:33	21	55±6	72±8	1.1±0.2	0.42		UMKH
191	030821	23:24:20	40	120±10	180±20	1.9±0.2	0.16	0.03±0.02	
192	030822	12:40:42	20	0.05±0.05	2.4±0.2	2.4±0.2	0.44		
193	030822	13:59:00	19	24±1	44±5	1.4±0.2	0.48		
194	030822	18:40:28	11						UMKH
195	030827	16:08:40	94	5.8±3	65±3	11±0.2	0.04	0.14±0.01	UMKRC
196	030830	06:00:22	56	0.1±0.05	8.6±0.4	8.3±0.2	0.10		
197	030830	12:34:54	13	0.05±0.05	2.4±0.3	2.5±0.2	0.88		
198	030830	18:37:30	71	20±0.8	120±5	9.6±0.2	0.07	0.44±0.01	UKR
199	030831	15:06:26	85	52±3	190±9	7.8±0.2	0.05	0.32±0.01	UMKR
200	030901	22:41:21	47	0.1±0.05	7.2±0.4	7±0.2	0.13		
201	030902	05:15:02	44	0.15±0.1	5.3±0.3	5.3±0.2	0.14		
202	030903	15:43:15	14	2.3±0.6	9.6±1	1.9±0.2	0.72	0.01±0.01	UMK
203	030904	17:50:12	26	16±1	47±5	1.4±0.2	0.31		
204	030905	07:51:43	19	10±0.8	28±3	1.6±0.2	0.48	0.04±0.01	
205	030908	02:46:06	83	12±0.8	110±7	6.1±0.2	0.05	0.13±0.01	UMK
206	030912	15:09:48	35	0.05±0.1	3.9±0.2	3.9±0.2	0.20		
207	030912	18:55:20	13	0.1±0.05	2.3±0.3	2.2±0.2	0.88		
208	030916	21:59:18	20	0.95±0.3	7.9±0.6	4.3±0.2	0.46	0.09±0.01	MK
209	030918	17:11:06	16	0.05±0.05	2.1±0.2	2.1±0.2	0.60		
210	030918	18:17:41	26	28±0.9	49±5	2±0.2	0.31	0.06±0.01	
211	030919	21:10:34	23	12±0.9	38±4	1.9±0.2	0.37	0.01±0.04	UMKR
212	030926	16:52:27	12	0.15±0.05	2.7±0.3	2.6±0.2	0.98		
213	030929	09:00:53	15	0.05±0.05	2.3±0.3	2.6±0.2	0.67		
214	030929	14:27:15	5						K
215	031002	21:44:12	18	0.05±0.05	3±0.3	3.1±0.2	0.51		
216	031004	21:13:38	33	32±2	55±5	3.4±0.2	0.21	0.07±0.01	MKR
217	031006	08:32:08	26	0.3±0.05	4.5±0.4	4±0.2	0.31		
218	031008	10:11:50	11						UK
219	031010	18:42:27	13	0.05±0.05	2±0.2	2.1±0.2	0.83		
220	031011	17:11:46	16	0.15±0.05	2.6±0.3	2.7±0.2	0.65		
221	031013	22:41:25	15	0.1±0.05	2.6±0.2	2.6±0.2	0.68		
222	031014	16:48:31	20	0.15±0.05	3.1±0.3	2.8±0.2	0.45		
223	031014	19:06:47	30	58±1	29±6	2.4±0.2	0.25	0.05±0.01	UM
224	031016	23:54:01	16	21±3	25±4	1.5±0.2	0.63		UK
225	031019	22:00:54	28	58±4	97±10	3.8±0.2	0.27	0.25±0.01	KR
226	031020	02:10:04	39	49±2	130±9	2±0.2	0.17	0.21±0.01	UMKR
227	031021	03:44:42	18	0.05±0.05	2.5±0.2	2.6±0.2	0.51		
228	031021	07:07:05	38	0.05±0.05	5.9±0.3	5.9±0.2	0.17		
229	031024	09:24:10	44	3.1±0.3	34±2	5.9±0.2	0.14	0.06±0.01	UMKR
230	031026	01:26:29	25	0.2±0.05	5±0.3	4.5±0.2	0.32		MK
231	031107	18:24:06	75	19±3	170±10	4.5±0.3	0.06	0.00±0.01	MKR
232	031108	14:11:00	220	27±3	560±20	24±0.3	0.01	0.30±0.01	UMKR
233	031109	11:10:20	187	100±20	950±40	9.8±0.3	0.02	0.17±0.01	UMH
234	031111	16:45:12	374	3.9±0.7	350±7	47±0.3	0.01	0.05±0.01	UKHR
235	031124	17:04:12	36	33±4	91±9	1.6±0.2	0.19	0.06±0.01	
236	031127(1)	18:58:51	14	15±5	>29000	1500±300	0.73		KR
237	031127(1)	18:59:16	29	50±10	>110000	2000±400	0.26		MKC
238	031128	11:37:10	41	0.05±0.1	4.1±0.2	4.1±0.2	0.16		
239	031201	06:07:30	14	30±0.9	33±4	1.8±0.2	0.79	0.36±0.02	
240	031206	12:43:22	61	0.1±0.05	8.6±0.3	8.4±0.2	0.09		
241	031207	05:39:48	32	0.05±0.05	4.8±0.2	4.8±0.2	0.23		
242	031208	01:18:28	9						K
243	031210	11:51:06	14	0.7±0.1	5.6±0.5	2.1±0.2	0.75		
244	031214	10:10:49	1019	0.25±0.05	250±1	210±0.5	0.00		MK
245	031216	18:25:11	58	0.15±0.1	7.8±0.4	7.3±0.2	0.09		
246	031216	21:41:18	30	88±5	110±10	1.5±0.2	0.25		MK
247	031217	06:56:25	35	0.05±0.05	5.4±0.2	5.4±0.2	0.20		
248	031219	05:39:03	92	6.8±1	98±4	8.2±0.2	0.05	0.08±0.01	MKH
249	031219	15:01:07	73	0.3±0.1	13±0.5	11±0.2	0.07		
250	031223	08:54:42	20	9.8±0.5	28±3	1.9±0.2	0.43		MK

Num	Date	UTC	σ	T_{90} [s]	C_{int} [kcnts]	C_{max} [kcnts/0.25 s]	V/V_{max}	$V_{f=0.45}$	Conf.
251	031225	08:52:21	27	78±3	78±10	3.2±0.2	0.28	0.29±0.01	K
252	031225	23:00:13	31	3.9±0.4	28±2	3.1±0.2	0.24		MK
253	031228	23:08:05	64	0.15±0.1	8.5±0.4	8±0.2	0.08		
254	040103	20:45:30	25	0.05±0.05	2.7±0.2	2.8±0.2	0.33		
255	040107	05:33:48	16	16±2	22±3	1.5±0.2	0.64	0.07±0.02	K
256	040107	09:03:14	37	43±6	110±10	2.3±0.2	0.18	0.02±0.01	
257	040107	09:40:35	19	0.05±0.05	2.4±0.2	2.4±0.2	0.47		
258	040108	09:18:58	12	0.05±0.05	1.4±0.2	1.4±0.2	0.92		
259	040112	07:51:44	19	0.15±0.2	2.5±0.2	2.5±0.2	0.48		
260	040117	13:22:39	29	0.05±0.05	4.5±0.3	4.6±0.2	0.26		
261	040119	10:50:27	26	0.15±0.2	4.1±0.2	4.1±0.2	0.30		
262	040130	15:12:22	59	0.2±0.05	7.5±0.4	7±0.2	0.09		
263	040201	19:33:08	21	0.15±0.05	4.2±0.3	4.2±0.2	0.42		
264	040202	10:54:33	15	0.05±0.05	2.5±0.2	2.5±0.2	0.66		
265	040202	13:17:06	33	0.2±0.05	5±0.4	4.8±0.2	0.21		
266	040202	13:29:52	36	0.3±0.05	10±0.4	7.2±0.2	0.19		U
267	040204	14:34:56	26	2.1±0.3	18±1	3±0.2	0.30	0.03±0.01	K
268	040205	20:44:38	16	0.1±0.2	2.3±0.2	2.3±0.2	0.60		
269	040207	22:11:56	47	24±1	94±5	5.8±0.2	0.13	0.34±0.01	UKR
270	040208	19:53:20	34	0.15±0.05	5.7±0.3	5.5±0.2	0.20		
271	040209	03:36:47	25	9.4±2	35±3	1.9±0.2	0.32		MKH
272	040210	11:11:13	40	8.4±0.3	25±2	8.8±0.2	0.16	0.27±0.01	K
273	040211	14:14:40	34	0.05±0.1	4.3±0.2	4.3±0.2	0.21		
274	040211	15:02:05	15	6.1±0.8	15±2	1.9±0.2	0.66	0.10±0.01	MKR
275	040211	19:01:09	12	0.05±0.1	1.6±0.1	1.6±0.2	0.95		
276	040219	18:21:37	15	0.1±0.05	2.5±0.2	2.5±0.2	0.66		
277	040220	00:55:08	99	12±2	160±7	6±0.2	0.04	0.02±0.01	MKHR
278	040225	10:02:13	7						KR
279	040301	09:50:01	12	0.25±0.05	3.1±0.3	2.6±0.2	0.98		
280	040302	12:23:59	164	9.4±0.3	180±5	26±0.3	0.02	0.10±0.01	MKR
281	040310	01:08:58	20	0.05±0.05	3.2±0.2	3.2±0.2	0.45		
282	040312	00:02:35	29	0.15±0.05	5.6±0.3	5.6±0.2	0.26		KR
283	040316	01:56:01	89	38±4	270±10	2.5±0.2	0.05		
284	040317	08:46:47	12	0.15±0.2	2±0.2	2±0.2	0.96		
285	040320	20:22:38	51	18±1	100±5	6±0.2	0.11	0.38±0.01	MK
286	040320	20:40:59	28	7.4±0.2	19±2	4.5±0.2	0.27	0.24±0.01	
287	040322	07:29:02	132	0.1±0.05	27±0.4	27±0.3	0.03		K
288	040324	10:21:10	167	0.15±0.05	41±0.5	37±0.3	0.02		KR
289	040324	22:22:08	15	0.05±0.05	2.4±0.2	2.4±0.2	0.66		
290	040327	20:35:54	12	0.1±0.2	1.9±0.2	1.9±0.2	0.91		
291	040328	01:25:24	19	0.05±0.05	3.3±0.3	3.3±0.2	0.47		
292	040329	11:10:49	380	2±0.1	170±3	69±0.3	0.01	0.10±0.01	KR
293	040330	13:14:38	13	7.2±0.3	14±2	1.4±0.2	0.87		MR
294	040330	17:00:31	127	0.8±0.2	27±0.9	22±0.3	0.03		
295	040403	04:09:00	25	0.1±0.05	3.5±0.3	3.5±0.2	0.32		
296	040404	10:58:51	7						K
297	040408	06:21:41	28	0.35±0.1	5.1±0.4	4.7±0.2	0.28		
298	040413	13:09:56	18	0.05±0.05	3.2±0.2	3.2±0.2	0.53		
299	040416	18:20:22	25	0.05±0.05	3.9±0.3	4±0.2	0.33		
300	040416	19:59:26	21	1.5±0.05	6.3±0.9	4.8±0.2	0.42		
301	040417	08:05:11	5						K
302	040421	06:40:05	26	0.1±0.2	4.4±0.3	4.3±0.2	0.31		
303	040423	06:08:07	20	0.55±0.05	8.2±0.6	3.7±0.2	0.43		
304	040425	14:31:53	15	0.1±0.05	2.5±0.3	2.5±0.2	0.65		
305	040425	16:23:31	191	7.9±1	200±7	21±0.3	0.02	0.04±0.01	MKHR
306	040502	06:36:55	115	19±3	180±8	11±0.2	0.03	0.06±0.01	MKR
307	040503	00:11:34	18	0.1±0.05	2.7±0.3	2.6±0.2	0.52		
308	040505	13:18:17	18	0.05±0.05	2.7±0.2	2.7±0.2	0.51		
309	040506	02:45:38	15	13±4	23±3	1.4±0.2	0.69	0.01±0.01	K
310	040507	10:43:18	22	40±4	66±8	1.9±0.2	0.38	0.12±0.01	K
311	040511	13:01:49	21	29±3	58±6	1.2±0.2	0.41		KH
312	040520	04:12:30	19	0.1±0.05	3.2±0.3	3.1±0.2	0.49		
313	040528	16:55:38	85	20±2	140±6	5.6±0.2	0.05	0.01±0.01	K
314	040601	06:33:09	18	21±2	42±4	1.5±0.2	0.53		RK
315	040603	15:40:50	17	11±1	28±3	1.5±0.2	0.59		KHR
316	040612	06:23:58	17	0.1±0.05	2.7±0.3	2.7±0.2	0.57		

Num	Date	UTC	σ	T_{90} [s]	C_{int} [kcnts]	C_{max} [kcnts/0.25 s]	V/V_{max}	$V_{f=0.45}$	Conf.
317	040612	21:43:45	41	1.6±0.4	25±1	7.5±0.2	0.16	0.02±0.01	
318	040613	04:42:46	40	0.05±0.1	5.1±0.3	5.1±0.2	0.16		
319	040615	11:22:30	110	47±8	340±20	5.1±0.2	0.04	0.03±0.01	K
320	040704	00:48:45	41	82±3	160±20	3.6±0.2	0.15	0.33±0.01	
321	040709	00:58:06	20	180±4	110±10	1.9±0.2	0.44		
322	040712	18:32:25	28	0.35±0.05	8.9±0.5	6.2±0.2	0.28		
323	040715	07:44:41	29	0.1±0.05	4.4±0.3	4.2±0.2	0.26		
324	040716	03:02:25	28	29±1	72±6	2.2±0.2	0.27	0.20±0.01	
325	040728	00:08:57	22	0.2±0.05	5.5±0.3	4.9±0.2	0.40		
326	040805	07:20:20	34	0.05±0.05	4.3±0.2	4.3±0.2	0.21		
327	040817	15:57:29	11						K
328	040818	01:29:03	80	14±1	120±7	8.9±0.2	0.06	0.17±0.01	MK
329	040818	17:31:41	40	190±5	230±30	2.4±0.2	0.16		
330	040822	21:21:54	12	0.5±0.1	4.3±0.4	2.8±0.2	0.96		KR
331	040823	03:18:43	141	35±4	330±10	17±0.3	0.02	0.29±0.01	K
332	040823	07:35:46	20	3.7±0.05	7.6±1	4±0.2	0.45	0.24±0.03	
333	040826	14:29:21	21	0.05±0.1	3.2±0.2	3.2±0.2	0.41		
334	040829	02:45:52	61	0.25±0.05	9.1±0.5	8.3±0.3	0.09		
335	040829	06:48:42	901	6.2±1	1100±20	73±0.4	0.00	0.01±0.01	
336	040829	08:38:47	20	38±0.8	43±6	1.5±0.2	0.46		KHR
337	040829	21:20:46	47	9.5±0.4	73±4	3.9±0.2	0.13	0.13±0.01	
338	040830	18:40:40	12	9.8±0.7	20±2	1.7±0.2	0.89	0.20±0.01	
339	040901	11:39:50	90	0.15±0.05	14±0.5	13±0.3	0.05		
340	040904	13:11:50	75	0.4±0.2	14±0.6	12±0.3	0.06		
341	040905	10:58:25	29	0.6±0.05	5±0.5	4.1±0.2	0.26		
342	040905	19:29:48	14	0.3±0.05	4.2±0.4	3.2±0.2	0.73		
343	040917	04:28:19	37	0.15±0.05	5±0.3	5±0.2	0.18		
344	040921	20:04:45	28	0.05±0.05	4.5±0.3	4.6±0.2	0.27		
345	040925	22:28:55	57	24±3	130±9	4.9±0.2	0.10	0.24±0.01	KR
346	040926	04:03:06	180	7.8±0.8	260±8	17±0.3	0.02	0.23±0.01	MKR
347	041010	10:36:07	19	0.9±0.05	3.7±0.6	2.6±0.2	0.50		
348	041010	20:06:02	81	0.3±0.05	12±0.5	11±0.3	0.06		
349	041011	17:01:57	27	4.8±0.4	31±2	2.7±0.2	0.28		MK
350	041013	22:56:26	28	0.25±0.05	8.5±0.4	5±0.2	0.27		MKR
351	041015	10:22:15	23	3.3±0.2	23±2	3.1±0.2	0.35	0.03±0.01	MKR
352	041016	04:39:35	8						KHR
353	041018	11:12:36	31	0.35±0.05	4.4±0.4	3.8±0.2	0.24		
354	041019	17:07:15	64	0.05±0.1	8.1±0.3	8.1±0.3	0.08		
355	041025	10:29:08	13	0.1±0.05	2.6±0.3	2.6±0.2	0.81		
356	041025	18:30:28	16	0.35±0.05	4.3±0.4	3.1±0.2	0.64		
357	041025	22:47:50	35	17±1	75±5	4.2±0.2	0.20	0.35±0.01	MKH
358	041027	18:18:39	17	15±1	35±4	1.1±0.2	0.55		KH
359	041101	01:49:36	19	1.4±0.1	12±0.8	3.1±0.2	0.48	0.14±0.01	
360	041104	04:17:07	26	1.2±0.05	15±0.9	3.8±0.2	0.30	0.02±0.01	
361	041106	12:39:17	21	0.25±0.05	3.9±0.3	3.6±0.2	0.42		
362	041107	15:49:10	23	20±1	46±4	2.8±0.2	0.38	0.07±0.01	KHR
363	041114	15:38:44	23	0.15±0.2	4±0.2	4±0.2	0.36		
364	041115	12:48:24	17	0.05±0.05	2.8±0.2	2.8±0.2	0.55		
365	041116	00:10:07	20	0.1±0.05	3.2±0.3	3.2±0.2	0.43		
366	041116	14:42:39	22	0.9±0.05	7.8±0.6	5.1±0.2	0.40	0.11±0.03	K
367	041117	15:17:49	52	20±2	120±7	3.1±0.2	0.11		MKR
368	041118	13:46:52	22	0.1±0.05	5.1±0.3	5.1±0.2	0.38		
369	041119	14:43:46	9						KH
370	041120	19:23:36	11						KR
371	041121	18:25:28	32	66±3	94±9	3.8±0.2	0.23	0.47±0.01	KH
372	041206	06:24:26	144	5±0.5	150±3	18±0.3	0.02	0.02±0.01	
373	041206	06:48:45	22	21±2	47±5	1.4±0.2	0.40		
374	041206	11:02:22	15	17±2	28±5	1.6±0.2	0.69		
375	041211	11:31:47	32	17±3	61±5	3.6±0.2	0.22	0.06±0.01	HS
376	041211	23:57:41	575	5.90±0.70	660±10	44.0±0.3	0.00	0.11±0.01	S
377	041212	18:34:17	1788	20±5	3100±50	120±0.4	0.00	0.04±0.01	
378	041213	06:59:36	28	0.05±0.05	5.1±0.3	5.1±0.2	0.27		
379	041213	08:17:53	19	0.15±0.05	3.5±0.3	3.3±0.2	0.49		
380	041219	01:42:00	78	130±9	360±30	3.9±0.2	0.06	0.01±0.01	HIXS
381	041226	17:22:26	330	12±2	550±10	22±0.3	0.01	0.04±0.01	
382	041229	16:21:00	21	170±10	140±20	1±0.2	0.40		

Num	Date	UTC	σ	T_{90} [s]	C_{int} [kcnts]	C_{max} [kcnts/0.25 s]	V/V_{max}	$V_{f=0.45}$	Conf.
383	041230	06:25:59	27	8.7±1	38±3	2.4±0.2	0.28		
384	041230	10:13:40	37	0.05±0.05	6.3±0.3	6.4±0.2	0.18		
385	050112	11:10:23	177	0.4±0.05	53±0.8	32±0.3	0.02		

Chapter 3
Discovery of the near-IR afterglow and of the host of GRB 030528

A. Rau, J. Greiner, S. Klose, M. Salvato, J. M. Castro Cerón, D. H. Hartmann, A. Fruchter, A. Levan, N. R. Tanvir, J. Gorosabel, J. Hjorth, A. Zeh, A. Küpcü Yoldaş, J. P. Beaulieu, J. Donatowicz, C. Vinter, A. J. Castro-Tirado, J. P. U. Fynbo, D. A. Kann, C. Kouveliotou, N. Masetti, P. Møller, E. Palazzi, E. Pian, J. Rhoads, R. A. M. J. Wijers & E. P. J. van den Heuvel
Astronomy & Astrophysics 427, 815 (2004)

Abstract: The rapid dissemination of an arcmin-sized *HETE-2* localization of the long-duration X-ray flash GRB 030528 led to a ground-based multi-observatory follow-up campaign. We report the discovery of the near-IR afterglow, and also describe the detection of the underlying host galaxy in the optical and near-IR bands[1]. The afterglow is classified as "optically dark" as it was not detected in the optical band. The *K*-band photometry presented here suggests that the lack of optical detection was simply the result of observational limitations (lack of rapid and deep observations plus high foreground extinction). Simple power law fits to the afterglow in the *K*-band suggest a typically decay with a slope of α=1.2. The properties of the host are consistent with the idea that GRB hosts are star forming blue galaxies. The redshift of GRB 030528 can not be determined accurately, but the data favour redshifts less than unity. In addition, we present an optical and near-IR analysis of the X-ray source CXOU J170354.0–223654 from the vicinity of GRB 030528.

3.1 Introduction

Optical and near-IR afterglows play a crucial role in the understanding of the phenomenon of long duration Gamma-ray bursts (GRB). While prompt γ-ray emission has been known since 1973 (Klebesadel et al. 1973), major breakthrough in GRB research came with the discoveries of the first X-ray afterglow (Costa et al. 1997) and optical transient (van Paradijs et al. 1997). Firm evidence for the cosmological origin of GRBs was first obtained with the determination of the redshift of z=0.835 for GRB 970508 from absorption lines in the optical afterglow (Metzger et al. 1997). To date, afterglows for 75 well localized long duration GRBs have been detected and 36 redshifts from emission lines in the underlying host galaxy and/or absorption features in the optical afterglow were determined (see J. Greiner's web

[1]Based on observations collected at the European Southern Observatory, La Silla and Paranal, Chile by GRACE under ESO Program 71.D-0355.

page[2]). For nearly all well localized bursts an X-ray afterglow was found whenever X-ray observations were performed, but only 53 bursts were also detected in the optical and/or near-IR band. One day after the GRB, optical transients exhibit *R*-band magnitudes that are typically in the range of ∼19–22 and K_s-band magnitudes of 16–19. Optical/near-IR afterglow light curves can be characterized by a power law in time, $F \propto t^{-\alpha}$, with $\alpha \sim 1.3$ (van Paradijs et al. 2000). For the remaining 23 GRBs with X-ray and/or radio afterglow no optical and/or near-IR transient could be detected. For this group of bursts the term "dark burst" was introduced. GRBs detected in the near-IR but lacking an optical afterglow constitute a sub-group, and can be labeled "optically dark bursts".

In many cases observational limitations can account for the non-detection in the optical or near-IR-band. A slow reaction time, a location in a crowded field, possibly high Galactic foreground extinction, or unfavorable observing conditions, like bright moon and twilight, can explain non-detections of the counterparts. *HETE-2* revealed that rapid and accurate localizations of the prompt emission in nearly all cases lead to the detection of an optical transient (Lamb et al. 2004). However, this does not provide a valid explanation for all dark bursts (Klose et al. 2003). In some cases , e.g. GRB 970828 (Groot et al. 1998; Djorgovski et al. 2001) and GRB 990506 (Taylor et al. 2000) even rapid (less than half a day after the GRB) and deep ($R>23$) observations did not reveal an afterglow, despite a clearly fading source in the X-ray and/or radio band.

There are many reasons for the non-detection of the optical transients of bursts with known X-ray or radio afterglows (e.g., Fynbo et al. 2001a; Lazzati et al. 2002). In addition to the observational biases mentioned above, the existence of "dark bursts" may reflect a broad distribution of physical parameters of the GRB itself or of its environment, as in the case of GRB 990506 (see Taylor et al. 2000). The rapidly decaying radio afterglow of this burst together with the non-detection in the optical could be due to an extremely low-density medium surrounding the GRB.

Since the spectroscopic confirmation of SN2003dh underlying the afterglow of GRB 030329 (Hjorth et al. 2003; Stanek et al. 2003) it is now widely believed that long-duration GRBs are associated with the death of massive stars (e.g., Heger et al. 2003). Because of the short lifetime of these progenitors of $\sim 10^6$ years, they do not propagate far from their birth place in star forming regions. Consequently, the optical and near-IR emission could suffer from significant attenuation in the dusty medium. The X-ray and radio afterglow emission may still be observable. Whether a burst is "dark" or has a detectable optical/near-IR transient would therefore depend on the conditions of the ISM in the vicinity of the GRB. However, it is conceivable that dust destruction by the prompt emission and early afterglow phase alters the circumstances (Galama & Wifers 2001; Galama et al. 2003).

Another possibility to explain "dark bursts" is to place them at high redshift (Lamb et al. 2000). The observed redshift distribution of GRBs is very broad and currently ranges between z=0.0085 to z=4.5 with a broad peak around $z \sim 1$ (e.g., Jakobsson et al. 2004). GRBs at still higher redshifts are expected based on the association with massive stars discussed above. However, the sensitivity of stellar mass loss to metalicity combined with the requirement that jets must successfully emerge from the stellar envelope suggests that single,

[2] http://www.mpe.mpg.de/∼jcg/grbgen.html

massive stars in the early universe may not result in observable GRBs (e.g., Heger et al. 2003). Alternative scenarios, some perhaps including binary stars, may very well produce GRBs at redshifts above z=6, where the Lyman alpha absorption edge will be shifted through the optical into the near-IR band. The resulting Lyman alpha suppression could then easily account for the lack of optical detections. On the other hand, observations show that the high-z explanation for "darkness" can not apply in all cases. For example, GRB 970828 and GRB 000210 revealed underlying host galaxies at positions coincident with those of the X-ray and radio afterglows (Djorgovski et al. 2001; Piro et al. 2002) for which spectra indicate redshifts of z=0.958 and z=0.8463, respectively.
Here we report on the discovery of the near-IR afterglow of the optically dark GRB 030528 and it's underlying host galaxy. After describing the prompt emission properties and afterglow searches by other teams (Sect. 2), we present our optical and near-IR observations (Sect. 3) and their reduction (Sect. 4). We show the properties of the near-IR afterglow and of the host galaxy (Sect. 5) and discuss the results in the context of dark bursts (Sect. 6).

3.2 GRB 030528

On May 28, 2003 the *HETE-2* French Gamma-ray Telescope (FREGATE) and the Wide-field X-ray Monitor (WXM) triggered on a long-duration Gamma-ray burst (HETE trigger #2724) at 13:03 UTC. The event was moderately bright with a fluence[3] of S=5.6$\times10^{-6}$ erg cm^{-2} and a peak flux on a one second time scale of 4.9$\times10^{-8}$ erg cm^{-2} s^{-1} in the 30-400 keV band (Atteia et al. 2003). The burst duration (given as T_{90}, which is the time over which a burst emits from 5% of its total measured counts to 95%) was T_{90}=49.1 s (30-400 keV) and the high energy spectrum peaked at 32 keV. The burst is classified as an X-ray flash according to the fluence ratio $S_{(2-30keV)}/S_{(30-400keV)}$=1.13$\pm$0.15.The properties of XRFs, X-ray rich bursts and GRBs apparently form a continuum (Lamb et al. 2004). At 107 min after the onset of the burst a confidence circle with 2′ radius centered at RA(J2000)=17h04m02s, DEC(J2000)=$-22^\circ38'59''$ derived from the HETE-2 Soft X-ray Camera (SXC) was released to the community. Figure 3.1 shows a K_s-band finding chart centered on this initial error circle.
Despite several rapid response observations, no optical afterglow was found in this crowded field in the Galactic Plane (LII=0.°0249, BII=11.°267). Table 3.1 provides a list of upper limits. Later, a correction of the initial *HETE-2* error circle had to be applied. The radius of the confidence circle increased to 2.′5 and the centroid was displaced by 1.′3. This modification was announced on May 31, 2.4 days after the burst (Villasenor et al. 2003; Fig. 3.1).
A 26.1 ksec *Chandra* observation performed on June 3 (5.97–6.29 days after the burst) of the revised *HETE-2* confidence circle revealed several X-ray sources in the 0.5–8 keV band (Butler et al. 2003a). Two of these, C1=CXOU J170400.3–223710 and C10=CXOU J170354.0–223654 were located inside our field of view. Following these detections, we inspected earlier multi-epoch near-IR SofI images and found that one source, coincident with C1, exhibited significant fading (Greiner et al. 2003b) which made this source the most likely af-

[3] http://space.mit.edu/HETE/Bursts/Data

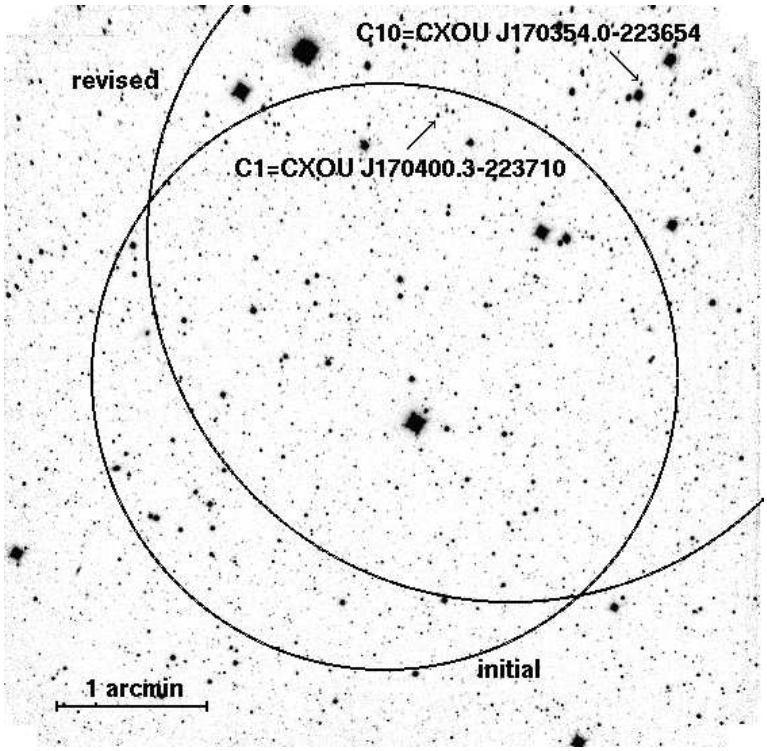

Figure 3.1. 15 min exposure K_s-band SofI image obtained on May 29, 2003. The initial and revised *HETE-2* SXC confidence circles are indicated together with the positions of two X-ray sources detected by *Chandra* (see text). North is up and East to the left.

Table 3.1. Time after the burst, filters and limiting magnitudes of published optical/near-IR observations for the afterglow of GRB 030528.

t	Filter	lim. mag	Ref.
106 s	white	15.8	Torii 2003
252 s	white	16.0	Uemura et al. 2003
0.097 d	*R*	18.7	Ayani & Yamaoka 2003
0.496 d	white	20.5	Valentini et al. 2003
5.831 d	K_s	19.5	Bogosavljevic et al. 2003
7.653 d	*I*	21.5	Mirabal & Halpern 2003

terglow candidate. A second *Chandra* observation (20 ksec exposure on June 9) showed that only one of the X-ray sources, C1, was in fact fading (Butler et al. 2003b). This observation confirmed the identification of C1 as the afterglow of GRB 030528. The X-ray observations are described by Butler et al. 2004. C1 is inside the initial *HETE-2* error circle. Therefore, the optical non-detections mentioned above, are not a result of it's later revision. Follow-up observations in the radio (Frail & Berger 2003) did not detect C1, or any other source inside the revised error circle.

3.3 Observations

Shortly (0.6684 days) after the initial $2'$ confidence circle was released, ToO imaging with the 3.58 m ESO-New Technology Telescope (NTT) equipped with the Son of ISAAC (SofI) infrared spectrograph and imaging camera at La Silla/Chile were initiated (Tab. 3.2). SofI is equipped with a 1024×1024 HgCdTe Hawaii array with 18.5μm pixel size and a plate scale of $0\farcs29$ per pixel. It has a field of view of $5\farcm5$. During the first two nights ($\sim$0.7 and $\sim$1.7 days after the burst) imaging in J, H and K_s was performed. During the fourth night ($\sim$3.6 days post-burst) only K_s-band imaging was carried out. The seeing conditions during the observations of this very crowded field were good for the first and third epoch ($\sim 0\farcs8$) but less favorable for the second epoch ($1\farcs1$–$1\farcs6$). All of the above imaging was centered on the initial *HETE-2* error circle. Due to the later increase and shift of the confidence circle and the $5\farcm5$ field of view of NTT-SofI, the observations do not cover the entire revised error circle (see Fig. 3.1).
At $\sim$14.9 days after the burst, one K-band observation was performed with the 3.8 m United Kingdom Infra-Red Telescope Fast-Track Imager (UKIRT UFTI) on Mauna Kea under good seeing conditions ($0.6''$). UFTI consists of a 1024x1024 HgCdTe Rockwell array with 18.5 μm pixels and a plate scale of $0\farcs09$ per pixel, giving a field of view of $92''\times92''$.
Nearly-Mould I-band photometry was obtained with the Mosaic2 imager at the 4 m Blanco Telescope at the Cerro Tololo Inter-American Observatory (CTIO) 6.6 and 32.6 days after the burst. The Mosaic2 consists of eight 2048x4096 SITe CCDs with a pixel size of 15 μm. The plate scale of $0\farcs27$ per pixel at the 4 m Blanco-Telescope produces a field of view of $36'\times36'$.
In addition, late time J_s-band imaging was performed with the Infrared Spectrometer And Array Camera (ISAAC) at the 8.2 m ESO Very Large Telescope (VLT) Antu in Paranal/Chile 111, 121, 124, and 125 days after the burst. ISAAC is equipped with a 1024×1024 pixel Rockwell Hawaii HgCdTe array with a 18.5 μm pixel size. The plate scale of $0\farcs147$ per pixel provides a $2\farcm5\times2\farcm5$ field of view.
Further, late epoch V and R-band observations were obtained with the Danish Faint Object Spectrograph and Camera (DFOSC) at the Danish 1.54m Telescope at La Silla/Chile 381–386 days after the burst. DFOSC consists of a 2048×4096 EEV/MAT CCD with a pixel size of 15 μm and a plate scale of $0\farcs39$ per pixel. As the instument optics does not utilise the full chip area, only 2148×2102 pixels are illuminated, giving a field of view of $13\farcm3\times13\farcm3$. These and the above mentioned observations are summarized in Tab. 3.2.

Table 3.2. Observation log. $< dt >$ stands for mid-observation time after the burst. Magnitudes and flux densities are corrected for Galactic foreground extinction. $^{(1)}$: all ISAAC J_s observations combined.

Date (Start UT)	$< dt >$ (days)	Telescope/Instrument	Filter	Exposure (min)	Seeing	Brightness (mag)	log Flux Density (erg/cm^2/s/Å)
2003 May 29 04:58	0.6684	NTT-SofI	J	15	0.8″	20.6±0.3	–17.73±0.12
2003 May 29 05:16	0.6809	NTT-SofI	H	15	0.8″	20.3±0.4	–18.05±0.16
2003 May 29 05:32	0.6920	NTT-SofI	K_s	15	0.8″	18.6±0.2	–17.83±0.08
2003 May 30 04:54	1.6673	NTT-SofI	J	20	1.6″	>20.2	<–17.57
2003 May 30 05:16	1.6826	NTT-SofI	H	20	1.1″	>19.9	<–17.89
2003 May 30 05:40	1.6993	NTT-SofI	K_s	20	1.1″	18.9±0.3	–17.95±0.12
2003 Jun 01 04:07	3.6486	NTT-SofI	K_s	60	0.8″	19.6±0.5	–18.23±0.20
2003 Jun 04 02:10	6.5604	Blanco-Mosaic2	I	40	1.2″	21.4±0.3	–17.63±0.12
2003 Jun 12 08:55	14.8680	UKIRT-UFTI	K	116	0.6″	19.6±0.1	–18.23±0.04
2003 Jun 30 03:00	32.5951	Blanco-Mosaic2	I	40	1.1″	21.2±0.3	–17.55±0.12
2003 Sep 17 00:12	111.4820	VLT-ISAAC	J_s	50	0.6″	21.0±0.2	–17.89±0.08
2003 Sep 27 00:27	121.4966	VLT-ISAAC	J_s	60	0.9″	21.1±0.3	–17.93±0.12
2003 Sep 29 23:38	124.4743	VLT-ISAAC	J_s	94	0.7″	20.7±0.1	–17.77±0.04
2003 Oct 01 00:04	125.4799	VLT-ISAAC	J_s	60	0.6″	20.7±0.2	–17.77±0.08
2004 Jun 15–18	382.5	D1m54-DFOSC	R	75	1.4″	22.0±0.2	–17.55±0.08
2004 Jun 18–19	384.5	D1m54-DFOSC	V	135	1.5″	21.9±0.2	–17.19±0.08
2003 Sep 17 – Oct 01		ISAAC-combined$^{(1)}$	J_s	264		20.8±0.1	–17.81±0.04

3.4 Data Reduction

The NTT-SofI and VLT-ISAAC near-infrared images were reduced using ESO's *Eclipse* package (Devillard 1997). The reduction of the Blanco-Mosaic2 data was performed with *bbpipe*, a script based on the *IRAF/MSCRED*, the UKIRT-UFTI observation was reduced using *ORACdr* and the DFOSC data were reduced with *IRAF*. Astrometry was performed using *IRAF/IMCOORDS* and the coordinates of stars in the field provided by the 2MASS All-Sky Point Source Catalog[4]. For the photometry we used *IRAF/DAOPHOT*. To account for the distortions in the SofI images caused by the position of C1 at the edge of the field of view (see Fig. 3.1), we used stars contained in the 2MASS Catalog from the vicinity of the source for the photometric calibrations of the J, J_s, H, K and K_s fields. The stars are listed in Tab. 3.3. We only used the stars for which magnitude uncertainties in the relevant bands were provided. The Mosaic2 *I*-band images were calibrated using the USNOFS field photometry of Henden (2003), in particular the three stars B, C & G (Fig. 3.2). The photometric measurements are partly hampered by the combination of instrumental distortions and the high density of sources in the field. The crowdedness of the field also affected the set of comparison stars. Only source F (Fig.3.2) is sufficiently isolated to provided high quality calibration. The photometry for A, B, C, D, E and G is less accurate in comparison to F, but not by much. In any case all individual uncertainties are taken into account in the error analysis. The DFOSC *V* and *R*-band calibration was performed using observations of the standard star G153-41 (Landolt 1992).

Table 3.3. Stars used for the flux calibration of the imaging data for C1 (Fig. 3.2). *I*-band magnitudes are from field photometry provided by Henden (2003) and *J*, *H* & K_s-band magnitudes are taken from the 2MASS All-Sky Point Source Catalog. $^{(1)}$: no *I*-band magnitudes available, $^{(2)}$: no uncertainties provided by 2MASS.

Star	RA (J2000) hh:mm:ss	DEC (J2000) dd:mm:ss	I [mag]	J [mag]	H [mag]	K_s [mag]
A	17:03:58.6	–22:37:33	$^{(1)}$	14.97±0.03	14.26±0.05	14.04±0.05
B	17:03:59.3	–22:37:18	14.60±0.02	13.37±0.02	12.64±0.03	12.46±0.02
C	17:04:00.3	–22:37:06	16.33±0.10	15.50±0.07	14.87±0.08	14.76±0.11
D	17:04:02.5	–22:37:10	$^{(1)}$	16.09±0.11	15.58±0.11	15.48±0.21
E	17:04:02.9	–22:37:37	$^{(1)}$	16.57±0.13	16.15±0.17	$15.76^{(2)}$
F	17:04:02.4	–22:37:37	$^{(1)}$	15.96±0.08	15.48±0.10	15.20±0.18
G	17:04:00.4	–22:36:58	17.44±0.20	16.43±0.11	15.88±0.12	$15.38^{(2)}$

To establish the proper photometric zero-points for the different instruments used in this study we cross-checked stellar colors (of non-saturated stars in the field) against a set of theoretical colors along the main sequence. We utilized synthetic stellar spectra from the library of Pickles (1998) and convolved those with the filter transmission curves and efficiencies of SofI, ISAAC, Mosaic2 and DFOSC. A good match to within a zero-point accuracy of ± 0.05 mag is obtained in all bands.

[4] http://irsa.ipac.caltech.edu/applications/Gator/

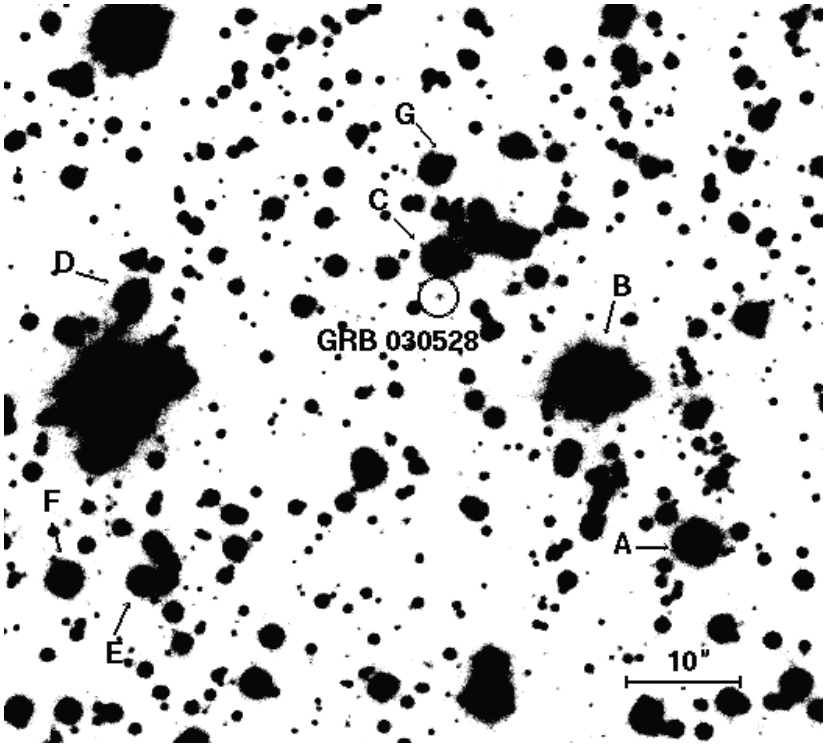

Figure 3.2. Combined late time VLT/ISAAC J_s-band image from September 2003 with a total exposure of 264 min. The position of GRB 030528 is marked by the circle, while the letters (from A-G) label the 2MASS stars used for the flux calibration (see also Tab. 3.3). The image size is $\sim 75'' \times 75''$ and North is up and East to the left.

The 2MASS catalog provides the standard J, H & K_s-band magnitudes. In addition to these bands we also present observations obtained in J_s and K. The J_s-band filter has a width of 0.16 μm and is narrower than J-band filter (0.29 μm) and the K-band filter is broader than the K_s-band filter with a width of 0.35 μm (instead of 0.27 μm). Furthermore, the K_s-band is centered at 2.16 μm while the K-band is centered at 2.20 μm. However, since J_s and K have respectively higher and lower transmission than the J and K_s, the net effect is that J-$J_s \leq 0.05$ (K-$K_s \leq 0.02$).
All magnitudes are corrected for Galactic foreground extinction according to the prescription given by Schlegel et al. (1998). For the coordinates of the afterglow of GRB 030528 we find $E(B-V)$=0.60, A_K=0.22 mag, A_H=0.35 mag, A_J=0.54 mag, A_I=1.17 mag, A_R=1.61 mag and A_V=2.00 mag.

3.5 Results

We now describe our results on the near-IR afterglow and on the optical/near-IR observations of the underlying host galaxy of GRB 030528 and discuss host properties in terms of population synthesis models. We apply the same methodology to the source C10, which is unrelated to the GRB, but defer the description to Appendix A.

C1 is the brightest X-ray source in the initial *Chandra* field at a flux level of 1.4×10^{-14} erg cm^{-2} s^{-1} at 0.5–8 keV (Butler et al. 2004). This value was calculated assuming a power law spectrum with a slope of Γ=1.9 and taking into account Galactic foreground extinction due to a neutral hydrogen column density of 1.6×10^{21} cm^{-2}. At the X-ray position of C1 a faint object in our SofI J, H & K_s-band observations $\sim$0.7 days post-burst is apparent. The source is near the detection limits in J and H, but significantly detected in K_s. The magnitudes, corrected for foreground extinction in the Galaxy, are J=20.6$\pm$0.3, H=20.3$\pm$0.4 and K_s=18.6$\pm$0.2 (see also Tab.3.2).
Seeing conditions during the second night (t $\sim$1.6 days post-burst) only allow us to derive brightness limits for C1 in the J and H band but we were able to detect the source at K_s=18.9$\pm$0.3. The J and H-band data are insufficient to test variability, and the two K_s-band measurements are formally consistent with a constant source. However, on June 1 (3.6 days post-burst) fading became apparent. At that time the source had declined to K_s=19.6$\pm$0.5, corresponding to a change by roughly $\sim$1 mag within three days. Fig. 3.3 shows the light curve of the source in K_s together with all near-IR observations presented here and the near-IR upper limits published in the GRB Coordinates Network (GCN)[5].

In contrast to the K-band variability, no fading is observed in the I-band observations taken 6.6 and 32.6 days after the burst. The source is persistent at a brightness of I=21.3$\pm$0.3, which we interpret as the I-band magnitude of the host galaxy. Similarly, comparing the late time ($>$100 days post-burst) ISAAC J_s-band observations with the SofI J-band data from the first night (t $\sim$0.6 days post-burst), the source also remains constant within the uncertainties of the measurements. Thus, the decay of the near-IR afterglow is only detected in the K_s-band.
In order to compare the afterglow decay in the near-IR with that in the X-ray band, we estimate the power law slope, α, from the few K/K_s-band data shown in Fig. 3.3. Obviously, the uncertainties in the photometry and the poor sampling of the light curve do not allow us to derive an accurate description of the afterglow behavior. A major source of uncertainty is introduced by the fact that we do not know when a jet break may have occurred. If the break occurred before our first K_s-band observation at t=0.7 days the subsequent decay slope may have been close to α=1.2. If the afterglow is best described by a single power law, the shallowest slope could be around α=0.7. In that case, the afterglow contribution to the K-band flux at 14.9 days post-burst is not negligible. Slopes much steeper than α=1.2 can be imagined upon arbitrarily placing the break time close to t=3 days. This is likely to be the case considering typical break times of $t\sim$0.4–4 days. Therefore, it appears reasonable that the post-break near-IR slope falls in the range of α=0.7–2. The significant uncertainties in the slopes leave the possibility that the near-IR and X-ray (α=2.0$\pm$0.8; Butler et al. 2004) decays are parallel.
The K-band image from an UKIRT/UFTI observation 14.9 days after the burst shows that the image of the source is extended relative to the point spread function of the field in East-West direction ($\sim1.5''\times0.8''$) (Fig. 3.4). This elongation is consistently seen in the late time

[5] http://gcn.gsfc.nasa.gov/gcn/gcn3_archive.html

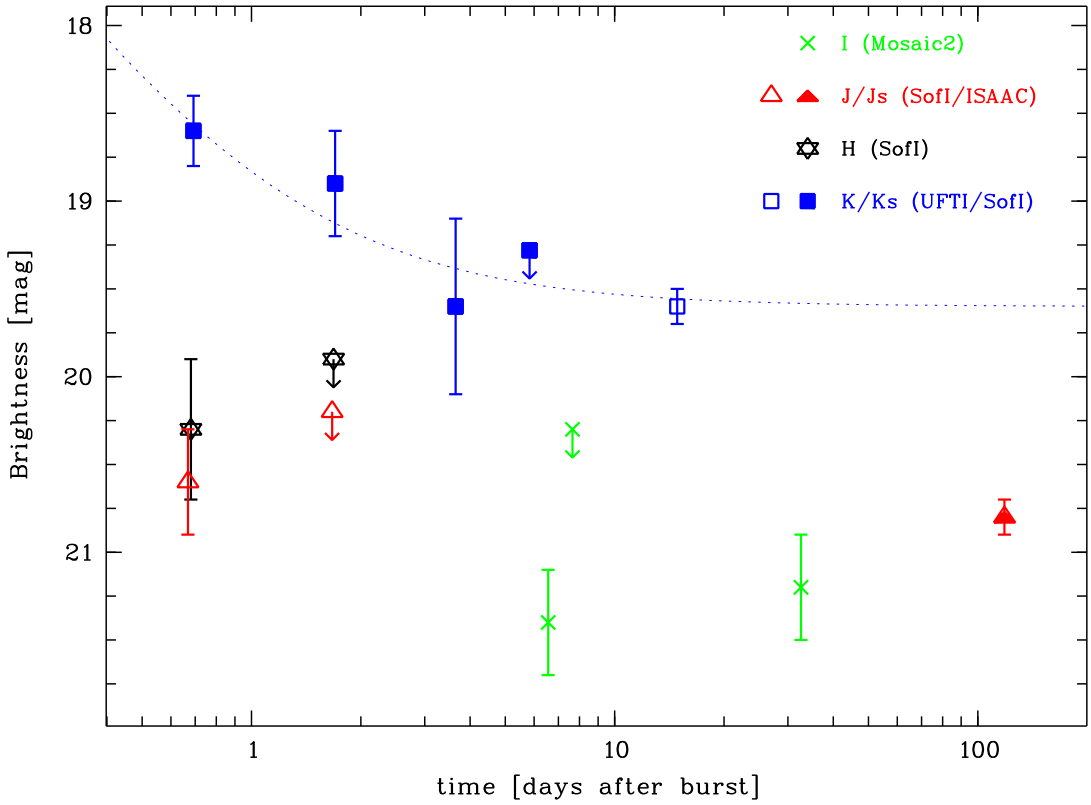

Figure 3.3. Foreground extinction corrected magnitudes in I (marked by a green cross), J/J_s (red triangle/filled triangle), H (black star) and K/K_s (blue square/filled square). For J and H only upper limits exist for t$\sim$1.7 days. The K_s-band upper limit at t=5.8 days is from observations with the WIRC at the Palomar 200-inch Hale telescope (Bogosavljevic et al. 2003) and the I-band upper limit at t=7.6 days from the 1.3 m McGraw-Hill telescope at the MDM observatory (Mirabal & Halpern 2003). The dotted line corresponds to a decay with a power law slope of α=1.2 with the host magnitude fixed to K=19.6.

ISAAC J_s-band images. The center of the source is located at RA(2000)=17h04m00.3s, DEC(2000)=–22°37′10s. The positional coincidence with the afterglow suggests that this is the underlying host galaxy of GRB 030528. We cannot exclude a residual point-like contribution to the total flux, including the afterglow and possibly an additional supernova (Zeh et al. 2004). A free fit to the K-band afterglow light curve gives a host magnitude of K=19.9$\pm$0.7. Assuming that after about 10 days all fluxes at shorter wavelengths (V–J) are exclusively due to the host galaxy, we find a host magnitude of J=20.8$\pm$0.1, an average I-band magnitude of I=21.3$\pm$0.3, R=22.0$\pm$0.2 and V=21.9$\pm$0.2. In the H-band we use the early SofI measurement of H=20.3$\pm$0.4 as an upper limit to the host brightness.
These broadband photometric measurements can be used to constrain the redshift range and galaxy classification of the host. Therefore, we applied the photometric redshift technique described in Bender et al. (2001). Thirty template spectra of a variety of galaxy types (from ellipticals to late type spirals as well as irregulars) were convolved with the filter curves and efficiencies used in our observations. The templates consist of local galaxy spectra (Man-

nucci et al. 2001; Kinney et al. 1996) and semi-empirical templates (Maraston 1998; Bruzual & Charlot 1993) and cover a wide range of ages and star formation histories. Varying the redshift between z=0 and z=10 we determine a probability density function via Bayesian statistic using eigenspectra. This photometric redshift method was earlier applied and calibrated e.g. on more than 500 spectroscopic redshifts of galaxies from the Munich Near-Infrared Cluster Survey with an rms scatter of 0.055 and no mean bias (Drory et al. 2003).

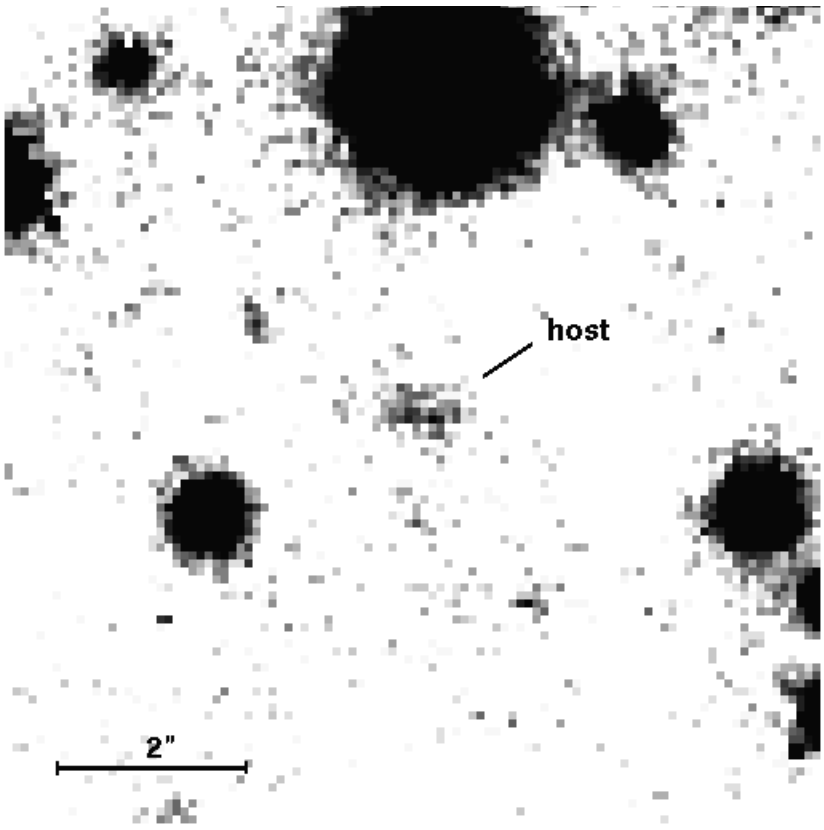

Figure 3.4. 116 min exposure *K*-band image taken with the 3.8 m UKIRT equipped with the UFTI on June 12, 14.9 days after the prompt emission. North is up and East to the left. The potential host galaxy (RA(2000)=17h04m00.3s, DEC(2000)=–22°37′10″) of GRB 030528 shows an elongation in East-West direction.

Fig. 3.5 and Fig. 3.6 show the resulting redshift probability density function together with the photometric measurements of the galaxy and two fitting galaxy template spectra. Late type star forming galaxies lead to significantly better matches to the observations (reduced χ^2<1) in contrast to ellipticals (reduced χ^2>2). The lack of *U*-band observations for GRB 030528 and the poor quality of the photometry reduces the power of the method and results in a relatively unconstrained redshift range. For late type galaxies redshifts beyond of z=4 appeared to be ruled out, while for ellipticals redshifts should not exceed $z = 0.2$. For completeness we also considered stellar spectra, and find that all available templates produce fits worse than those for elliptical galaxies (reduced χ^2>2.2; not plotted here).

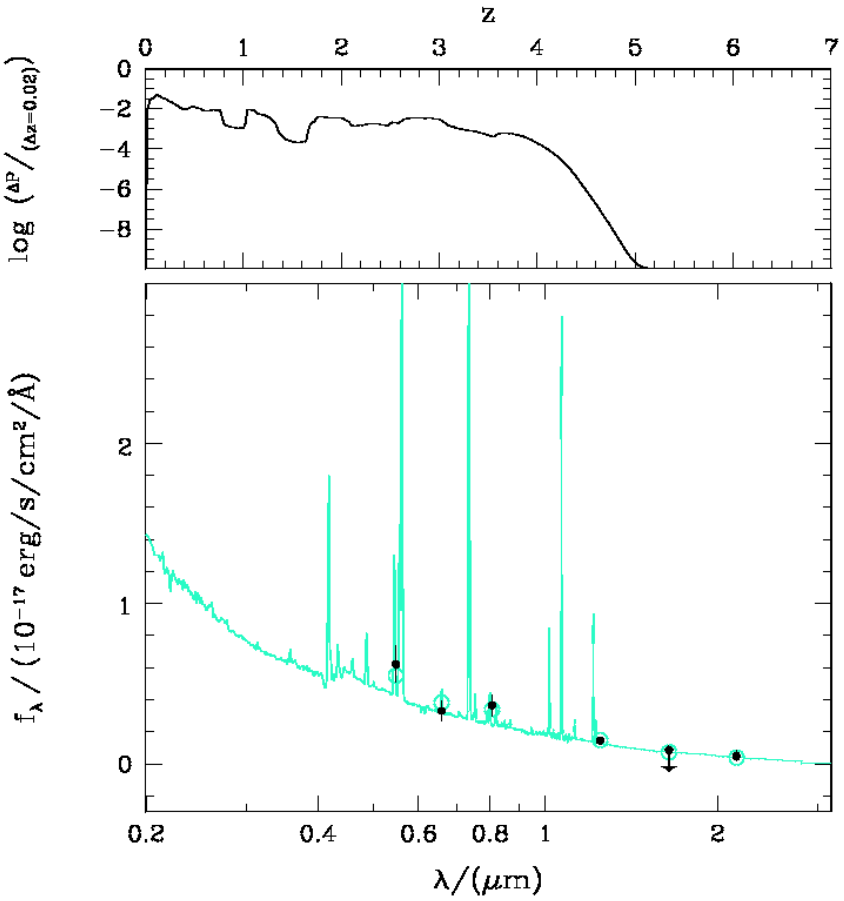

Figure 3.5. Results of the photometric redshift fit of C1 with template spectra following Bender et al. (2001). Upper panel: The probability density of the redshift of the object for late type galaxies. The probability for the redshift drops above $z \sim 4$ and has several maxima below. Lower panel: The photometric measurements (black points) together with the best fitting late type galaxy at a redshift of z=0.2 (cyan solid line). Empty circles correspond to the expected magnitudes in the observed photometric bands.

3.6 Discussion

The discovery of the near-IR afterglow and optical/near-IR host galaxy of GRB 030528 presented here, again demonstrates the importance of rapid, deep multi-wavelength follow-up observations. In this particular case rapid and deep near-IR observations were obtained, but the afterglow would probably not have been identified without the *Chandra* observations in the X-ray band. Guided by the X-ray data, we discovered the afterglow in a crowded field at a position significantly affected by image distortions. However, it took additional X-ray observations to confirm the near-IR-candidate. The chain of events for GRB 030528 emphasizes that observational programs directed at the identification and study of GRB afterglows depend critically on at least three ingredients; rapid response, deep imaging, and multi wavelength coverage. Lacking any one of these, GRB 030528 would have most likely

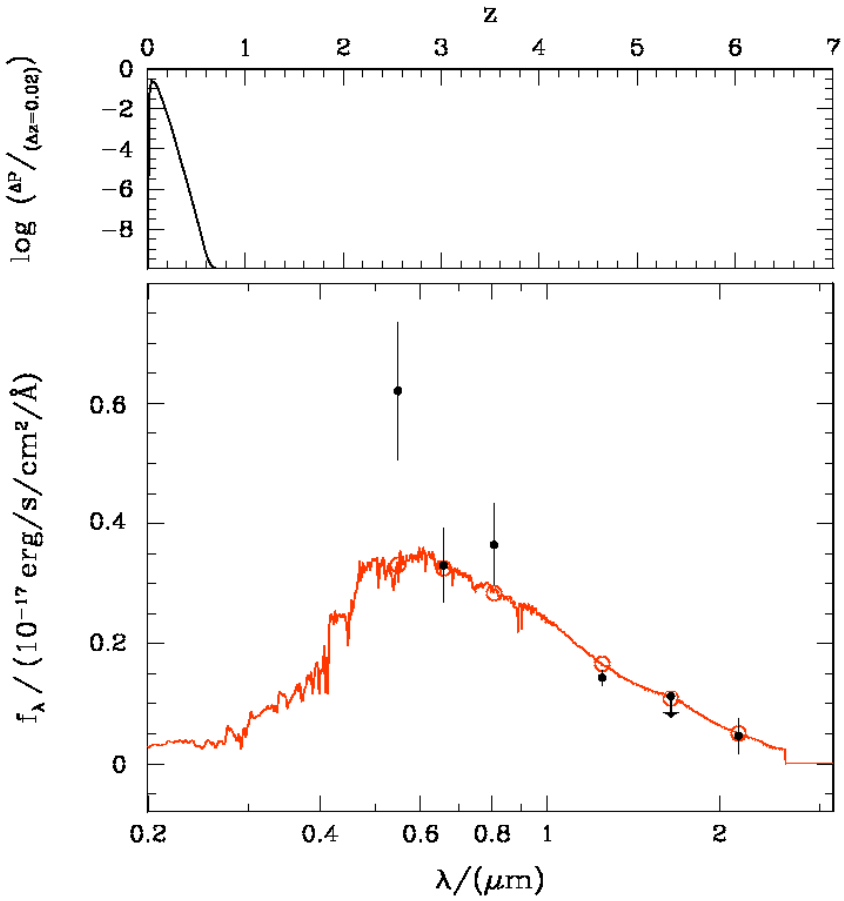

Figure 3.6. Same as Fig. 3.5 for early type galaxies.

been labeled as a “dark burst”. The fact that it was caught in the near-IR still attaches the label “optically dark” GRB, and one wonders if this is an instrumental effect or intrinsic.

The non-detection of the optical afterglow may have several reasons. The lack of early, deep optical observations is perhaps the most important. Using the decay observed in the K_s-band (Fig. 3.3) we estimate the R-band magnitude at the time of the early observations at the Bisei Observatory (Ayani & Yamaoka 2003) which provide a upper limit of $R>18.7$ at t=0.097 days. Ignoring the possibility of a break in the power law decay one predicts $K_s \sim 16.5$ at that time. With the typically observed afterglow colors of $R–K \sim 2–5$ mag (Gorosabel et al. 2002) this corresponds to R=18.5–21.5. Applying the Galactic foreground extinction correction the observable brightness should have been R=20.1–23.1. An early break in the light curve would suggest an even dimmer source. Clearly the depths of the Bisei observation did not reach a level required to capture the afterglow of GRB 030528. Depending on the $R–K$ colour, the afterglow might have been detected if it would not had suffered from the large Galactic foreground extinction. Thus, the position in the Galactic Plane additionally hampered the optical detection. It is obvious that this GRB is yet another example of a burst which maybe “falsely accused of being dark”. *HETE-2* observations indeed suggest that “optically dark” burst may mostly be due to a shortage of deep and rapid ground-based

follow-up observations and adverse observing conditions (Lamb et al. 2004).

A further challenge to the task of finding afterglows is the competition in brightness between the afterglow and the host galaxy. Except for extremely early observations the afterglow flux may be comparable or significantly less than the integrated flux from a normal galaxy. This obviously poses a challenge as the signal-to-noise ratio is essential for any detection algorithm.

Considering the luminosity functions for the host galaxies and the afterglows one potentially encounters a further challenge. A bright afterglow against the backdrop of a faint host is probably easy to identify, while a faint afterglow from a bright host could more easily escape detection. Figure 3.7 demonstrates that the *K*-band afterglow of GRB 030528 was indeed very faint when compared to all *K*-band detections of afterglows reported in the literature so far. Only the *K*-band afterglow of GRB 971214 was fainter at the time of its discovery (Ramaprakash et al. 1998). On the other hand, Fig. 3.7 also shows that most *K*-band afterglows detected by mid 2004 occupy a region, which spans over only 3 magnitudes. Assuming that $K \sim 19.6$ measured at t=14.9 days is in fact the magnitude of the host (an underlying supernova contribution might introduce a small upwards correction) this galaxy would be among the brightest GRB hosts in the K_s-band to date.

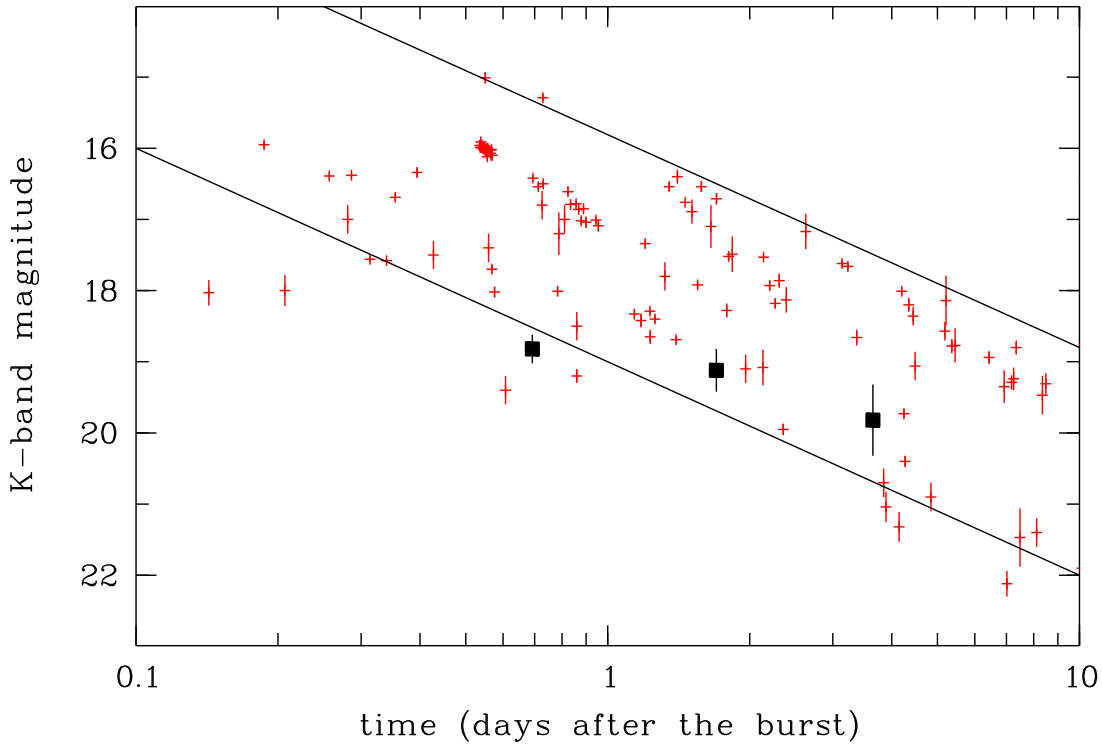

Figure 3.7. Published *K*-band magnitudes of all GRB afterglows observed by May 2004 (red dots; references listed in Appendix B) in comparison to the faint *K*-band afterglow of GRB 030528 (black filled squares). Data are not corrected for Galactic extinction. The straight lines indicate a decay with a slope $\alpha = 1.2$.

Based on the few photometric data points for the afterglow, some of which only provide upper limits due to the contribution of the host, we derive a rough lower limit on the spectral slope, $\beta > 0.4$. Such a spectral slope would not be atypical. Also, the temporal decay is in the range of the standard value of $\alpha = 1.3$ (van Paradijs 2000).
The near-IR afterglow was significantly detected only in the K_s-band. Does the non-detection in the *J* and *H*-bands require large intrinsic extinction? Both, the *J*-band and the *H*-band addresses the above question to some extent. Assuming a typical afterglow law for the spectral energy distribution of $F_\nu \propto \nu^{-\beta}$ with β=0.8 (0.4) we estimate foreground extinction corrected *J* and *H*-band magnitudes at t=0.6 days post burst. The expected *J*-band magnitude of $J\sim$20.4 ($\sim$20.6) is consistent with the observed value of J=20.3$\pm$0.4. As the host seems to dominate the *J*-band emission at that time, no constraint on the intrinsic extinction of the afterglow can be set. However, the expected *H*-band magnitude of $H\sim$19.5 ($\sim$19.6) is significantly brighter than the observed value of H=20.6$\pm$0.3 and thus indicative of some additional intrinsic extinction. Nevertheless, the data only allow us to derive a rough estimate for the observer frame extinction of $A_V>2$. From estimates of the effective neutral hydrogen column density in the X-ray band (Butler et al. 2004) it is clear that intrinsic extinction in the host galaxy may account for at most a few magnitudes in the *R*-band. These two approaches yield comparable values, but the uncertainties are large in either case.
The *R*-*K*$\sim$2.4 mag color of the host seems to be consistent with the colors in the sample of GRB host galaxies detected in the *K*-band (le Floc'h et al. 2003). Our spectral template fitting (see section 5) is consistent with the idea that GRB host galaxies are actively star forming blue galaxies as emphasized by le Floc'h et al. 03 . It is perhaps fair to assume that the host of GRB 030528 is similar to the host sample discussed by these authors. le Floc'h et al. find that GRB hosts appear to be sub-luminous at approximately 8% of L_* in a Schechter distribution function. If, for simplicity, we assume that the host of GRB 030528 has an absolute brightness of exactly this value (corresponding M_K=–22.25) the *K*-band magnitude derived from the fit to the afterglow light curve of K=19.9$\pm$0.7 implies a redshift of $z\sim$0.4–0.6 (for currently accepted cosmological parameters). Applying the pseudo redshift indicator of Atteia (2003) to the *HETE-2* data gives z'=0.36, which is close to the above value. The assumed absolute magnitude is uncertain by about $\pm$2 mag and pseudo redshifts are also uncertain to within a factor two to three. It is thus clear that the redshift of the host of GRB 030528 is by no means established. However, it seems reasonable to interpret the observations to imply redshifts of the order of unity or less. At z=0.4 the angular extent of 1.″5 of the host (see Fig. 3.4) implies a linear dimension of $\sim$8.7 kpc (assuming standard cosmology). This would suggest the host to be a blue compact star forming galaxy.

In summary, we have demonstrated that observations in the near-IR hold the promise to detect afterglows that escape in the optical band because of possible reddening. Despite the success of the discovery of the afterglow of GRB 030528 coverage was insufficient to establish a well sampled light curve and to derive an accurate redshift. However, our detection of the host galaxy provides indirect evidence for a low redshift. Despite a significant allocation of observing time at large aperture telescopes, the sampling of this afterglow fell short of optimal coverage and depth. The well recognized shortage of global resources is likely to present a major hurdle to afterglow programs in the *Swift*-era when the burst detection rate

is expected to increase dramatically.

Acknowledgements: This work is primarily based on observations collected at the European Southern Observatory, Chile, under the GRACE proposal 71.D-0355 (PI: E.v.d.Heuvel) with additional data obtained at the Cerro Tololo Inter-American Observatory and the United Kingdom Infra-Red Telescope. We are highly indebted to the ESO staff, in particular C. Cid, C. Foellmi, P. Gandhi, S. Hubrig, R. Johnson, R. Mendez, J. Pritchard, L. Vanzi & J. Willis for the prompt execution of the observing requests and all additional effort related to that. We thank the anonymous referee for insightful and helpful comments and P. Reig for his attempt to observe the host with the 1.3 m telescope at Skinakas Observatory. This publication makes use of data products from the Two Micron All Sky Survey, which is a joint project of the University of Massachusetts and the Infrared Processing and Analysis Center/California Institute of Technology, funded by the National Aeronautics and Space Administration and the National Science Foundation. This research has made use of data obtained from the HETE science team via the website http://space.mit.edu/HETE/Bursts/Data. HETE is an international mission of the NASA Explorer program, run by the Massachusetts Institute of Technology.

3.7 Appendix A - CXOU J170354.0–223654

We here summarize our results on the optical and near-IR observations of C10=CXOU J170354.0–223654. At the X-ray position a source is detected in the SofI J, H and K_s as well as in the Mosaic I-band and DFOSC V and R-band images (Fig. 3.8, RA(2000)=17:03:54.0, DEC(2000)=-22:36:53). C10 is outside the field of view of the ISAAC and UFTI observations. Tab. 3.4 lists the brightness and flux density values for all observations with C10 in the field of view. The source shows no significant variation in any band. Likewise, the two *Chandra* observation also indicate that C10 is constant in the X-ray band. This makes an association with GRB 030528 very unlikely.

The counterpart of C10 appears point like in the optical/near-IR images (Fig. 3.8). This allows both, a stellar and a Galactic nature of the object. In case of a star, the distance of the source in the Galaxy and thus the degree of extinction is unknown. Exploring the range from a nearby location (quasi unextinguished) to the opposite side of the Milky Way (foreground extinction assumed as given above) we derive ranges for the near-IR colors of J-K=0.2–0.6 mag and I-K=0.6-1.6 mag. Due to the unknown extinction, the optical colours span an even wider range. The colors constrain the spectral type to G–K for a main sequence star or supergiant (Johnson 1966). Fig. 3.9 shows an example fit of the spectrum of a G0 star to our photometric data (lower panel; dotted line). However, the ratio of X-ray to bolometric flux can be used to test the stellar origin of C10. From the observed *Chandra* counts in the energy range of 0.5–8 keV (a total of 17.5 counts in 45 ksec) we derive the X-ray flux as $F_x \sim (3.3–4.2) \times 10^{-15}$ erg cm^{-2} s^{-1} (assuming a power law shape with Γ=1.9). The lower value gives the flux corrected for the hydrogen column in the Galaxy ($N_H = 1.6 \times 10^{21}$ cm^{-2}) while the upper limit results for an object with N_H=0. Using the colors and bolometric corrections for G–K main sequence stars given by Johnson (1966) together with the observed K-band

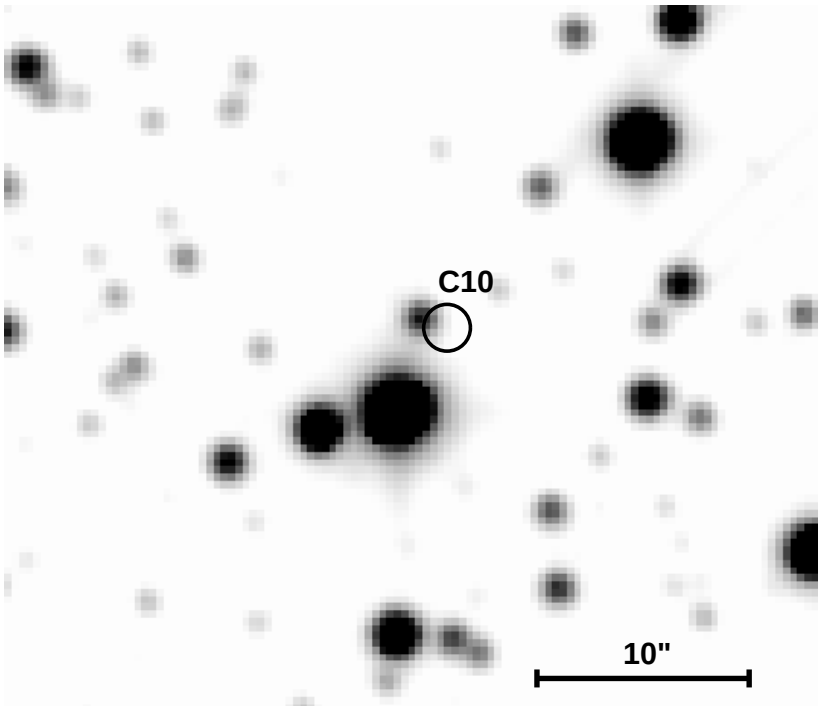

Figure 3.8. V-band image of the field around C10 taken with the Danish 1.54m Telescope in June 2004. Coincident with the *Chandra* position (error circle as given in Butler et al. (2003a)) we detect a point like source. North is up and East to the left.

Table 3.4. Brightness and flux densities of C10 corrected for foreground extinction in the Galaxy (assuming an extragalactic origin).

$< dt >$ (days)	Filter	Brightness (mag)	log Flux (erg/cm^2/s/Å)
0.6684	J	16.04±0.05	–15.91±0.02
1.6673	J	16.20±0.24	–15.97±0.09
0.6809	H	15.78±0.05	–16.24±0.02
1.6826	H	15.86±0.08	–16.27±0.03
0.6920	K_s	15.69±0.06	–16.67±0.02
1.6993	K_s	15.76±0.10	–16.69±0.04
3.6486	K_s	15.62±0.06	–16.64±0.02
6.5694	I	16.42±0.05	–15.80±0.02
32.5951	I	16.36±0.05	–15.77±0.02
382.5	R	16.81±0.05	–15.47±0.02
384.5	V	17.07±0.05	–15.26±0.02

magnitudes and filter width, we estimate the bolometric flux to be F_{bol}=(0.8–4)$\times 10^{-13}$ erg cm^{-2} s^{-1}. The resulting ratio of log(F_x/F_{bol})=-1.8±0.5 exceeds significantly the value typically observed for G–K stars (-4.5 to -6.5; Pallavicini et al. (1981)). Therefore, although the photometric data allow an association of C10 with a single star, the X-ray properties make

this very unlikely. Nevertheless, we can not exclude an X-ray binary system in the Galactic Plane with the X-ray radiation coming from an accretion disk around a black hole or from a neutron star surface and the optical/near-IR emission being produced by the accretion disk, outflow and secondary star.

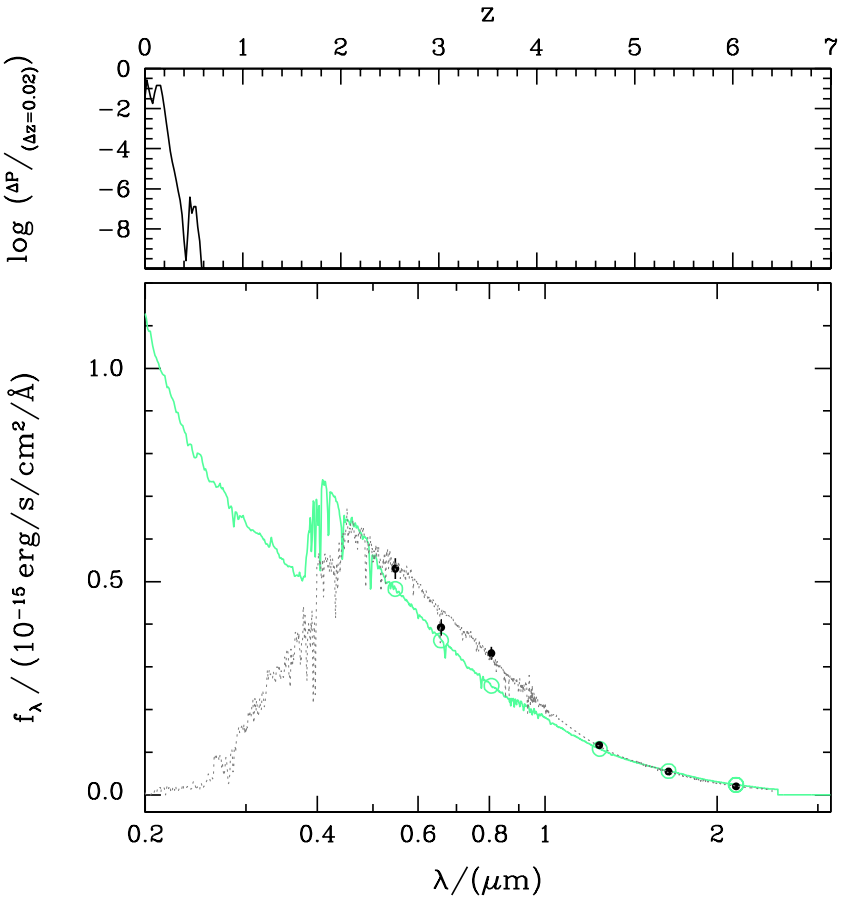

Figure 3.9. Same as Fig. 3.5 for C10. Upper panel: A global maximum of the probability density is evident at z <0.2. Lower panel: Best fitting (late type) galaxy model (cyan solid line) and best fitting (G0) stellar spectrum (black dotted line).

C10 can also be associated with a galaxy behind the Milky Way. Similarly to the analysis of C1, we applied the photometric redshift technique of Bender et al. (2001). Fig. 3.9 shows the redshift probability density function and the best fitting galaxy spectrum. A fit of a late type galaxy template to the data shows no sufficient match (reduced χ^2 ∼2.3). Early type galaxies are excluded by the fit with a reduced χ^2>6. The redshift for the best fitting galaxy template is z <0.2. Given the point-like appearance of the source, z=0.1 would require a compact small galaxy. As for a star, we use the X-ray properties to test for a possible galaxy nature of C10. From the best fitting galaxy template spectrum the expected *B*-band flux can be estimated. A late type galaxy with the observed multicolor magnitudes as shown in Fig. 3.9, has $F_B \sim 3.6\times10^{-13}$ erg cm^{-2} s^{-1}. Using the extinction corrected X-ray flux given above, we derive $\log(F_x/F_B)$=–2.6 consistent with the observations of normal galaxies (Fabbiano 1989).

The applied photometric redshift method does not allow us to estimate the redshift probability for AGNs. As shown above, templates of stars and normal galaxies have problems to fit the data. The appearance as a point source together with the X-ray properties instead make an association of C10 with an AGN the most likely solution. Spectroscopic observations are necessary to confirm this result.

3.8 Appendix B - K-band afterglow light curve data

We used the following bursts for the compilation of *K*-band afterglow light curves in Fig.3.7: GRB 970508 (Chary et al. 1998), GRB 971214 (Gorosabel et al. 1998; Ramaprakash et al. 1998), GRB 980329 (Larkin et al. 1998; Reichart et al. 1999), GRB 980613 (Hjorth et al. 2002), GRB 990123 (Kulkarni et al. 1999; Holland et al. 2004), GRB 991208 (Bloom et al. 1999), GRB 991216 (Vreeswijk et al. 1999; Garnavich et al. 2000; Halpern et al. 2000), GRB 000131 (Andersen et al. 2000), GRB 000301C (Kobayashi et al. 2000; Jensen et al. 2001; Rhoads & Fruchter 2001), GRB 010222 (Masetti et al. 2001), GRB 001011 (Gorosabel et al. 2002), GRB 000926 (Di Paola et al. 2000; Fynbo et al. 2001b), GRB 011121 (Price et al. 2002; Greiner et al. 2003c), GRB 011211 (Jakobsson et al. 2003), GRB 020305 (Burud et al. 2002), GRB 020322 (Mannucci et al. 2002), GRB 020405 (Masetti et al. 2003), GRB 020813 (Covino et al. 2003), GRB 021004 (Di Paola et al. 2002), GRB 021211 (Fox et al. 2003b), GRB 030115 (Kato & Nagata 2003; Dullighan et al. 2004), GRB 030227 (Castro-Tirado et al. 2003), GRB 030323 (Vreeswijk et al. 2004), GRB 030429 (Nishiyama et al. 2003; Jakobsson et al. 2004), XRF 030723 (Fox et al. 2003a; Fynbo et al. 2004), GRB 031203 (Malesani et al. 2004; Prochaska et al. 2004).

Chapter 4
The host of GRB/XRF 030528 - an actively star forming galaxy at z=0.782

A. Rau, M. Salvato & J. Greiner
Astronomy & Astrophysics 444, 425 (2005)

Abstract: An important parameter for the distinction of X-ray flashes, X-ray rich bursts and Gamma-ray bursts in the rest frame is the distance to the explosion site. Here we report on the spectroscopic redshift determination of the host galaxy of XRF/GRB 030528 using the ESO VLT FORS2 instrument. From the strong oxygen and hydrogen emission lines the redshift was measured to be z=0.782$\pm$0.001. Obtaining the line luminosities and ratios we find that the host is consistent with being an actively star forming galaxy with sub-solar metallicity. With a stellar mass of $\sim 10^{10}\,M_{\odot}$ the host is placed among the most massive GRB host galaxies at a similar redshift. Estimating the redshifted properties of the prompt emission, we find that XRF/GRB 030528 would be classified as an X-ray rich burst in the rest frame rather than an X-ray flash in the typically-used observer frame.

4.1 Introduction

The distribution of observer frame peak energies in νF_ν, E_{peak}^{obs}, of the prompt high-energy emission of Gamma-ray bursts (GRBs) ranges from several keV up to a few MeV with a clustering around 250 keV (Preece et al. 2000). Recently, special attention was drawn to the extreme low energy part of the distribution. Based on *Beppo-SAX* Wide-Field Camera observations (Heise et al. (2001) classified these events as so-called X-ray flashes (XRFs). XRFs are similar to long duration GRBs in various prompt burst properties (e.g. the duration and the low and high-energy spectral slopes) but are characterized by $E_{peak}^{obs} \leq 30$ keV. An operational classification based on the ratio of X-ray to γ-ray fluence, $\log(S_X(2\text{–}30\,\mathrm{keV})/S_\gamma(30\text{–}400\,\mathrm{keV}))$ in the observer frame, was proposed for events detected by the *HETE-2* satellite (Sakamoto et al. 2004). According to this definition, one third of all *HETE-2*-localized bursts are X-ray flashes with $\log(S_X/S_\gamma)>0$, another third are X-ray rich bursts (XRR) having $\log(S_X/S_\gamma)>-0.5$, with the rest being the "classical" GRBs (Lamb et al. 2005).
It has been suggested that XRFs represent the extension of GRBs to bursts with low peak energies and that XRFs, XRRs and GRBs form a continuum (Heise et al. 2001, Barraud et al. 2003). This was strengthened by the discoveries of X-ray (Harrison et al. 2001), optical (Soderberg et al. 2003) and radio (Taylor et al. 2001) afterglows for some XRFs with properties similar to those found for GRBs. Furthermore, for XRF 020903 (Soderberg et al.

2005b) and XRF 030723 (Fynbo et al. 2004) possible supernova bumps in the afterglow light curves have been reported similar to the observed associations of the deaths of massive stars with long-duration GRBs (e.g. Hjorth et al. 2003; Stanek et al. 2003; Zeh et al. 2004).
A variety of theoretical models has been proposed to explain the observed peak energies of XRFs. E.g., (i) a high baryon loading in the GRB jets can result in bulk Lorentz factors much smaller than those expected in GRBs (Dermer et al. 1999; Huang et al. 2002) (ii) Similarly, a low contrast between the bulk Lorentz factors of the colliding relativistic shells can produce XRF-like events (Barraud et al. 2005). (iii) For GRB jets which are not pointed directly at the observer the spectrum will be softer as well (Yamazaki et al. 2002). (iv) The peak energies of GRBs at high redshift will be moved to lower energies and can mimic XRFs in the observer frame (Heise et al. 2001).
An important discriminator between the individual models is the distance scale to the explosion site. A number of XRFs have been localized to arcminute accuracy in the past but only for a few could accurate distances be obtained so far. For XRF 020903 and XRF 030429 the redshift could be measured unambigously as z=0.251 (Soderberg et al. 2004) and z=2.66 (Jakobsson et al. 2005), respectively. A third event, XRF 040701, has a candidate host galaxy at z=0.2146 (Kelson et al. 2004) associated with one of the two tentatively fading X-ray sources in the error box (Fox 2004). For some more XRFs, upper limits on the redshift could be set from optical follow-up observations. In two cases, XRF 011030 and XRF 020427, host galaxies with typical properties of GRB hosts have been detected and photometric evidence suggests the redshifts to be $z<3.5$ (Bloom et al. 2003) and $z<2.3$ (van Dokkum & Bloom 2003), respectively. For XRF 030723 a firm upper limit of z=2.3 could be placed from the absence of Lyα absorption and prominent lines in the afterglow spectrum as well as from a light curve bump associated with possible underlying supernova (Fynbo et al. 2004).
Here we report on the spectral analysis of the host galaxy of GRB/XRF 030528. After summarizing the known properties of the burst and host (Sect. 2) we present the observations and data reduction (Sect. 3). The obtained host properties derived from the spectrum are shown in Sect. 4 and the implications in the context of XRFs and GRB/XRF host galaxies are discussed in Sect. 5.
We use a cosmology of Ω_m=0.27, Ω_λ=0.7 and H_0=70 km s^{-1} Mpc^{-1} throughout the paper. All photometric magnitudes are given in the AB system.

4.2 GRB/XRF 030528

The high energy transient was detected by *HETE-2* as a long-duration Gamma-ray burst (HETE trigger #2724)[1]. The event was moderately bright with a fluence of S=5.6$\pm$0.7$\times10^{-6}$ erg cm^{-2} and a peak flux on a one second time scale of 4.9$\times10^{-8}$ erg cm^{-2} s^{-1} in the 30-400 keV band (Sakamoto et al. 2005). The burst duration (given as T_{90}, which is the time over which a burst emits from 5% of its total measured counts to 95%) was T_{90}=49.2$\pm$1.2 s (30-400 keV) and the high energy spectrum peaked at 32$\pm$5 keV. With $\log(S_X/S_\gamma)$=0.04, the

[1] http://space.mit.edu/HETE/Bursts/Data

event was classified as an X-ray flash. Accordingly, we will refer to the event as XRF 030528 throughout this paper, while in other places (e.g. Butler et al. 2004; Rau et al. 2004b, R04b hereafter) the identifier GRB 030528 was used.

The burst occured in a crowded field of the sky near the Galactic Plane (LII=0.°0462 & BII=11.°2902) which lead to complication of the ground based optical follow-up observations by a significant Galactic foreground extinction. A faint near-IR afterglow was detected (Greiner et al. 2003) and at the same position a fading X-ray source was found with *Chandra* (Butler et al. 2003b).

In R04b we described the properties of the near-IR afterglow as well as a photometric study of the detected underlying host galaxy. The galaxy was found to be among the brightests observed GRB hosts with $K_{AB}\sim 21.8\pm 0.7$ mag. A fitting of template spectral energy distributions (SEDs) to the photometry in V, R, I, J_s, H & K showed that the host properties were consistent with that of a young star forming galaxy. Unfortunately, the lack of spectroscopy and the sparse photometric sampling of the SED did not allow us to determine the redshift accurately, but the data favor $z<1$.

4.3 Observations and data reduction

The host galaxy of XRF 030528 was observed with the Focal Reducer and low-dispersion Spectrograph 2 (FORS2) at the 8.2 m ESO Very Large Telescope (VLT) Antu in Paranal, Chile. Twelve exposures, each lasting 594s, were taken in two nights, on Apr. 12, 2005 and May 6, 2005. We obtained longslit spectroscopy using the 300V grism together with the order separation filter GG435, thus covering a spectral range of approx. 5200–9200 Å. Using a 1.″0 slit, the 3.3 Å pixel^{-1} scale leads to a resolution of 13.5 Å(FWHM) at 1.″0 seeing.

Flat-field, bias correction and cosmic ray removal was applied in the standard fashion using IRAF[2]. The wavelength calibration of the combined spectra was done using HgCdHe+Ar calibration lamps. The standard star LTT 7379 (spectral type G0) was used for the flux calibration of the spectra. In addition a correction for telluric absorption was performed using an observation of the telluric standard star EG 274 (spectral type DA).

Using the far-IR extinction maps of Schlegel et al. (1998) the Galactic foreground extinction in the direction of XRF 030528 is estimated as E(B–V)=0.62. Several authors have argued that the far-IR analysis overestimates the value of E(B–V) by up to $\sim$30 % for fields at low galactic lattitude. Dutra et al. (2003) suggest a rescaling of the Schlegel et al. extinction by 0.75 which results in an E(B–V)=0.46 for the line of sight towards the host of XRF 030528. For the following analysis we corrected the spectra according to the rescaled value and consider this as a lower limit of the foreground extinction. All presented spectral parameters (line fluxes & luminosities) and absolute magnitudes have to be considered as lower limits.

[2]IRAF is distributed by the National Optical Astronomy Observatories, which are operated by the Association of Universities for Research in Astronomy, Inc., under cooperative agreement with the National Science Foundation.

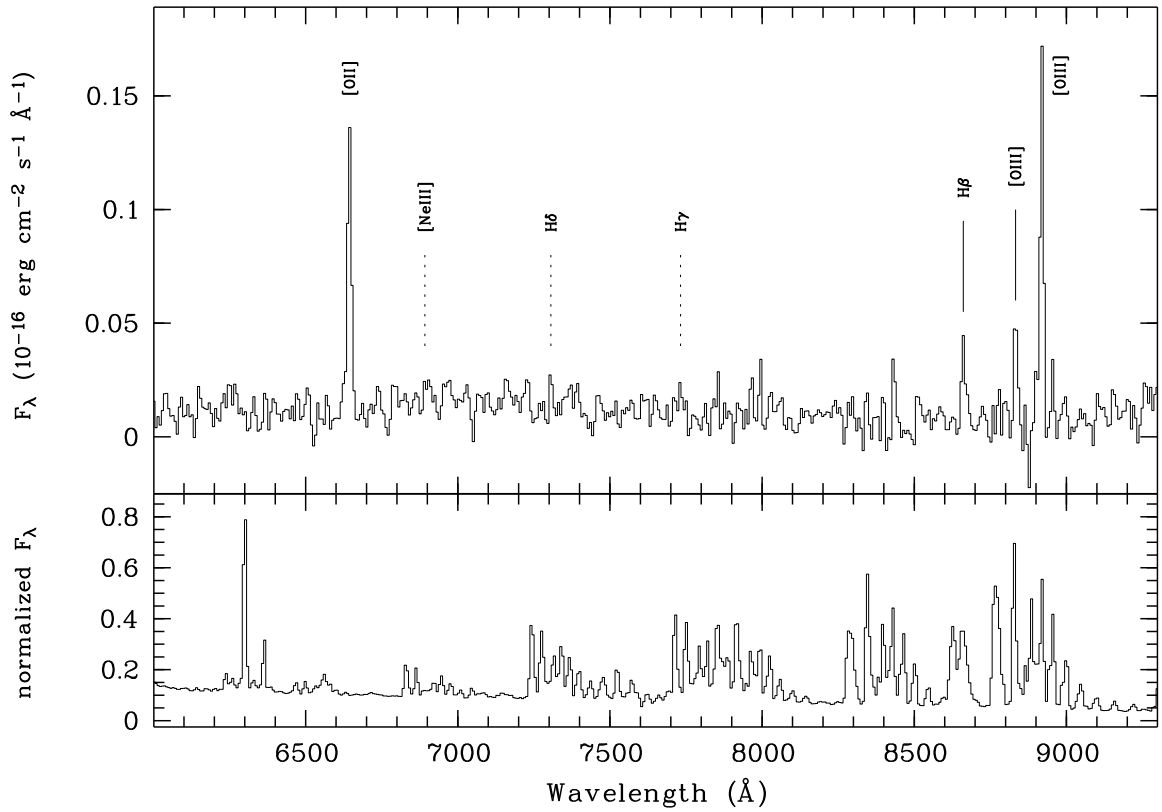

Figure 4.1. *top:* Final FORS2 long-slit spectrum of the host galaxy with an exposure of ∼2 hrs. The positions of the identified emission lines (solid lines) and a selection of undetected lines (dashed) are indicated. The host continuum is only marginally detected. Residuals of sky emission features are visible above 8000 Å. *bottom:* Normalized sky spectrum showing the prominent telluric emission lines.

4.4 Results

The final summed spectrum of the host galaxy is shown in Figure 4.1. A number of significant emission lines are detected which we identified as [OII] (λ3727 Å), Hβ (λ4861 Å), [OIII] (λ4959 Å) and [OIII] (λ5007 Å) at a helio-center corrected redshift of z=0.782±0.001. This corresponds to a luminosity distance of D_L=4.949±0.008 Gpc using the cosmological parameters given above. At this redshift Hβ and the [OIII] emission lines coincide with prominent sky emission features which complicates the accurate extraction of the line properties and effects possible weak detections of Hγ and Hδ in emission. Only [OII] falls into a wavelength range empty of sky features.

We measured the emission line strengths using a Gaussian fit in IRAF *splot*. The line fluxes are listed in Table 4.1 together with the estimated redshifts and the according line luminosities. The widths of the emission lines are consistent with the instrumental line width (560 km s^{-1} at λ=7000Å) and do not show signs of intrinsic broadening. Consistent with the photometric measurements in the V, R & I bands presented in R04b, the host continuum is only marginally traced. The resulting uncertainty in the continuum flux prevents us from deriving

sensitive equivalent widths for the lines.

Table 4.1. Line identifications. Columns: observer frame wavelengths λ_{obs}, corresponding emission line redshifts z, line fluxes and corresponding luminosities for the lines indicated in the spectrum shown in Fig. 4.1. Note that we do not apply a correction for underlying Balmer absorption.

Line	λ_{obs} Å	z	Flux 10^{-17} erg/s/cm^2	L 10^{41} erg/s
$[OII]$ λ3727	6644	0.783	15±1	4.4±0.2
$[NeIII]$ λ3869	6891	0.781	<1	<0.3
H_δ λ4102	7306	0.781	<2.5	<0.7
H_γ λ4340	7732	0.781	<2.5	<0.7
H_β λ4861	8661	0.782	4.8±0.4	1.4±0.2
$[OIII]$ λ4959	8833	0.781	4±1	1.2±0.3
$[OIII]$ λ5007	8919	0.781	20±1	5.9±0.3

The spectrum is uncorrected for possible intrinsic extinction in the host galaxy. In order to get an estimate of the extinction we used the Balmer line ratios and fits to the spectral energy distribution using the host photometry presented in R04b. Due to the shift of Hα to the near-IR only the ratios of Hγ/Hβ and Hδ/Hβ can be used to estimate E(B–V). Comparing the line ratios derived from the strict upper limits of the line fluxes for Hγ and Hδ with the theoretical values (Brocklehurst 1971) we find that no constraints for the extinction can be obtained. In an independent attempt we applied SED fitting to the broad-band photometry in V,R,I,J_s,H & K using HyperZ (Bolzonella et al. 2000) and theoretical spectral model templates of Bruzual & Charlot (1993). The sparse photometric sampling of the host together with the considerable uncertainties provides lower and upper limits of A_V=0 and A_V=2.5, respectively (χ^2<1). Thus, only a lower limit of the intrinsic extinction A_V=0 can be derived. Therefore, the line strengths given in Table 4.1 have to be considered as strict lower limits.
The unextincted star formation rate (SFR) can be derived from the luminosity of the [OII] emission line, e.g. using the typical applied calibration of Kennicutt (1998, K98 hereafter), SFR($M_\odot yr^{-1}$)=1.4±0.4×$10^{-41}L_{[OII]}$. Taking the measured line luminosity as a lower limit for the real luminosity we estimate the unextincted star formation to be >6±2 $M_\odot yr^{-1}$. A measure for the extinction corrected SFR was proposed by Rosa-Gonzalez et al. (2002, RG02 hereafter), SFR($M_\odot yr^{-1}$)=8.4±0.4×$10^{-41}L_{[OII]}$. They derived "unbiased" SFR expressions, e.g. computed from the [OII] line luminosity and the UV continuum. Correcting for the effects of underlying stellar Balmer absorption their SFR estimators bring into agreement the rates measured with different indicators, including the far-IR. According to this calibrator we derive an extinction=corrected SFR of 37±4 $M_\odot yr^{-1}$.
The UV continuum directly probes the emission from young massive stars and thus is another measure of the unextincted fraction of the ongoing star formation. The optimal rest frame wavelength (1500–2800 Å) lies outside of our spectroscopic coverage (>2950 Å at z=0.782), and the continuum is only marginally traced. Therefore, we used the best fitting SED to derive the flux at rest frame 2800 Å. The resulting lower limit for the UV SFR is 4±1 $M_\odot yr^{-1}$ when applying the K98 estimator, SFR($M_\odot yr^{-1}$)=1.4±0.4×$10^{-28}L_{\nu,UV}$, and

$17\pm3\,M_{\odot}yr^{-1}$ for the corresponding extinction corrected calibrator of RG02, SFR($M_{\odot}yr^{-1}$) = $6.4\pm0.4\times10^{-28}L_{\nu,UV}$. For clarity, the results are summarized in Table 4.2. The derived star formation rates are about a factor of two lower than the corresponding values obtained using the [OII] emission line as an indicator, which is fully consistent with the spread generally obtained when using various SFR indicators (e.g. Hopkins et al. 2001).

Table 4.2. Star formation rates and specific star formation rates for different indicators (column 1: [OII] & UV continuum at 2800 Å) and calibrators (column 2: Kennicut 1998 & Rosa-Gonzalez et al. 2002). The derived SFRs are given in column 3 and the columns 4 and 5 show the specific SFRs for an $L_{\star,B}$ galaxy and per unit solar mass, respectively.

		SFR	specific SFR	
		$[M_{\odot}yr^{-1}]$	$[M_{\odot}yr^{-1}]$	$[M_{\odot}yr^{-1}\,M_{\odot}{}^{-1}]$
[OII]	K98	6 ± 2	12 ± 3	2×10^{-10}
	RG02	37 ± 4	74 ± 6	1.2×10^{-9}
UV	K98	4 ± 1	8 ± 2	1×10^{-10}
	RG02	17 ± 3	34 ± 4	5×10^{-10}

The metallicity of the host galaxy can be derived from the oxygen and hydrogen emission lines using the indicator R_{23}=log(([OII]+[OIII])/Hβ) (Pagel et al. 1979). This emipirical indicator is not unique and typically provides a double branch solution. This degeneracy can generally be broken using other strong emission lines (e.g. [NII] λ6584 Å). For the host of XRF 030528 these lines are not available but the value of R_{23} falls onto the turnover of the two branches. Using the calibrations compiled in McGaugh (1991) we find 12+[log(O/H)]=7.7–8.5, which corresponds to a metallicity of 0.1–0.6 solar.

Knowing the redshift we determined the absolute magnitudes and luminosities of the host galaxy in various photometric bands. The rest frame absolute magnitudes (AB system, K-correction only) were derived using spectral template fitting in HyperZ with the intrinsic extinction fixed to zero. The resulting magnitudes are shown in Table 4.3 together with the respective magnitudes of an $L_{\star}$ galaxy in a Schechter distribution function and the luminosities of the host in units of $L/L_{\star}$.

The host galaxy is of the order of $L_{\star}$ in the U-band and subluminous at longer wavelengths, as expected for an actively star forming galaxy. Note that the use of the Schlegel et al. extinction value (E(B–V)=0.62) without the correction suggested by Dutra et al. (see above) would affect mainly the bands shortwards of the rest frame B-band (roughly corresponding to the observer frame R). The corresponding luminosities for E(B–V)=0.62 are $L_U\sim2.2L_{\star,U}$ and $L_B\sim0.9L_{\star,B}$, both a factor of two brighter than the results for E(B–V)=0.43. Therefore, the magnitudes and luminosities given in Table 4.3 have to be understood as lower limits.

In addition to the star formation rate and luminosities we can also derive an estimate of the stellar mass in the host galaxy applying various methods. Using the correlation between the mass and rest frame B and V-band magnitudes of Bell et al. (2005), assuming a Kroupa (2001) initial mass function, we estimate the mass to be $\sim2\times10^{10}\,M_{\odot}$. As the correlation assumes a wide range in stellar ages the obtained masses of galaxies with recent starburst activity, like the host of XRF 030528, will be overestimated. Nevertheless, the obtained

Table 4.3. Absolute magnitudes of the host galaxy in various photometric bands (AB system) together with the absolute magnitudes of an $L_\star$ galaxy in a Schechter distribution function and the luminosity of the host in units of $L/L_\star$. Values for $M_\star$–5 log h_{70} obtained for a range in redshift consistent with the redshift f our host galaxy were adopted from Dahlen et al. (2005) (U, B, R_c & J) and Cowie et al. (1996) (K). The uncertainties in M and $L/L_\star$ do not contain the uncertainty in the Galactic reddening (see Sect. 3)

rest frame band pass	M [mag]	$M_\star$ - 5 log h_{70} [mag]	$L/L_\star$
U	-20.5±0.1	-20.3±0.1	1.2±0.2
B	-20.7±0.1	-21.4±0.1	0.5±0.1
R_c	-21.1±0.1	-22.3±0.1	0.35±0.05
J	-21.4±0.1	-23.0±0.2	0.25±0.05
K_s	-21.6±0.1	-23.5±0.2	0.17±0.05

mass is of the same order as the stellar mass derived from the rest frame K-band mass-to-light ratio of 0.8 (Brinchmann & Ellis 2000) of $\sim 9\times10^9\,M_\odot$.
Using the luminosity of the host and its stellar mass the specific star formation rate in units of $M_\odot yr^{-1}$ for an $L_{\star,B}$ galaxy and per unit mass can be estimated. The specific star formation rates for the RG02 SFR calibrators are 74±6 and 34±4 $M_\odot yr^{-1}$ for an $L_{\star,B}$ galaxy derived from the [OII] and UV estimators, respectively and 1.2×10^{-9} and $5\times10^{-10}\,M_\odot yr^{-1}\,M_\odot{}^{-1}$, respectively (see also Table 4.2).

4.5 Discussion

Accurate distance measurements for extragalactic high-energy transients like XRFs, XRRs and GRBs are important to discriminate between the proposed theoretical models and for the application of the events as cosmological probes. While the redshift distribution of classical GRBs now contains ∼50 events covering a redshift range from z=0.0085 to z=4.511, the distance scale of XRFs is much less determined. The redshift measurement of XRF 030528 presented here gives the third secure distance to an XRF obtained so far and shows that XRFs, classified according to the *HETE-2* X-ray to γ-ray fluence ratio in the observer frame, cover a range consistent with that of the classical GRBs (Fig. 4.2).
A possible scenario associates XRFs with GRBs at high redshift (Heise et al. 2001). The three obtained XRF distances indicated that this can not be true for at least some of the events. Nevertheless, the shift of the rest frame peak energy to lower values in the observer frame cannot be neglected. For XRF 030528 the observer frame peak energy of E^{obs}_{peak}=32±5 keV corresponds to E^{rest}_{peak}=57±9 keV at a redshift of z=0.782. We modeled the high energy spectrum of the burst using a Band function (Band et al. 1993) with parameter values given for XRF 030528 in Sakamoto et al. (2005) and classified it according to the *HETE-2* scheme in the rest frame. The obtained value of $\log(S_X/S_\gamma)$∼–0.17 demonstrates that XRF 030528 would be defined as an X-ray rich burst at its rest frame rather than an XRF.
A similar estimate was obtained for XRF 030429 (z=2.66). For this event $E^{obs}_{peak}=35^{+12}_{-8}$ keV

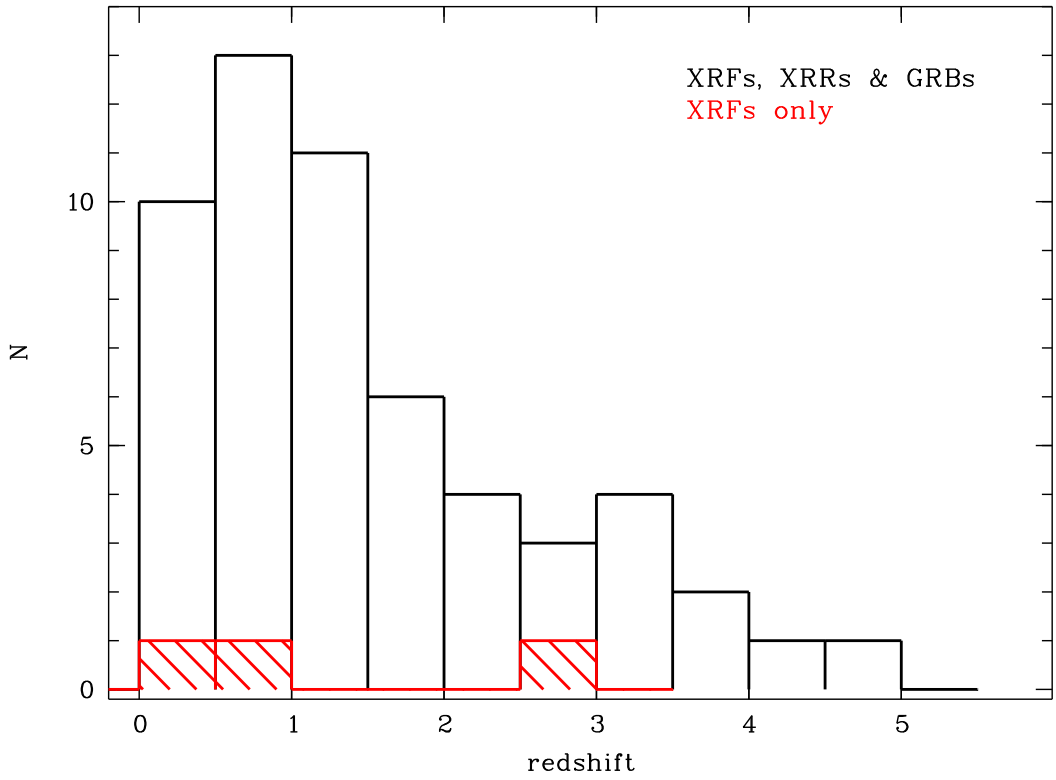

Figure 4.2. Distribution of accurately measured redshifts for XRFs, XRRs and GRBs together (empty histogram) and XRFs only (hatched). The total sample contains 55 bursts with GRB 050803 (Bloom et al. 2005) being the latest entry. The XRFs are 020903, 030528 and 030429 at z=0.251, 0.782 and 2.66, respectively.

(Sakamoto et al. 2005) shifts to E^{rest}_{peak}=128^{+43}_{-30} keV in the rest frame. This corresponds to $\log(S_X/S_\gamma)\sim$–0.43 which places the burst at the borderline between "classical" GRBs and XRRs. From the three XRFs with accurately known redshift only for XRF 020903 (E^{rest}_{peak}=6 keV) does its classification remain that of an XRF also in the rest frame. However, this event was especially soft and the physical similarity to bursts like XRF 030528 or 030429 is uncertain.

As shown above, the identification of bursts based on observer frame fluence ratios is in most cases only an operational classification. Naturally, a more sophisticated seperation would need to be based on rest frame rather than observer frame properties. Nevertheless, it becomes increasingly evident that XRFs, XRRs and GRBs form a continuum of objects, a situation that questions the necessity of such a classification of events (both in the observer and in the rest frame) and evaluates it purely operationally.

Knowing the redshift, the isotropic equivalent energy for the prompt emission of XRF 030528 can be determined to be $E_{iso,\gamma}$=2.0±0.7×10^{52} erg in the 2–400 keV observer frame energy range. Together with E^{rest}_{peak}=57 keV, XRF 030528 falls at the lower end of the correlation of $E_{iso,\gamma}$ and E^{rest}_{peak} (Lloyd-Ronning & Ramirez-Ruiz 2002; Amati et al. 2002). Assuming the validity of the relationship between E^{rest}_{peak} and the collimation-corrected total energy, E_γ,

proposed by Ghirlanda et al. (2004), the collimation fraction of the burst can be estimated. Equation (3) of Ghirlanda et al. (2004) gives E_γ=4.8$\pm$0.7$\times10^{49}$ for E^{rest}_{peak}=57 keV. This implies a collimation factor of 2.4×10^{-3} and an opening angle of 4°, which is in the typical range for GRB jets (Frail et al. 2001).

The principal aim of the observation presented here was the estimation of the redshift of XRF 030528 and thus the further establishment of the distance scale of XRFs. XRF 030528 is no longer an XRF but an XRR in the rest frame. The good quality of the spectroscopic data provided us with the possibility to study also the underlying host galaxy in more detail. From the rest frame UV continuum and the [OII] emission line luminosity star formation rate, values ranging from 4 to 37 $M_\odot yr^{-1}$ were obtained. Despite the large uncertainty of the estimate, we can conclude that the host galaxy exhibits a significant level of ongoing star formation, similar to what was found by Christensen et al. (2004) in a sample of 10 GRB host galaxies.
XRF 030528 occurred in a galaxy which appears sub-luminous in the near-IR ($\sim0.2L_{\star,K}$) and rest-frame optical bands ($\sim0.5L_{\star,B}$). This is also typical for the hosts of long-duration GRBs studied so far (e.g., Sokolov et al. 2001; le Floc'h et al. 2003; Christensen et al. 2004). Furthermore, the gas in the host was found to be of sub-solar metallicity (0.1–0.6 z) using the emission line indicator R_{23}, in agreement with a recent study of three low-z GRB host galaxies by Sollerman et al. (2005). This suggests that the host of XRF 030528 is indeed an actively star forming galaxy as emphasized in R04b.
Only a small number of estimates for the stellar mass content in GRB host galaxies have been performed so far (e.g. Sokolov et al. 2001; Chary et al. 2002). For the host of XRF 030528 we obtained the stellar mass using two independent indicators applied to the absolute magnitudes derived from the photometry presented in R04b. Both methods gave consistent results of $M\sim10^{10}$ $M_\odot$, which places the host among the most massive GRB hosts at a similar redshift. Note that the previous mass estimates were obtained using synthesis model fitting while we used indicators based directly on the absolute B & V and K-band magnitudes.
At a redshift of z=0.782, the angular extent of the host galaxy ($\sim1\farcs5$; R04b) corresponds to a linear size of $\sim$11 kpc (ignoring possible inclination effects). This indicates that the host is not a dwarf galaxy but is more comparable in size with a spiral galaxy like the Milky Way.
The comparison of the specific star formation rate and the stellar mass of the host galaxy with galaxies in the FORS Deep Field and GOODS-South field at similar redshift shows that it falls into the group of young actively star forming galaxies (Feulner et al. 2005). This indicates once more (e.g., Bloom et al. 2003; Soderberg et al. 2004; Fynbo et al. 2004) that XRFs are associated with star forming regions in the universe as are GRBs and again suggests the similarity between these events. Unfortunately, the sparse afterglow and host photometry prevents us from deriving an accurate constraint on a supernova associated with XRF 030528. The obtained K-band brightness 14.8 days post-burst provides an upper limit for the absolute magnitude of any supernova of K=–21.6 mag, around 2 mag brighter than most luminous core-collaps supernova observed in the near-IR (Mannucci et al. 2003).
While the indications that in many properties XRFs, XRRs and GRBs form a continuum in many properties are increasingly evident, the origin of the soft spectral peak in XRFs is not revealed for all events. In the case of XRF 030528 we showed that the classification in the

observer frame differs from that obtained in the rest frame. At least in XRF 020903, the only "real" XRF with a known distance so far, this is not true. In order to distinguish between the individual models and to estimate the rest frame properties of the events accurately, redshift measurements for XRFs are still very important. These require accurate localizations which will be provided by the ongoing *HETE-2* mission as well as, with a lower rate, by the *Swift* instruments. Nevertheless, the detection of very soft events like XRF 020903 at high redshift ($z>1$) will require sensitive instruments at even lower energies.

Acknowledgments: This work is based on observations collected at the European Southern Observatory, Chile, under proposal 075.D-0539. We thank D. Hartmann & S. Savaglio for the fruitful discussions. We thank the anonymous referee for valuable comments.

Chapter 5
Constraining the GRB collimation with a survey for orphan afterglows

A. Rau, J. Greiner & R. Schwarz
Astronomy & Astrophysics in press (2006)

Abstract: Gamma-ray bursts are believed to be produced in highly-relativistic collimated outflows. Support for this comes among others from the association of the times of detected breaks in the decay of afterglow light curves with the collimation angle of the jets. An alternative approach to estimate a limit on the collimation angle uses GRB afterglows without detected prompt-emission counterparts. Here we report on the analysis of a dedicated survey for the search of these orphan afterglows using the Wide Field Imager at the 2.2 m telescope at La Silla, Chile. We monitored $\sim$12 deg^2 in up to 25 nights typically spaced by one two nights with a limiting magnitude of R=23. Four previously unknown optical transients were discovered and three of these associated with a flare star, a cataclysmic variable and a dwarf nova. The fourth source shows indications for an extragalactic origin but the sparse sampling of the light curve prevents a reliable classification. We discuss the results in the context of the collimation of GRBs.

5.1 Introduction

There is now conspicuous observational and theoretical evidence that the radiation of cosmic gamma-ray bursts (GRBs) is produced in highly relativistic collimated outflows. A jet geometry was originally invoked as a solution for the "energy crisis" by reducing the total energy output of a GRB by factor of $\Omega_\gamma/4\pi$, where Ω_γ is the solid angle into which gamma-rays are emitted (e.g., Rhoads 1997; Fruchter et al. 1999). Evidence for the collimation was provided by the theoretically predicted (e.g., Sari 1999; Gruzinow 1999; Ghisellini & Lazzati 1999) and observed polarization evolution of optical afterglows (e.g., Covino et al. 1999; Wijers et al. 1999; Greiner et al. 2003).

More convincing signatures of the jet geometry were identified already earlier in the broad-band breaks observed in the optical and radio afterglow light curves of several long duration GRBs (e.g., Stanek et al. 1999; Harrison et al. 1999). The opening angles, which have been inferred from these "jet breaks" for a number of radio afterglows, vary from 1° to more than 25°, with a strong concentration near 4° (Frail et al. 2001). However, breaks obtained from the radio afterglow light curves occur typically much later than those observed at optical wavelengths. This suggests that either the optical transients typically radiate into a smaller

solid angle than the radio transients or that the radio breaks are not associated with the jet opening angle.
A consequence of the collimation is that the prompt γ-ray emission will be detected if the viewing angle of the observer is equal to or smaller than the opening angle of the jet, θ_{jet}. This implies that only for a fraction of all bursts in the Universe γ-ray photons will reach the Earth. The total GRB rate will be higher than the observed rate by a factor of roughly $\theta_{jet}^{-2} \propto \Gamma^2$ in case of a universal jet structure, where Γ is the bulk Lorentz factor of the ejecta. For a quasi-universal Gaussian-type jet, the rate will be generally smaller. Nevertheless, GRBs which are not pointed directly at the observer can in principle be discovered through their afterglow radiation at longer wavelengths.
In the standard internal-external fireball model (e.g. Rees & Meszaros 1992, 1994) the afterglow is produced when the initially highly relativistic ejecta plows into the ambient medium. The afterglow emission is radiated into a solid angle of $\Omega_A \sim 1/\Gamma$, along the line of motion. When the jet decelerates, Ω_A increases until it reaches 4π. Therefore, so-called "off-axis" orphan afterglows can be detected for bursts which are beamed outside of the field of view of the observer (e.g., Rhoads 1997; Perna & Loeb 1998; Dalal et al. 2002). The light curves of these off-axis orphan afterglows will initally be faint, brightening up to a viewing angle dependent maximum and become similar to regular GRB afterglows after the jet break later on (Rhoads 1999; Nakar & Piran 2003).
It is theoretically reasonable to assume that the optical afterglow might be emitted from a slower moving material (a lower Γ) than the initial γ-ray beam. Therefore, so-called "on-axis" orphan afterglows are expected when the narrow γ-ray emission misses the observer by a small amount but the wider optical emission region falls within the observation cone (Nakar & Piran 2003). These afterglows will exhibit similar light curves as regular afterglows with detected prompt emission.
Observations of orphan afterglows can help to study the initial opening angle of the jets and to place a constraint on the collimation of the optical afterglow emission (Rhoads 1997). Especially on-axis orphans are suitable as they are substantially brighter then off-axis orphans and thus easier to detect in a dedicated survey (Nakar & Piran 2003). Additionally, Dalal et al. (2002) pointed out, assuming uniform jet with constant jet-break time and luminosity at the break time for an on-axis observer, that for small angles the afterglow beaming angle scales with the jet opening angle. Therefore, the number of detectable off-axis orphan afterglows would be independent of the jet opening angle and similar for moderately wide jets ($\sim 20\,^\circ$) and for arbitrarily narrow jets ($< 0.01\,^\circ$). In contrast, Totani & Panaitescu (2002) found a strong dependence of the orphan rate on the jet opening angle assuming a constant total energy in the afterglow jet.

In this paper we present a survey for optical orphan afterglows with a wide-field imaging instrument (see Sect. 2) and will give an estimate on the GRB collimation derived from the detection rate of on-axis orphan afterglows. A small number of surveys dedicated to the search of untriggered optical GRB counterparts were performed over the past years. No candidate event was found in 125 hrs monitoring in a field of 256 deg^2 with ROTSE-I to a limiting magnitude of 15.7 (Kehoe et al. 2002). Vanden Berk et al. (2002) searched for color-selected transients within 1500 deg^2 of the Sloan Digital Sky Survey (SDSS) down

to R=19 and found only one unusual radio-loud AGN showing strong variability (Gal-Yam et al. 2002). The automatized RAPTOR wide-field sky monitoring system allows to image 1300 $\deg^2$ at a time down to a magnitude of $\sim$12.5 (Vestrand et al. 2004). A couple of interesting optical transients were found in the *B*, *V* and *R*-band Deep Lens Survey transient search, within an area of 0.01 $\deg^2$ with a limiting magnitude of 24. None of those could be positively associated with a GRB afterglow (Becker et al. 2004). Recently, Rykoff et al. (2005) performed the search using the ROTSE-III telesope array without detecting any candidate afterglow events. They placed an upper limit on the rate of fading optical transients with quiescent counterparts dimmer than $\sim$20th magnitude at a rate of less than 1.9 $\deg^{-2}$ yr^{-1}.
The paper is structured as follows. In Sect. 2 we describe the observational strategy, instrumentation and selected survey fields as well as the data reduction and transient detection method. The candidate transients are presented in Sect. 3 and the transient detection efficiency in Sect. 4. A discussion of the results in the context of GRB collimation is given in Sect. 5.

5.2 Observations and data reduction

5.2.1 Strategy, instrumentation & survey fields

A search for GRB afterglows or other transient phenomena in the sky requires a thorough strategy due to the random occurence of the events in space and time. As a continuous monitoring of a large field with a large apperture telescope could only be considered overambitious in many cases, we developed our strategy using the knowledge of the properties of observed optical afterglows at the time when the survey was proposed (1999).
The primary idea was to take multiple deep observations of a number of selected sky fields. The observing scheme was chosen such that the survey would be sensitive enough ($R\sim$23 mag) to provide the detection of a GRB orphan afterglow in at least two epochs together with earlier and later upper limits. To combine the availability of a large aperture telescope together with the observed brightness decay of GRB afterglows, we decided to perform consecutive observations of a given field in every 2nd night. Over this time span, on-axis orphan afterglows will be brighter than *R*=21 in most cases. Instead, off-axis orphans are expected to be fainter and will dominate below that brightness (Nakar & Piran 2003).
We obtained imaging data during three periods (May-June, August & September-October) in 1999 and monitored 7 different sky fields in up to 25 nights each. Each field is composed out of 2 to 8 separate sub-fields and a total of 38 sub-fields were selected. This corresponds to an area of $\sim$12 square degrees being imaged throughout the campaign. A list of all fields together with the number of sub-fields and the maximum number of observing nights is provided in Table 5.1. Note that due to changes of the observing conditions during a night not always a complete monitoring of a given field could be accomplished.
A total of 39 nights were scheduled using the the Wide Field Imager (WFI) at the MPG/ESO 2.2 m telescope in La Silla, Chile. Due to weather constrains only 31 nights could at last partly be used for observations. Unfortunately, the lost nights caused unfavorable interrup-

tions of the otherwise gap-less observing schedule of each period and lead to a significantly decreased detection sensitivity for orphan afterglows.
The distribution of the time delay between two consecutive observations of a given pointing is shown in Figure 5.1. While the majority of the survey could be observed with the proposed gap of two days between consecutive observations, $\sim$15 % suffered from larger gaps due to inappropriate weather conditions. In addition to the regular 2-day schedule a small number of nights were included in which multiple observations of selected fields (F1, F3 & F5) were performed within one night. This would allow to identify and distinguish possible short-term variable sources (e.g. CVs) in these fields.

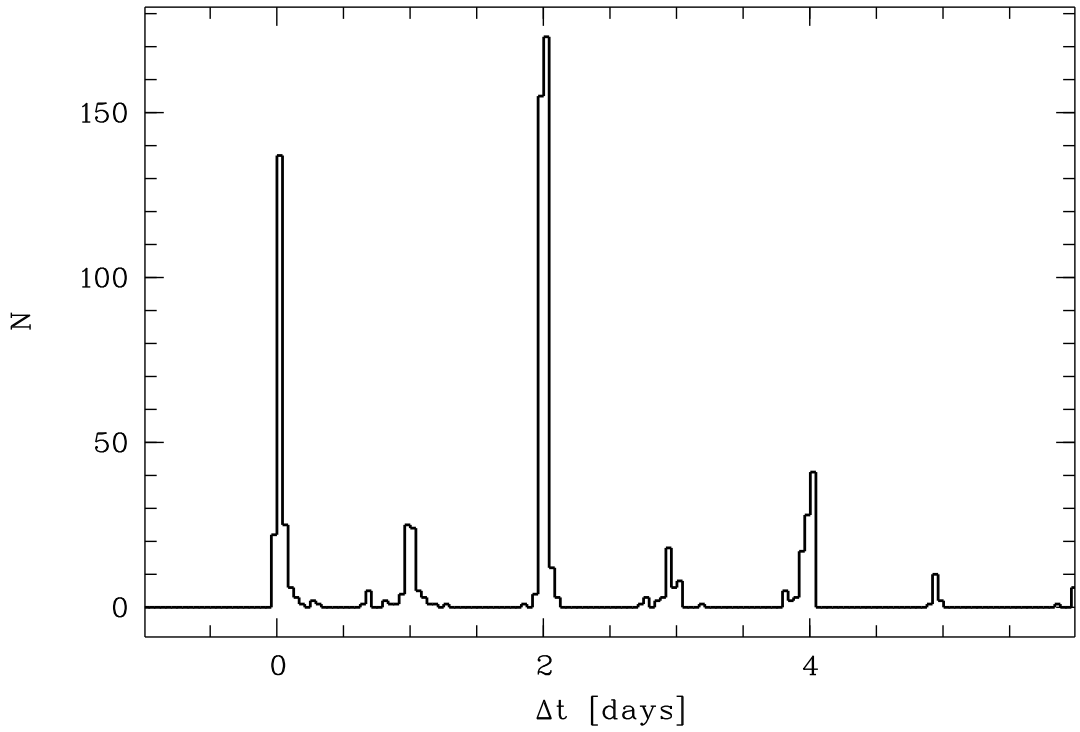

Figure 5.1. The distribution of time between consecutive observations of individual subfields with 1 hrs binning.

The photometry was taken with WFI mainly in the *R*-band together with a small number of pointings performed using the *V* and *I*-band filters. The typical exposure time was 420 s per pointing. The instrument consists of a mosaic of 4×2 CCDs each 2046×4128 pixel in size which, together with the plate scale of 0.238 arcsec/pixel, provided a sky coverage of $34' \times 33'$ per image. A gap of $\sim$2 arcsec exists between neighboring CCDs of the imager. Throughout the data acquisition the observing conditions varied strongly (see Figure 5.2). The majority of the data were taken at a seeing of $\sim$1" but a small fraction of the observations suffered from significantly worse seeing. Due to the low limiting magnitude and the loss of all but the brightest sources we neglected date taken under seeing conditions above $2\farcs4$ ($\sim$10 pixel FWHM). This corresponds to an additional loss of $\sim$10 % of the campaign data.
The selection of the fields was more or less random with respect to the search for orphan afterglows with the exception of the field SA113 (our F6). This field included a number

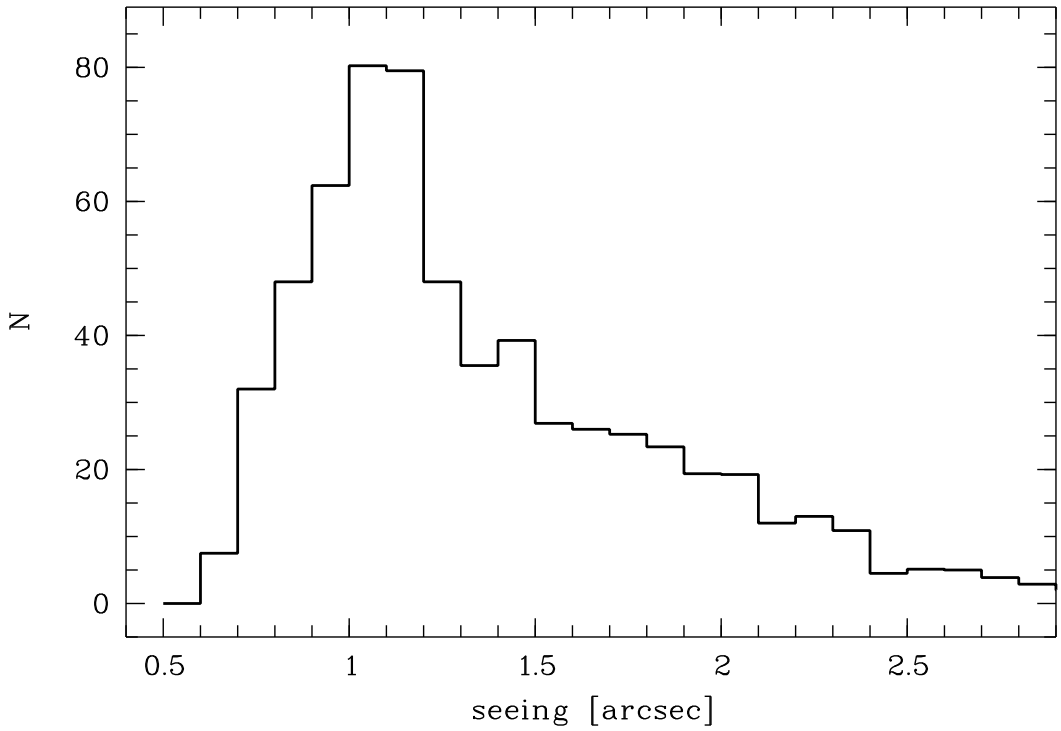

Figure 5.2. Seeing distribution for all pointings.

Table 5.1. Observation log. The first four columns provide the ID, central coordinates and number of sub-fields. The last column represents the amount of nights with seeing $<2\farcs4$ in which pointings of a given field were obtained.

Field	RA(2000)	Dec(2000)	sub-fields	# of nights
F1	01h32m	–43°12′	4	15
F2	03h33m	–27°37′	4	12
F3	13h28m	–21°40′	8	11
F4	16h20m	+04°00′	8	12
F5	21h26m	–43°22′	8	23
F6	21h41m	+00°30′	2	25
F7	21h52m	–27°32′	4	21

of Landoldt standard stars which would allow an absolute photometric calibration of the survey (Landoldt 1992; see below). F6, together with a second field (F4), is also covered by the SDSS[1]. This provided us with the opportunity to identify possible transient sources in these fields down to $R\sim22$ mag using the SDSS multi-band informations. Bright stars and significant foreground extinction were avoided during the field selection.

[1] http://www.sdss.org/

5.2.2 Data reduction

Nearly 700 images were obtained throughout the survey. For the automatic reduction and analysis of this large amount of data a Perl-based pipeline was developed which uses a number of well tested software packages. The basic image reduction was performed using *IRAF*[2]*/MSCRED*. For each night of observations a common bias frame was produced and subtracted from the science images. Flat field correction was performed using daily super-sky-flats produced from all science observations of a given night without significant illumination by the Moon or other bright sources.

The astrometric solutions were obtained on CCD-basis with the *WIFIX/ASTROMETRIX*[3] package by comparing the positions of detected sources with those compiled in the USNO-A2.0 catalog (Monet et al. 1998). The resulting astrometric precision is indicated in Figure 5.3 where the difference in the position of isolated sources detected in a sub-field of F6 in multiple observations is shown. About 80 % of the sources lie within 1/2 detector pixel ($0\farcs119$) compared to a reference observation taken on May 31, 1999. More than 99 % of the sources are detected within a circle of $0\farcs4$ radius. Note that the double peaked shape of the distribution in Figure 5.3 is artificial, resulting from the numerical rounding of the pixel coordinates in the source detection algorithm.

The source detection in the images was performed in each of the 8 WFI CCDs separately. We used the *IRAF/DAOPHOT* package to measure the source flux inside a Gaussian-shaped point-spread-function. The search for transient sources does not gain significant benefit from an absolut photometric calibration which would be connected with an unavoidable additional systematic zero-point uncertainty. Instead, we obtained the variability informations using the technique of differential photometry. We selected an ensemble of at least 20 local, non-saturated, non-variable reference stars for each sub-field. By deriving the median brightness offset of these stars with respect to the brightness of the same stars obtained in a reference image of a given sub-field (typically the one with the smallest seeing), the photometric offset between the two observations could be estimated. This was sucessively done for all observations of a given sub-field and thus provided a common photometric zero-point for all pointings of the respective sub-field.

Absolut photometric calibration was obtained based on observations in one photometric night (October 12, 1999) of the field SA113 (our F6). This field contains a number of Landoldt standard stars with well tabulated optical photometry (Landoldt 1992)[4] As all photometric standard stars were saturated in the regular 420 s image taken for our survey, we obtained a shorter exposure (20 s) during the same night. In this 20 s frame six non-saturated standard stars were contained and the photometric zero point for this image was obtained (systematic uncertainty of ΔR=0.1 mag). This allowed to produce a sample of secondary standard stars in the field down to a limiting magnitude of $R\sim21$ corresponding to a 5σ

[2] *IRAF* is distributed by the National Optical Astronomy Observatories, which are operated by the Association of Universities for Research in Astronomy, Inc., under cooperative agreement with the National Science Foundation.

[3] http://www.na.astro.it/∼radovich/wifix.htm

[4] The tabulated Cousin *R*-band magnitudes were transformed to the WFI *R*-band filter system using the colour and extinction terms given at http://www.ls.eso.org/lasilla/Telescopes/2p2T/E2p2M/WFI/zeropoints/.

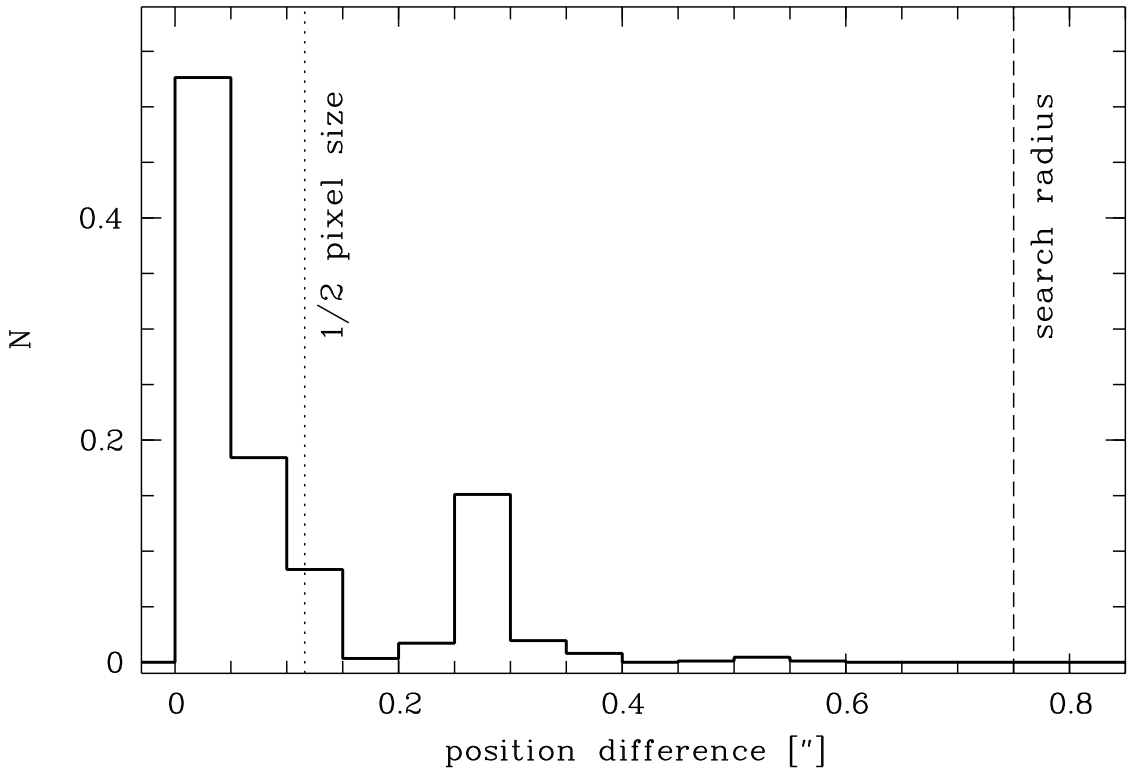

Figure 5.3. Normalized distribution of the distances of ∼40 isolated sources detected during the whole survey in the field F6-1 compared to the respective reference positions obtained from an observation taken on May 31, 1999 (solid line). The dotted and dashed lines indicate the size of 1/2 detector pixel and the search radius for the source tracing algorithm, respectively. The selected sources span ∼5 mag in brightness and are distributed over the entire detector field of view.

detection.

The field F6 was observed in nearly all nights of the survey. This allowed to obtain accurate photometric calibration for the other six fields based on the zero points derived from the secondary standards in F6 in a common night. For each field one photometric night was chosen and the photometric calibration of all further observations were calibrated with respect to this night. The photometry in all fields was additionally corrected for Galactic foreground extinction (A_R=0.02–0.25) (Schlegel et al. 1998).

Figure 5.4 shows the resulting photometric quality for an example field (F4) obtained under good seeing conditions (0.″8). The uncertainties represent the detection uncertainties in the instrumental magnitude system and do not include the uncertainties resulting from the absolute photometric calibration ($\Delta R\sim$0.1 mag). A limiting magnitude of $R\sim$23 at 10σ was reached in this observation. As discussed above, the observing conditions varied strongly throughout the survey. Thus, the achieved limiting magnitude ranged between $R\sim$19 and $R\sim$23, depending on the seeing and Moon illumination. Sources brighter than $R\sim$16 were saturated in a good night.

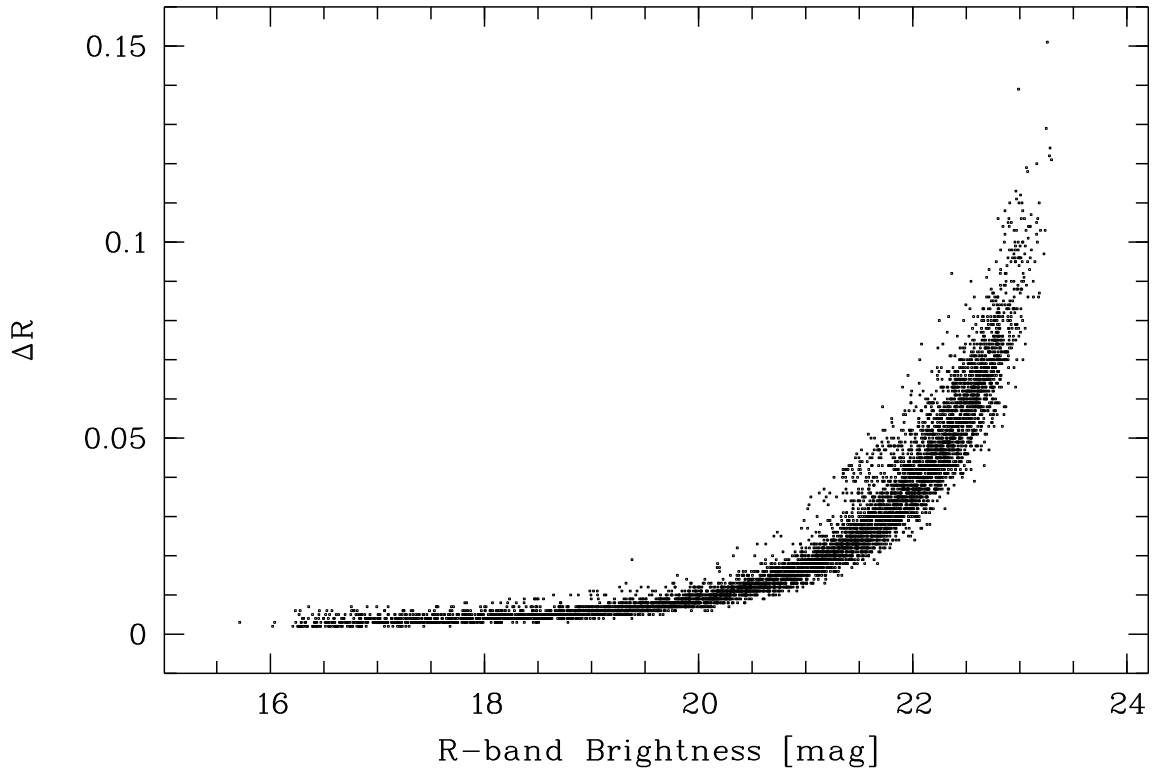

Figure 5.4. Photometry obtained for an observation of the field F4 on May 22, 1999. The seeing during the time of the imaging was 0.″8 and a limiting magnitude of $R\sim23$ mag with 10σ was reached. Sources brighter than $R\sim16$ mag are saturated.

5.2.3 Transient detection method

For each of the seven fields a master table including the coordinates and magnitudes of all detected sources in all observations was produced. Herein, we assigned detections within a distance of 0.″75 to a detection obtained in a reference image together and consider this as one source.

Light curves were obtained for all detected sources and candidate transient objects were selected based on the deviation of their light curve from their mean light curve. For all candidates with single detections or $\Delta R>0.75$ mag ($\sim$12000) light curves plots as well as thumbnail images of all pointings were produced. These were examined by eye in order to remove spurious transients arising from nearby bright stars, extended objects, stray light effects at the edge of the FoV, bad focus or detections which were consistent with faint stars at the limiting magnitude of the individual pointings. The strategy of the survey was aimed to catch a possible orphan afterglow in at least two consecutive observations. Therefore, we considered only sources with at minimum two detections for further investigations. A number of fast moving objects (e.g. air planes, terrestrial satellites) could be identified by the trace in the images which they left during the 420 s exposure. Solar system objects (e.g. asteroids) are especially abundant in the survey fields located close to the ecliptic plane (F3, F6 & F7). These sources appear either as one-time detections or show significant

motion between subsequent observations and could be identified accordingly. Of the ∼12000 candidates only four remained and were double checked with the positions of known sources compiled in the SIMBAD[5] and NED[6] databases and if possible correlated with the SDSS 4th release and the DSS[7].

5.3 Results

5.3.1 Candidate transients

Throughout the survey four new transient sources with detections in at least two images were found. We identified one candidate cataclysmic variable, one dwarf nova, one flare star and one candidate extragalactic transient superimposed on an underlying faint object. For the latter an orphan afterglow nature is considered possible. Below we give a brief description of each of the transient sources (see also Table 5.2).

Table 5.2. Candidate transient sources. The minimum and maximum obtained brightnesses as well as the putative classification are given.

Name	Brightness [mag]		Putative
	min	max	classification
J132653.8-212702	20.3±0.1	19.5±0.1	CV, eclip. binary
J132813.7-214237	21.3±0.1	19.9±0.1	extragalactic
J161953.3+031909	19.9±0.1	17.5±0.1	dwarf nova
J215406.6-274226	22.5±0.2	20.0±0.1	flare star

J132653.8-212702

The source was initially detected in F3 during the first night of observations on May 22, 1999 (MJD 51321.0045). The field was observed four times during that night and the source exhibited a significant brightness increase from R=20.4 to R=19.7 within 80 min (Fig. 5.5a). It was observed again on May 31/June 2, June 17/19 and August 4/6 and showed a flaring of ΔR=0.2–0.4 mag during each of these epochs. No X-ray or optical counterpart was detected in the ROSAT All-Sky survey (taken 1990) and SIMBAD or NED, respectively. The rapid variability excludes slowly varying objects and is consistent with a cataclysmic variables and eclipsing binaries. No orbital period could be obtained due to the sparse sampling of the light curve. The confirmation of the nature of this source requires further monitoring of the variability or simultaenous observations in multiple colours.

[5] http://simbad.u-strasbg.fr/
[6] http://nedwww.ipac.caltech.edu/
[7] http://archive.stsci.edu/cgi-bin/dss_form

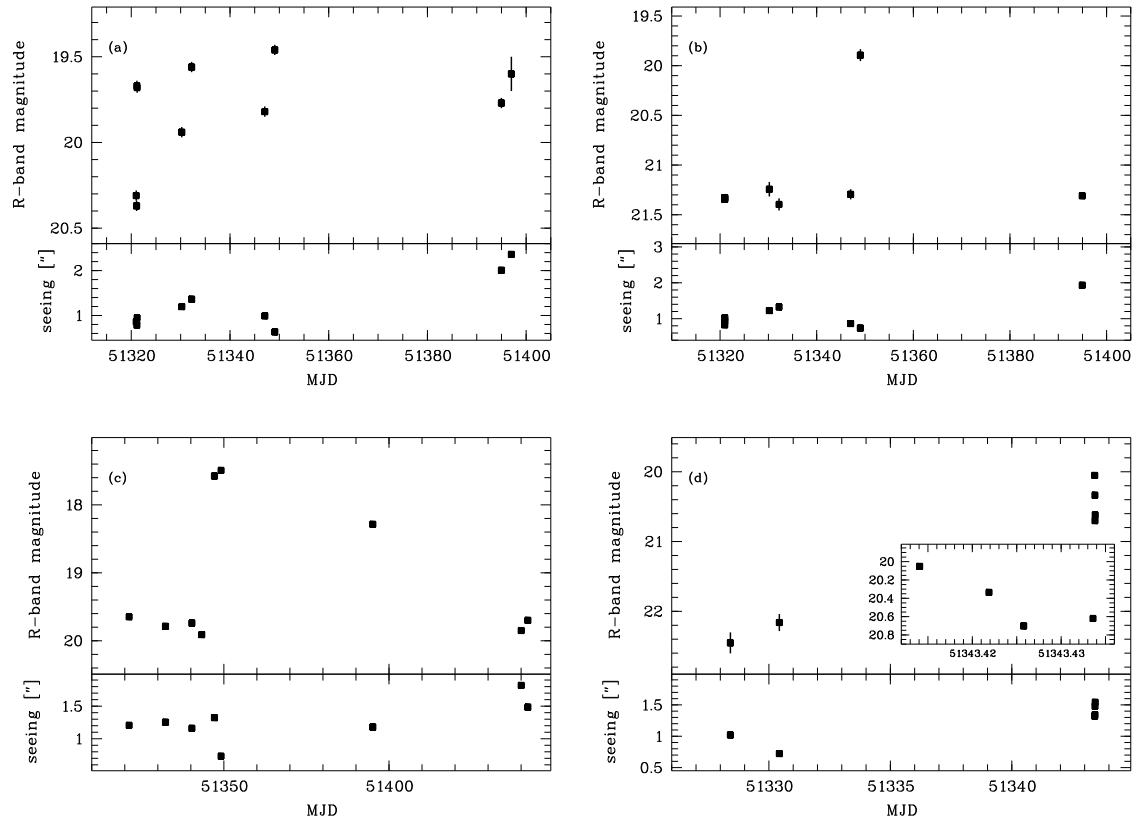

Figure 5.5. Light curves of the four transient source candidates (top) and seeing evolution (bottom). Error bars are smaller than the symbol size if not visible. **top left:** The candidate cataclysmic variable J132653.8-212702. **top right:** J132813.7-214237, extragalactic transient candidate. **bottom left:** J161953.3+031909, a dwarf nova. **bottom right:** J215406.6-274226, a possible flare star or afterglow candidate. The inset shows the detailed light curve at the time of the flare.

J132813.7-214237

The source was detected on June 20.07 UT 1999 (MJD 51349.0430) at it's maximum brightness of R=19.9 (Fig. 5.5b). Unfortunately, the observing period finished after the observation of the outburst and the next R-band pointing was performed more than six weeks later on August 04. Thus, a decay of the source could not be monitored. A faint (R=21.3) persistent point source was found at the position of the transient in images taken before and after the outburst. The ROSAT All-sky survey did not show a source at the position of J132813.7-214237 at 3σ flux upper limit of 5.5×10^{-13} erg cm^{-2} s^{-1}. Similarly, no counterpart was found in the SIMBAD and NED databases. The object is visible near the limiting magnitude of the DSS in the B and R-band and not detected in the DSS I-band. A detailed analysis revealed that the transient source was offset by $\sim0\farcs8$ from the position of the persistent counterpart (Fig. 5.6). This might suggest an extragalactic origin of the transient assuming the persistent counterpart can be associated with a candidate host galaxy. Nevertheless, this vague assumption based in the available observational data requires a confirmation by an accurate distance measurement.
The lacking observational coverage of the the decay light curve of J132813.7-214237 leaves the identification of the origin of the source an open question. Assuming the extraggalactic nature of the faint persistent source, the flaring source could for e.g., be associated with a supernova explosion occuring in this galaxy. The brightening of $\sim$1.5 mag in $\sim$2 days is very steep compared to observerd supernova though (Leibundgut et al. 1991). Another explanation is that of a forground flares stare close to the line of sight towards the persistent background sources. Furthermore, J132813.7-214237 might be a potential orphan afterglow. In order to test this hypothesis we searched for triggered GRBs which occurred during the time between the preceding observation (June 18.05 UT) and the outburst. We found 5 cataloged[8] GRBs during this period (BATSE #7609 & 7610 and IPN #2066, 2067 & 2069; K.Hurley, private communication). None of those has a position consistent with J132813.7-214237 which allows to exclude an association with a triggered GRB. Regardless, J132813.7-214237 can also be due to an untriggered or orphan afterglow and is the best such candidate found during our survey.

J161953.3+031909

This candidate was detected as a constant source (R=19.9) during the first four observations of the field F4 in May and June 1999 and exhibited a sudden brightening by ΔR=2.4 mag between the pointings on June 14.29 UT (MJD 51343.2950) and June 17.14 UT (Fig. 5.5c). The following observation on June 19.15 UT showed the source unchanged and later observations indicate a subsequent decay over 50–90 days back to the quiescent brightness. The optical light curve suggests the classification of J161953.3+031909 as a dwarf nova. This is strengthened by the detection of a faint X-ray source in the ROSAT all-sky survey. During an exposure of 320 sec on August 12/13, 1990 a total of 9 source photons were detected, corresponding to a mean vignetting-corrected count rate of 0.033 cts s^{-1} (this is below the significance threshold of the all-sky survey catalog, so this source is not contained in the

[8] http://grbcat.gsfc.nasa.gov/grbcat/grbcat.html

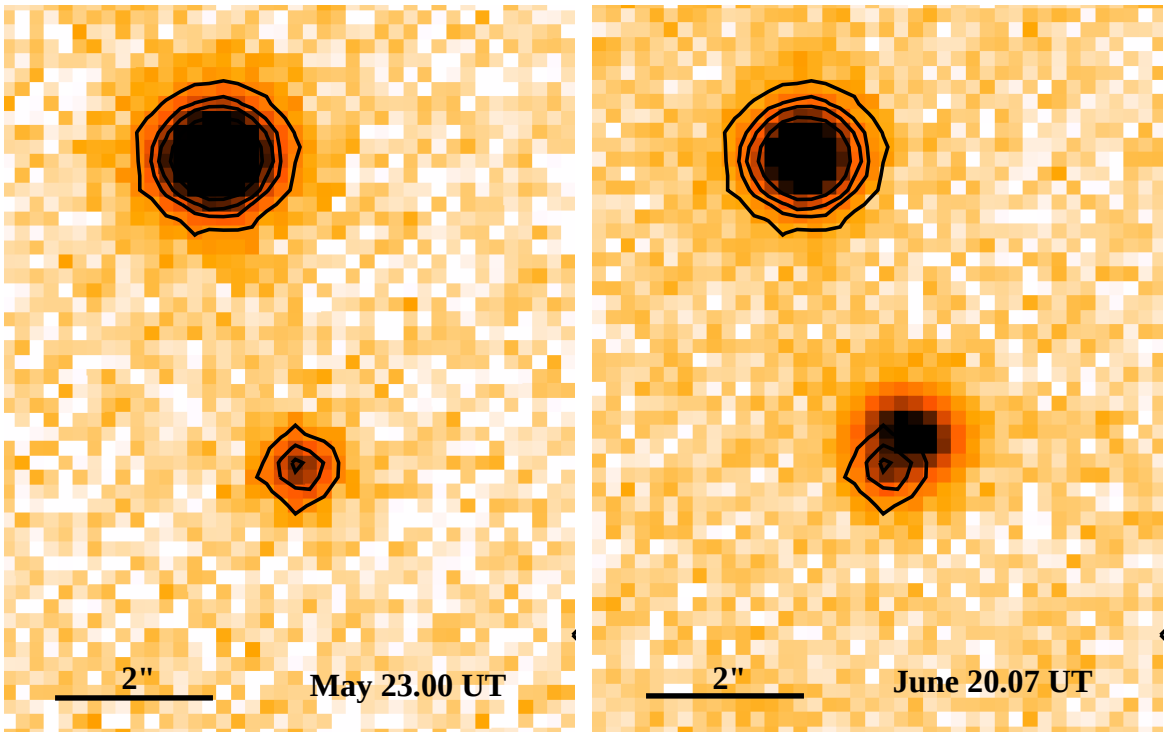

Figure 5.6. left: Image of of the J132813.7-214237 (center source) and a nearby bright star from an observation taken on May 23.00 UT when the source had a brightness of R=21. Flux contours are overplotted for both objects. North is up and East to the left. **right:** Same field observed on June 20.07 UT together with the flux contours from May 23.00 UT. The flaring source shows an offset of $\sim 0\farcs8$ with respect to the quiescent counterpart.

1RXS catalog of Voges et al. 1999). Adopting a thermal bremsstrahlung model with 1 keV temperature and half of the Galactic foreground absorption, an unabsorbed flux in the 0.1-2.4 keV band of $(7.0\pm1.0)\times10^{-13}$ erg cm^{-2} s^{-1} (or $(9\pm2)\times10^{-13}$ erg cm^{-2} s^{-1} bolometric) is derived. Using the quiescent optical brightness, this implies a ratio of L_X/L_{opt} = 0.6, consistent with SU UMa stars (Verbunt et al 1997). With an X-ray luminosity of 1.1×10^{32} [D/1 kpc] erg s^{-1}, the implied distance is of order a few hundred parsec. No entry was found in the SIMBAD and NED databases.

J215406.6-274226

This source was initially detected in two epochs of the field F7 as a faint object with R=22.5 (Fig. 5.5d). On June 14.41 UT 1999 (MJD 51343.4150) it was found ΔR=1.9 mag brighter than previously measured. Fortunately, during this night four images of the field were taken and the rapid fading of J215406.6-274226 by ΔR=0.7 mag in around 20 min, corresponding to a decay with t^{-1}, was discovered (inset of Fig. 5.5d). Unfortunately, the further fading could not be monitored as the position of the source fell into the gap between two CCDs for the following twelve pointings. While the rapid decay would be consistent with the observations of early GRB afterglows, also a flare star offers a possible explanation. Given the range of absolute magnitudes for nearby M-dwarfs of M_V=12–16 (Reid et al. 1995) the observed quiescent brightness would place J215406.6-274226 at a distance of 0.2–1.2 kpc.

No X-ray or optical counterpart was detected in the ROSAT All-Sky survey and SIMBAD or NED, respectively. No source is detected in the DSS *B* and *R*-band images but a faint source ($\sim 7\sigma$) is visible in the DSS *I*-band. The quiescent counterpart could not be resolved and further observational effort is required for a more solid classification of the object.

5.4 Efficiency for orphan afterglow detection

The detection efficiency for on-axis optical afterglows was estimated using a set of Monte-Carlo simulations folded with the observing schedule of the survey. We simulated afterglows with random sky coordinates, light curve parameters and explosion times distributed over the periods in which observations were taken. For all afterglows with positions inside one of the monitored fields, the expected magnitudes of the afterglows in the first and second observation of the field after the burst were calculated.

The afterglow light curves were described by a broken power law and parameterized by the pre-break slope, α_1, break time, t_b, post-break slope, α_2 and initial *R*-band magnitude, R_{in}. The initial magnitude corresponds to the brightness with which an afterglow is created. A relatively flat decay plus a steeper flux decrease after the jet break is typically observed for optical afterglows associated with detected long-duration GRBs and is also expected for on-axis orphans as well as "regular" afterglows of untriggered bursts. As described earlier, off-axis orphans will show a different behavior. They are expected to be fainter than on-axis orphans at early times and follow the post-break decay of on-axis afterglows after an initial phase of re-brightening. It appears safe to assume that on-axis afterglows will be the majority at a limiting magnitude of R=19–21 and off-axis orphans will dominate only at lower magnitudes (Nakar & Piran 2003). As the survey strategy foresees to consider only sources as candidate orphans with at least two detections spaced by two nights, off-axis orphans with maximum brightness of $R>21$ will in most cases be to faint to be identified. While bright off-axis orphans could in principle have been detected in the survey, we do not include them in the simulations and focus solely on untriggered and on-axis orphans.

The expected number of detected afterglows in the survey depends on the choices for α_1, α_2, t_b and R_{in}. The ranges for the slopes and break time were obtained from observed light curves of 38 optical afterglows compiled in Zeh et al. (2005). Accordingly, we used Gaussian distributions for $-1.8<\alpha_1<-0.4$ and $-2.8<\alpha_2<-1.4$ and an uniform distribution for t_b ranging from 0.4–4 days. The most influencing parameter for the outcome of the simulations is the initial magnitude of an candidate afterglow. Rapid optical follow-up observations of BATSE bursts with LOTIS and ROTSE-I (Park et al. 1999; Akerlof et al. 2000; Kehoe et al. 2001) and recent *Swift*/UVOT detections indicated that the preponderance of early afterglows does not get brighter than $R\sim 14$. Furthermore, *HETE-2* follow-up and UVOT observations showed that around 50 % of the afterglows might be brighter than $R\sim 18.5$ for 30 minutes after the burst (e.g., Lamb et al. 2004).

In order to test the influence of the limits of R_{in} on the expected number of afterglows in the survey, we performed two simulations with 10^6 bursts per year and full sky, each. The initial magnitudes were uniformly distributed between $9<R_{in}<20$ and $13<R_{in}<23$, respectively. In addition, a distribution proportional to $0.2\times R_{in}$ in the range of $13<R_{in}<23$ was simulated.

The latter corresponds to the observations of afterglows presented in Zeh et al. (2005) and is expected to reproduce the reality more closely than an uniform distribution. Each simulation was repeated 10^3 times and the mean detection rates at a given *R*-band magnitude were obtained.
The results of the simulations are presented in Figure 5.7. Here we show the normalized (devided by the total number of simulated events) probability for a first-time detection of a simulated afterglow brighter than a given magnitude. The normalized probability represents the chance to detect the afterglow in a simulation with one single event over the year and full sky. The expectation for a second observation of a candidate afterglow for the model with non-uniform distribution of R_{in} is included as well. Naturally, the probability to detect an afterglow increases with the depth of the survey. More transients are expected to be detected above a certain magnitude for afterglow models with brighter R_{in}. Due to the lower number of bright afterglows and the increasing probability with diminishing initial brightness, the non-uniform distribution gives the lowest expectation rates. At the limiting magnitude of the survey of $R\sim23$ the probability to detect a random afterglow in at least one observation is approximately 3×10^{-7}. The detection rate of events in at least two consecutive observations is lower by a factor of ~3. In the more optimistic models, the probability for a single detection reaches up to 2×10^{-6}.

5.5 Discussion

The Monte Carlo simulations described in the previous section provide us with the number of afterglows (per year and full sky), N_{MC}, which correspond to the probability of identifying one event in two consecutive observations of the survey. For the three tested afterglow parameterizations we find values between N_{MC}=1.5$\times10^6$ and N_{MC}=1$\times10^7$.
Throughout the survey, four unidentified optical transients were discovered and one of these sources shows indications for an extragalactic origin (see Sect. 3.1.2). Nevertheless, the flaring of the source was only detected in a single observation and thus the fading could not be monitored. An unambiguous identification of the transient with a GRB afterglow is therefore not possible which leaves us with the result of having no clear orphan or untriggered afterglow detected in the data. Therefore, N_{MC} obtained from the simulations can be interpreted as an upper limit on the true number of on-axis afterglows per year and full sky. For $N>N_{MC}$ one or more on-axis orphans would have been expected in the data.
As advertised earlier, on-axis orphan afterglows can be used to place a constraint on the collimation of the optical afterglow emitting region relative to the collimation of the γ-ray emitting jet. The collimation factor, f_c, corresponds to the ratio of the true rates of on-axis optical afterglows, N_A, and long-duration GRBs which produce observable optical afterglows, N_γ, pointed at the Earth. With $N_{MC}>N_A$, an upper limit for the collimation can be derived from $f_c<N_{MC}/N_\gamma$. Obtaining N_γ is not trivial as several uncertain factors influence the number of GRBs for which afterglows are in principle detectable. In a simplified model N_γ can be written as

$$N_\gamma = N_{\gamma,obs} \cdot f_X \cdot f_D \cdot f_S \tag{5.1}$$

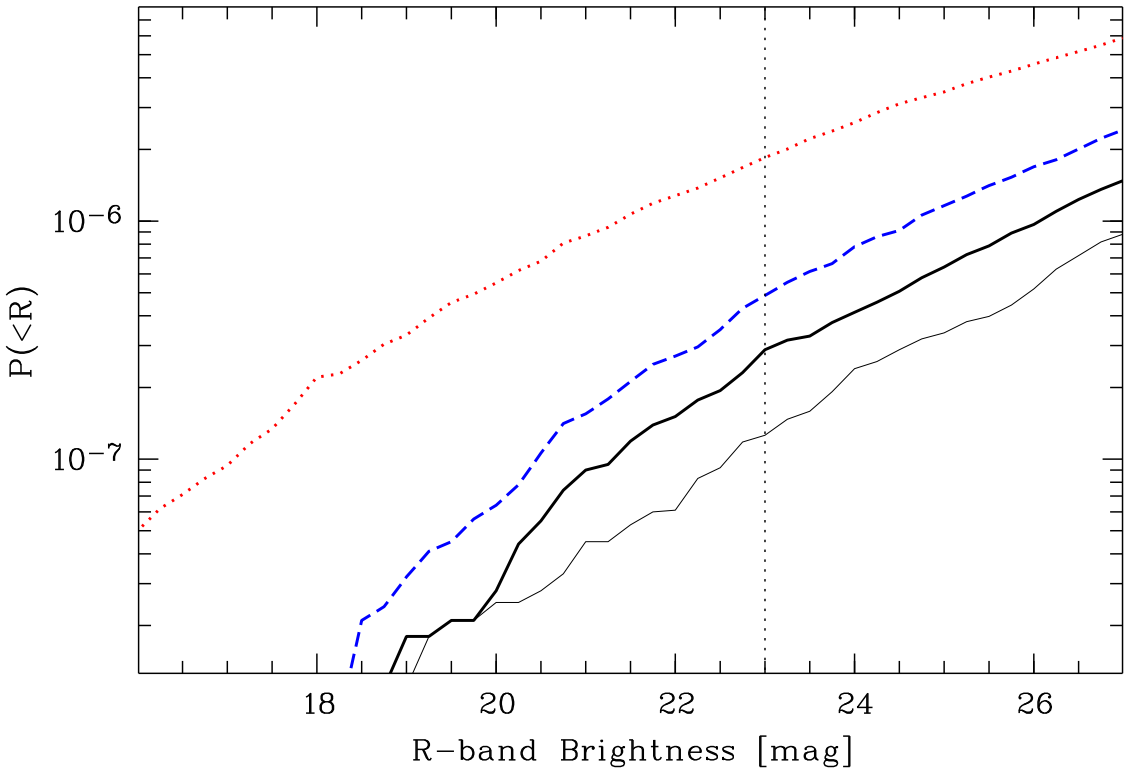

Figure 5.7. Probability distributions for the detection of a random afterglow for three different models of the initial brightness. The dotted and dashed functions represent uniform distributions of R_{in}=9–20 and R_{in}=13–23, respectively. The thick and thin solid lines correspond to the first-time and second-time observations for a distribution proportional to $0.2\times R_{in}$ in the range of R_{in}=13–23. The vertical dotted line marks the limiting magnitude of the presented survey.

where $N_{\gamma,obs}$ is the observed rate of long-duration GRBs with a specific γ-ray instrument corrected for sky coverage, f_X corrects for events outside the instrument's energy range, f_D is the correction factor for optically dim or dark afterglows of long-duration bursts (e.g., intrinsically faint, absorbed, high-z)and f_S corrects for possible afterglows associated with short bursts. Using the full sky GRB rate measured with BATSE of $\sim$666 yr^{-1} (Paciesas et al. 1999) and correcting for the ratio of long to short bursts (2:1; Kouveliotou et al. 1993), we obtain $N_{\gamma,obs}\sim$444. The *HETE-2* population of high energy bursts revealed a composition of X-ray flashes (Heise et al. 2001), X-ray rich bursts and "normal" GRBs in equal parts (Lamb et al. 2005). X-ray flashes and X-ray rich bursts show similar afterglows as observed for GRBs but have softer prompt emission spectra. As BATSE was less sensitive at lower energies than *HETE-2* a fraction of these events might have been missed. This could require a correction factor as large as f_X=2.

In general, not for all rapidly followed GRBs an associated optical transient can be found. Some detected afterglows were faint already early on and would have fallen below the limiting magnitude reached in our survey. The fraction of these events was found to be of the order of 10 % (e.g., Lamb et al. 2004; Jakobsson et al. 2004; Rol et al. 2005) which provides $f_D\sim$0.9. Only recently the first optical transients of short-duration GRBs were found (Price

et al. 2005a; Gal-Yam et al. 2005). Theory and observations hint that these afterglows are significantly fainter than the counterparts of long-duration bursts. Therefore, we neglect the influence of short burst afterglows and apply f_S=1.
Using the assumptions discussed above together with N_{MC}=1×10^7 we derive N_γ∼800 and f_C<12500 accordingly. This rather conservative upper limit is significantly higher than the beaming correction derived by Guetta et al. (2005) and Frail et al. (2001) of 75±25 and 500, respectively. The γ-ray beaming factor corresponds to the ratio of the overall rate of GRBs to the detected burst rate and should be an upper limit for f_C (corresponding to the case of isotropic afterglow radiation).
The high upper limit on f_C shows that the effective coverage of the performed observations were not sufficient to provide a strong constraint for the collimation. An approximately 25 times larger portion of the sky (∼325 deg^2) would have been required to reduce f_c to less than 500, assuming no orphan afterglow detection. We performed a further Monte Carlo simulation in order to estimate the properties for an "ideal" survey assuming a schedule of one observation per field every two nights over 150 nights with a limiting magnitude of R=23. We find that f_C<500 (<75, <10) would be reached with such a configuration and a 50 deg^2 (300 deg^2, 2500 deg^2) field. Although ambituous, a program like this is in the range of the near-future instrumentation (e.g., VLT Survey Telescope and Visible & Infrared Survey Telescope for Astronomy) which encourages to perform a comprehensive search for untriggered GRBs in the near future. In addition, spectroscopic follow-up observations of candidate orphans would be important to distinguish between afterglows and other optical transients.
The non-detection of an afterglow also provides a limit on the rate of other explosive events with similar fading behaviour. This includes events with minor or quashed high energy emission like failed GRBs (Huang et al. 2002) or so-called "dirty fireballs" (Dermer et al. 1999).

5.6 Conclusion

We presented the data reduction, analysis and results of an *R*-band survey dedicated to slowly variable optical transients. The survey strategy was designed specifically to search for afterglows of untriggered gamma-ray bursts. 12 deg^2 were monitored in up to 25 nights down to a limiting magnitude of R=23. Throughout the survey, four previously unknown transients were discovered. Based on the limited photometric data only putative classifications of the candidates could be obtained so far. The observations of three of the transients suggest them to be a cataclysmic variable, a flare star and a dwarf nova, respectively.
The fourth transient appeared in a single image as a bright source slightly offset with respect to an underlying quiesent object. The decay of the source could not be followed due to the lack of observations, thus the orgin of the transient is unresolved. However, the spatial association with the persistent source suggests an extragalatic origin. The steep brightness increase of ∼1.5 mag in ∼2 days appears a-typical for a supernova and thus makes the detected flaring source the best candidate for an orphan afterglow in our survey.
Simulations of the transient detection efficiency of the survey showed that the effective sky

coverage was not sufficient to obtain a strong constraint on the collimation of the optically emitting GRB outflow from the non-detection of suitable counterparts. Nevertheless, we found that a similar programs like the one described in this paper are feasible to be performed in the near future. Limits on the collimation ratio of the X-ray to gamma-ray emitting regions were already obtained in the past and strong ratios ($>$8) were ruled out (Grindlay 1999; Greiner et al. 1999). Tighter constrains on the optical emitting region will become available soon as well with the use of large dedicated surveys.

Acknowledgments: We thank the many observers who have assisted in the completion of this survey, including M. Braun, D. Clowe, J. Eislöffel, J. Fried, P. Heraudeau, R. Klessen, T. Kranz, I. Lehmann, R. Schmidt, C. Wolf, D. Woods and the helpful night assistants at La Silla. The WFI is a joint project between the European Southern Observatory, the Max-Planck-Institut für Astronomie in Heidelberg (Germany) and the Osservatorio Astronomico di Capodimonte in Naples (Italy). We thank Mario Radovich (INAF - Osservatorio Astronomico di Capodimonte) for making the WIFIX image reduction and astrometry package publicly available.

Chapter 6
Epilogue

In the preceding pages, the reader was given insight into three observational aspects of gamma-ray bursts. Following the arrival time sequence of signatures from these cosmological explosions, the prompt and afterglow emission as well as the host galaxy properties were investigated. A conclusion to each individual topic was already included at the end of the respective chapters, but a short wrap-up will be given here for the sake of completeness. The epilogue will be closed by a (personally biased) outlook into the near future of GRB research.

At first, the initial signature of a GRB, the prompt gamma-ray emission, believed to arise in internal shocks in ultra-relativistic collimated outflows, was studied based on the sample of events detected with the anti-coincidence shield of the *INTEGRAL* spectrometer SPI. SPI-ACS was shown to be successfully operating as an omnidirectional GRB detector above $\sim$80 keV. During the first 26.5 months of the mission, 236 burst candidates were detected and their properties were compiled in the first SPI-ACS GRB catalogue. For 179 SPI-ACS triggers a high-energy cosmic origin could be confirmed by observations with other gamma-ray instruments connected in the Interplanetary Network. Beside the known duration bimodality of long ($>$2 s) and short-bursts ($<$2 s), a large number ($>$150) of spurious very short ($<$100 ms) events was detected. I demonstrated that the origin of this population ($\sim$40% of the total sample) is significantly different from the that of the regular GRB sample, as shown both by the log$N$–logC_{max} distribution as well as by the $<V/V_{max}>$ test. The very short population appears consistent with a homogeneous distribution in an Euclidean space while events longer than 0.25 s show a deviation from homogeneity detected already for the BATSE bursts sample. Observations of simultaneous saturations in the spectrometer Germanium detectors and very short events in the SPI-ACS overall rate suggest a cosmic ray origin for a significant fraction of these events. Discounting the very short event population, the short burst distribution appears more as an extension of the long burst distribution to shorter durations rather than as a separate population.

In the second part of the thesis, I moved the focus from the high-energy prompt emission to the afterglow phase and underlying host galaxies, studied at optical and near-IR wavelengths. As example event for this part of the study I used the optically dark GRB/XRF 030528. I have demonstrated that observations in the near-IR range hold the promise to detect afterglows that escape in the optical band because of possible reddening. Despite the success of the discovery of the afterglow of GRB/XRF 030528 coverage was insufficient to establish a well sampled light curve and to derive an accurate redshift from photometry only. Accordingly, spectroscopy of the host was proposed and performed using the ESO VLT

FORS2 instrument. From the prominent oxygen and hydrogen emission lines a redshift of z=0.782±0.001 was obtained. Estimating the line luminosities and line ratios I showed that the observations of the host were consistent with that of an actively star forming galaxy with sub-solar metalicity, in agreement with theoretical predictions for the progenitor models of long duration bursts. With a stellar mass of $\sim 10^{10}\,M_{\odot}$ the host is placed among the most massive GRB host galaxies at a similar redshift.
Estimating the redshifted properties of the prompt emission, I showed that GRB/XRF 030528 would be classified as an X-ray rich burst in the rest frame rather than an X-ray flash in the typically-used observer frame. The physical motivation of the classification scheme of X-ray flashes, X-ray rich bursts and gamma-ray bursts in the observer frame seems therefore questionable and at best operational. As there are strong indications that the three classes form continua in their intrinsic and observed properties, already the necessity of a stringent separation can be put in doubt. Instead, the differences of the observed properties certainly arise from a continuous distribution of e.g. Lorentz factors of the ejecta, contrast of the Lorentz factors between different shells, viewing angles with respect to the jet-axis or redshift.
The final part of the thesis was dedicated to a survey for slowly varying optical transients such as 'orphan' and un-triggered GRB afterglows. The collimation of the ultra-relativistic outflows of GRBs leads to the natural consequence that only those bursts will be detected via their prompt gamma-ray emission, for which the observer lies within the opening angle of the jet. Nevertheless, GRBs which are not pointed directly at the observer can in principle be discovered as orphan afterglows, as the late time emission is expected to be radiated into a larger solid angle than the gamma-rays.
The survey was performed using the Wide Field Imager at the ESO/MPG 2.2 m telescope at La Silla (Chile) and covered approximately 12 deg^2 in up to 25 nights down to a limiting magnitude of R=23. Four previously unidentified transients were discovered from which three could be putatively classified as a cataclysmic variable, a flare star and a dwarf nova, respectively. The fourth transient appeared as a flaring source slightly offset with respect to an underlying quiescent object which suggests an extragalactic origin. As the decay of the source could not be followed due to a lack of observations, a distinction between a possible super nova, flare star or an orphan afterglow could not be obtained. Respective spectroscopic identification is proposed to the ESO/VLTs (Period 77) and awaits acceptance.
On-axis orphans are considered powerful tools to constrain the ratio of the optically emitting region to the region from which the prompt high-energy emission arises. Unfortunately, simulations of the transient detection efficiency of the survey showed that the effective sky coverage was not sufficient to obtain a strong constraint on this ratio. Nevertheless, I found that similar programs, like the one described in this work but with a larger coverage, have the prospect of leading to more stringent constraints on the collimation of GRB outflows in the near future.

Our knowledge of gamma-ray burst improved and still improves rapidly thanks to dedicated missions such as the *HETE-2* and *Swift* satellites. Thus, a present outlook of the prospects of GRB related research in the coming years might quickly be doomed of being outdated. Rather than giving you a comprehensive list of questions which will be raised and the methods to reveal their answers, I would only like to touch upon a small number of observational

issues in which I am personally interested in and that are in some way connected to the topics approached in this thesis.

Presently, the *INTEGRAL* mission is planned to continue until at least 2008, thus, SPI-ACS is expected to monitor the sky for the prompt emission of GRBs at least until this time. Although the number of accurate burst triangulations decreased since the shutdown of the *Ulysses* GRB detector in December 2003, SPI-ACS will further collect valuable data of gamma-ray transients. Its value was also demonstrated by the detection of the super outburst of the soft gamma-ray repeater SGR 1806-20 in December 2004. SPI-ACS was the first instrument for which the detection was reported to the community (Borkowski et al. 2004; Mereghetti et al. 2005). We detected also a large number of fainter SGR outbursts, successfully triangulated with the help of the IPN instruments and Helicon/Coronas-F, with the prospect of continuation over the rest of the mission. My analysis of the GRB sample showed among others that the short burst population of SPI-ACS appeared to be less prominent than expected from the BATSE mission. My result was based on the data of the first 2 years after the launch of *INTEGRAL* and suffers from a limited statistics. An analysis of the GRB sample of the entire mission, together with a detailed modelling of the expected rate of short bursts based on the BATSE spectral data and the SPI-ACS sensitivity, will reveal its significance.

BATSE studied the prompt emission in the 'standard' energy range of 50–300 keV in large detail and not much more new insight is expected here to come. On the other side, a number of open questions both for the lower and higher energies are still unsolved and might offer surprises in the near future. It has been proposed that ultrahigh energy (10^{19} eV) cosmic rays are accelerated by the blast waves associated with GRBs and that the synchrotron spectrum from protons and energetic leptons formed in the cascades initiated by photopion production could be detected with the *Gamma-ray Large Area Space Telescope* (GLAST) with launch anticipated in 2007 or with ground-based air Cherenkov telescopes like the *Antarctic Muon and Neutrino Detector Array* (AMANDA) or *IceCube*. The temporal decay of the induced high-energy gamma-ray afterglows is significantly slower than that of the primary electron synchrotron and associated synchrotron self-Compton radiation and thus provides a direct way to test the hadronic origin of a high-energy GRB afterglow.

At energies below the BATSE range, *BeppoSaX* and *HETE-2* probed already the nature of X-ray flashes. While the continuum of GRBs, XRRs and XRFs is now statistically confirmed, the question about the extent of this peak energy distribution arises. Is there a population of GRB-like bursts with peak energies in the ultraviolet range or even below that? Does the continuation expands all the way down from hard GRBs to optical transients associated with core collapse supernovae? What defines the 'fundamental plane' (if it exists) of these events? Can the appearance of an GRB-like event be predicted based on the spin, mass and metallicity of the progenitor and the distance and viewing angle of the observer with respect to the rotational axis, or which other 'ingredients' are required?

One of the major future applications of GRBs will be their use as probes of the very early Universe. A grand challenge in modern cosmology is posed by the question of how the first stars formed and what their impact was on the cosmic history. As the bright gamma-ray emission easily penetrates the Universe and reaches the observer from very high redshifts

(even beyond the re-ionization epoch), the detection of high-z bursts will allow to study their birthplaces and the begin of stellar, galaxy and structure formation. Opposite to Quasars, the GRB afterglow brightness decreases only mildly with redshift due to cosmic time dilation and favorable K-correction. Measuring the afterglow flux shortwards of the Lyman limit will help to constrain directly the epoch when the Universe was re-ionized.
In order to detect and identify high redshift bursts, dedicated instrumentation is required. NASA's *Swift* satellite provides accurate and rapid localizations for roughly 100 bursts per year. Out of these, less than a handful is expected to originate from $z>6.5$, thus, rapid identification is important in order to organize the best fitting follow-up strategy of the few high-z bursts with large optical and near-IR telescopes. The *Gamma-ray Burst Optical/Near-IR Detector* (GROND)[1] will investigate gamma-ray burst afterglows and other transients simultaneously in seven filter bands, thus ensuring rapid photometric redshifts with up to 0.5 z-accuracy in the range of $3.5<z<13$. Several dichroic beamsplitters will feed light into three NIR channels and four visual channels, each equipped with its own detector. GROND is expected to become operational in 2006 at the 2.2 m ESO/MPG telescope at La Silla.
The final point which I like to mention is the prospect for large surveys for untriggered and orphan afterglows of GRBs. Near-future instrumentation like the *VLT Survey Telescope* (VST) and the *Visible & Infrared Survey Telescope for Astronomy* (VISTA), both with a 1 deg^2 field of view, will allow to compile large sky surveys with possible first light in 2006 and 2007, respectively. I showed in Chapter 5 that already one observation every second night over 150 nights covering a 2500 deg^2 down to a limiting magnitude of R=23, would have the prospect of constraining the ratio of optical to gamma-ray emitting outflow to a value of $\sim$10. Although ambitious, these programs are in range and will allow to gain more insight into the collimation and beaming of GRB outflows.

[1] GROND is currently build by the MPE (PI: J. Greiner) in collaboration with the LSW Tautenburg and will be installed at ESO in 2006.

References

Akerlof, C., Balsano, R., Barthelmy, S., et al. , *ApJ*, **532**, L25 (2000)
Amati, L., Frontera, F., Tavani, M., et al. , *A&A*, **390**, 8 (2002)
Andersen, M.I., Hjorth, J., Pedersen, H., et al. , *A&A*, **364**, L54 (2000)
Atteia, J-L., Kawai, N., Lamb, D., et al. , *GCN*, **2256** (2003)
Atteia, J-L., *A&A*, **407**, L1 (2003)
Ayani, K., & Yamaoka, H., *GCN*, **2257** (2003)
Band, D., Matteson, J., Ford, L. et al. , *ApJ*, **413**, 281 (1993)
Barraud, C., Olive, J.-F., Lestrade, J.P., et al. , *A&A*, **400**, 1021 (2003)
Barraud, C., Daigne, F., Mochkovitch, R., & Atteia, J.-L., *A&A*, **440**, 809 (2005)
Becker, A.C., Wittman, D.M., Boeshaar, P.C., et al. , *ApJ*, **611**, 418 (2004)
Bell, E.F., Papovich, C., Wolf., C., et al. , *ApJ*, **625**, 23 (2005)
Bender, R., Appenzeller, I., Böhm, A., *in ESO/ECF/STScI Workshop on Deep Fields*, ed. S. Christiani (Berlin:Springer), 327 (2001)
Berger, E., Cowie, L.L., Kulkarni, S.R., et al. , *ApJ*, **588**, 99 (2003)
Bersier, D., McLeod, B., Garnavich, P.M., et al. , *ApJ*, **583**, L63 (2003)
Bhat, P.N., Fishman, G.J., Meegan, C.A., et al. , *Nature*, **359**, 217 (1992)
Bloom, J.S., Diercks, A., Kulkarni, S.R., et al. , *GCN*, **480** (1999)
Bloom, J.S., Frail, D.A & Sari, R., *AJ*, **121**, 2879 (2001)
Bloom, J.S., Kulkarni, S.R., & Djorgovski, S.G., *AJ*, **123**, 1111 (2002)
Bloom, J.S., Fox, D., van Dokkum, P.G., et al. , *ApJ*, **599**, 957 (2003)
Bloom, J.S., Perley, D., Foley R., et al. , *GCN*, **3758** (2005)
Bogosavljevic, M., Mahabal, A., & Djorgovski, S.G., *GCN*, **2275** (2003)
Bolzonella, M., Miralles, J.-M., Pello, R., *A&A*, **363**, 476 (2000)
Borkowski, J., Götz, D., Mereghetti, S., et al. , *GCN*, **2920**, (2004)
Brinchmann, J., & Ellis, R.S., *ApJ*, **536**, L77 (2000)
Brocklehurst, M., *MNRAS*, **153**, 471 (1971)
Bruzual, G. & Charlot, S., *ApJ*, **405**, 538 (1993)
Burud, I., Rhoads, J., Fruchter, A., & Griep, D., *GCN*, **1283** (2002)
Butler, N., Dullighan, A., Ford, P., et al. , *GCN*, **2269** (2003a)
Butler, N., Dullighan, A., Ford, P., et al. , *GCN*, **2279** (2003b)
Butler, N., Dullighan, A., Ford, P., et al. , *in AIP Conf. Proc. 727: Gamma-Ray Bursts: 30 Years of Discovery*, p.435 (2004)
Castro-Tirado, A.J., Gorosabel, J., Guziy, S., et al. , *A&A*, **411**, L315 (2003)
Cavallo, G. & Rees, M.J., *MNRAS*, **183**, 359 (1978)

Chary, R., Neugebauer, G., Morris, M., et al. , *ApJ*, **498**, L9 (1998)
Chary, R., Becklin, E.E., & Armus, L., *ApJ*, **566**, L229 (2002)
Christensen, L., Hjorth, J., Gorosabel, J., *A&A*, **425**, 913 (2004)
Cline, D. B., Matthey, C. & Otwinowski, S., *APh*, **18**, 531 (2003)
Coburn, W., & Boggs, S.E., *Nature*, **423**, 415 (2003)
Colgate, S.A., *Canadian Journ. of Phys.*, **46**, 476 (1968)
Costa, E., Frontera, F., Heise, J., et al. , *Nature*, **387**, 783 (1997)
Courty, S., Bjrnsson, G., Gudmundsson, E.H., *MNRAS*, **354**, 581 (2004)
Covino, S., Lazzati, D., Ghisellini, G., et al. , *A&A*, **348**, L1 (1999)
Covino, S., Malesani, D., Tavecchio, F., et al. , *A&A*, **404**, L5 (2003)
Cowie, L.L., Songaila A., Hu, E.M., & Cohen, J.G., *AJ*, **112**, 389 (1996)
Dahlen, T., Mobasher, B., Somerville, R.S., et al. , *ApJ*, **631**, 126 (2005)
Dalal N., Griest, K., & Pruet, J., *ApJ*, **564**, 209 (2002)
Dermer, C.D., Chiang, J., & Böttcher, M., *ApJ*, **513**, 656 (1999)
Dermer, C.D., astro-ph/0202254 (2002)
Devillard, N., The Messenger **87**, 19 (1997)
Dezalay, J.-P., Lestrade, J., Barat, C., Talon, R., Sunyaev, R., Terekhov, O., & Kuznetsov, A., *ApJ*, **471**, L27 (1996)
Di Paola, A., Speziali, R., Antonelli, L.A., et al. , *GCN*, **816** (2000)
Di Paola, A., Boattini, A., Del Principe, M., et al. , *GCN*, **1616** (2002)
Djorgovski, S.G., Frail, D.A., Kulkarni, S.R., et al. , *ApJ*, **562**, 654 (2001)
Djorgovski, S.G., Kulkarni, S.R., Frail, D.A., et al. , in *Discoveries and Research Prospects from 6-10m Class Telescopes*, ed. P. Guhathakurta, Proc. SPIE, vol. 4834, (2003)
Drory, N., Bender, R., Feulner, G., et al. , *ApJ*, **595**, 698 (2003)
Dullighan, A., Ricker, G., Butler, N., & Vanderspek, R., *in AIP Conf. Proc. 727: Gamma-Ray Bursts: 30 Years of Discovery*, p.467 (2004)
Duncan, R.C. & Thompson, C., *ApJ*, **392**, L9 (1992)
Dutra, C.M., Ahumada, A.V., Claria, J.J., Bica, E., & Barbuy, B., *A&A*, **408**, 287 (2003)
Eichler, D., Livio, M., Piran, T., & Schramm, D.N., *Nature*, **340**, 126 (1989)
Fabbiano, G., *ARA&A*, **27**, 87 (1989)
Farukhi, M. R., *IEEE* Vol. NS-29, p.1237 (1982)
Feulner, G., Gabasch, A., Salvato, M., et al. , *ApJL* submitted (2005)
Fishman, G. J., Meegan, C. A., Parnell, T. A., et al. , *GSFC 19th Intern Cosmic Ray Conf.*, Vol 3, p.343 (1985)
Fishman, G. J., Meegan, C. A., Wilson R. B., et al. , *in Proc. of the GRO Science Workshop, GSFC*, 2 (1989)
Fishman, G. J., Meegan, C. A., Wilson, R. B. et al. , *ApJS*, **92**, 229 (1994)
Fishman, G. J. & Meegan, C. A., *ARA&A*, **33**, 415 (1995)
Fox, D.W., Kaplan, D.L., Cenko, B., Kulkarni, S.R., & Nechita, A., *GCN*, **2323** (2003a)
Fox, D.W., Price, P.A., Soderberg, A.M., et al. , *ApJ*, **586**, L5 (2003b)
Fox, D.B., *GCN*, **2630** (2004)
Frail, D.A., Kulkarni, S.R., Nicastro, S.R. et al. , *Nature*, **398**, 261 (1997)
Frail, D.A., Kulkarni, S.R., Sari, R. et al. , *ApJ*, **562**, L55 (2001)

Frail, D.A., & Berger, E., *GCN*, **2270** (2003)
Fruchter, A., Thorsett, S.E., Metzger, M.R., et al. , *ApJ*, **519**, L13 (1999)
Fynbo, J.P.U., Jensen, B.L., Gorosabel, J., et al. , *A&A*, **369**, 373 (2001a)
Fynbo, J.P.U., Gorosabel, J., Dall, T.H., et al. , *A&A*, **373**, 796 (2001b)
Fynbo, J.P.U., Jakobsson, P., Møller, P., et al. , *A&A*, **406**, L63 (2003)
Fynbo, J.P.U., Sollerman, J., Hjorth, J., et al. , *ApJ*, **609**, 962 (2004)
Galama, T.J., Vreeswijk, P.M., van Paradijs, J., et al. , *Nature*, **395**, 670 (1998)
Galama, T.J. &, Wijers, R.A.M.J., *ApJ*, **549**, L209 (2001)
Galama, T.J., Reichart, D., Brown, T.M., et al. , *ApJ*, **587**, 135 (2003)
Gal-Yam, A., Ofek, E.O., Filippenko, A.V., Chornock, R., & Li, W., *PASP*, **114**, 587 (2002)
Gal-Yam, A., Cenko, S.B., Berger, E., Krzeminski, W., & Lee, B., *GCN*, **3681** (2005)
Garnavich, P.M., Jha, S., Pahre, M.A., et al. , *ApJ*, **543**, 61 (2000)
Ghirlanda, G., Ghisellini, G., & Lazzati, D., *ApJ*, **616**, 331 (2004)
Ghisellini, G., & Lazzati, D., *MNRAS*, **309**, L7 (1999)
Ghisellini, G., astro-ph/0301256 (2003)
Golenetskii, S., Mazets, E., Pal'shin, V. & Frederiks, D., *GCN*, **2487** (2003a)
Golenetskii, S., Mazets, E., Pal'shin, V. & Frederiks, D., *GCN*, **2488** (2003b)
Goodman, J., *ApJ*, **308**, L47 (1986)
Gorosabel, J., Castro-Tirado, A.J., Willott, C.J., et al. , *A&A*, **335**, L5 (1998)
Gorosabel, J., Fynbo, J.P.U., Hjorth, J., et al. , *A&A*, **384**, 11 (2002)
Greiner, J., Voges, W., Boller, T., & Hartmann, D., *A&AS*, **138**, 441 (1999)
Greiner, J., Peimbert, M., Esteban, C., et al. , *GCN*, **2020** (2003a)
Greiner, J., Rau, A., & Klose, S., *GCN*, **2271** (2003b)
Greiner, J., Klose, S., Salvato, M., et al. , *ApJ*, 599, **1223** (2003c)
Greiner, J., Klose, S., Reinsch, K., et al. , *Nature*, **426**, 157 (2003d)
Grindlay, J.E., *ApJ*, **510**, 710 (1999)
Groot, P.J., Galama, T.J., van Paradijs, J., et al. , *ApJ*, **493**, L27 (1998)
Gruzinov, A., *ApJ*, **525**, L29 (1999)
Guetta, D., Piran, T., Waxman, E., *ApJ*, **619**, 412 (2005)
Hakkila, J., Haglin, D. J., Pendleton, G. N. et al. , *ApJ*, **538**, 165 (2000)
Halpern, J.P., Uglesich, R., Mirabal, N., et al. , *ApJ*, **543**, 697 (2000)
Halzen, F., Zas, E, MacGibbon, J. H. & Weekes, T. C., *Nature* **353**, 807 (1991)
Harrison, F. A., Bloom, J.S., Frail, D.A., et al. , *ApJ*, **523**, L121 (1999)
Harrison, F.A., Yost, S., Fox., D.B., et al. , *GCN*, **1143** (2001)
Heise, J., in't Zand, J, Kippen, R.M., & Woods P.M., in Gamma-Ray Bursts in the Afterglow Era, ed. E. Costa, F. Frontera, & J. Hjorth (Berlin: Springer), 16 (2001)
Heger, A., Fryer, C.L., Woosley, S.E., Langer, N., & Hartmann, D.H., *ApJ*, **591**, 288 (2003)
Henden, A., *GCN*, **2267** (2003)
Hjorth, J., Bjornsson, G., Andersen, M.I., et al. , *Science*, **28**, 2073 (1999)
Hjorth, J., Thomsen, B., Nielsen, S.R., et al. , *ApJ*, **576**, 113 (2002)
Hjorth, J., Sollerman, J., Møller, P. et al. , *Nature*, **423**, 847 (2003)
Holland, S.T., Bersier, D., Bloom, J.S., et al. , *AJ*, **128**, 128 (2004)
Hopkins, A.M., Connolly, A.J., Haarsma, D.B., & Cram, L.E., *AJ*, **122**, 288 (2001)

Horvath, I., *ApJ*, **508**, 757 (1998)
Huang, Y.F., Dai, Z.G., & Lu, T., *A&A*, **355**, L43
Huang, Y.F., Dai, Z.G., & Lu, T., *MNRAS*, **332**, 735 (2001)
Hurley, K., *A&A*, **69**, 313 (1978)
Hurley, K., *in Gamma-Ray Bursts - Proceedings of the Gamma-Ray Burst Workshop - 1991*, Huntsville, AL, Eds. W. Paciesas and G. Fishman , AIP Conf. Proc. 265, p. 3 (1991)
Hurley, K., *in Proc. of the 2nd INTEGRAL Workshop, ESA SP*, 382, 491 (1997)
Hurley, K., Cline, T., Mitrofanov, I. et al. , *GCN*, **2296** (2003a)
Hurley, K., Cline, T., Mitrofanov, I. et al. , *GCN*, **2356** (2003b)
Hurley, K., Cline, T., Golenetskii, S. et al. , *GCN*, **2492** (2003c)
Jakobsson, P., Hjorth, J., Fynbo, J.P.U., et al. , *A&A*, **408**, 941 (2003)
Jakobsson, P., Hjorth, J., Fynbo, J.P.U., et al. , *A&A*, **427**, 785, (2004)
Jakobsson, P., Hjorth, J., Fynbo, J.P.U., et al. , *ApJ*, **617**, L21 (2004)
Jensen, B.L., Fynbo, J.U., Gorosabel, J., et al. , *A&A*, **370**, 909 (2001)
Johnson, H.L., *ARA&A*, **4**, 193 (1966)
Kato, D. & Nagata T., *GCN*, **1830** (2003)
Kehoe, R., Akerlof, C., Balsano, R., et al. , *ApJ*, **577**, L159 (2002)
Kelson, D.D., Koviak, K., Berger, E., & Fox, D.B., *GCN*, **2627** (2004)
Kennea, J.A., Burrows, D.N., Nousek, J., *GCN*, **3383** (2005)
Kennicutt, R.C., *ARA&A*, **36**, 189 (1998)
Kienlin, A. v. , Arend, N., Lichti, G.G., Strong, A.W. & Connell, P., in Proc. of the SPIE, Edited by J.E. Trümper & H.D. Tananbaum, Vol. 4851, pp. 1336 (2003a)
Kienlin A. v., Beckmann, V., Rau, A. et al. , *A&A*, **411**, L299 (2003b)
Kinney, A.L., Calzetti, D., Bohlin, R.C., et al. , *ApJ*, **467**, 38 (1996)
Klebesadel, R., Strong, I., & Olsen, R., *ApJ*, **182**, L85 (1973)
Klose, S., Henden, A.A., Greiner, J., et al. , *ApJ*, **592**, 1025 (2003)
Klose, S., Greiner, J., Rau, A., et al. , *AJ*, **128**, 1942 (2004)
Kobayashi, N., Goto, M., Terada, H., & Tokunaga, A.T., *GCN*, **577** (2000)
Kouveliotou, C., Meegan, C. A., Fishman, G. J. et al. , *ApJ*, **413**, L101 (1993)
Kulkarni, S.R., Djorgoski, S.G., Ramaprakash, A.N., et al. , *Nature*, **393**, 35 (1998)
Kulkarni, S.R., Djorgovski, S.G., Odewahn, S.C., et al. , *Nature*, **398**, 389 (1999)
Lamb, D.Q., & Reichart, D.E., *ApJ*, **536**, 1 (2000)
Lamb, D.Q., Ricker, G.R., Atteia, J.-L., et al. , *NewAstRev*, **48**, 423 (2004)
Lamb, D.Q., Donaghy, T.Q. & Graziani, C., *ApJ*, **620**, 355 (2005)
Landolt, A.U., AJ, **104**, 340 (1992)
Larkin, J., Ghez, A., Kulkarni, S.R., et al. , *GCN*, **51** (1998)
Lazzati, D., Covino, S., & Ghisellini, G., *MNRAS*, **330**, 583 (2002)
le Floc'h, E., Duc ,P-A., Mirabel, I.F., et al. , *A&A*, **400**, 499 (2003)
Leibundgut, B., Tammann, G.A., Cadonau, R., & Cerrito, D., *A&AS*, **89**, 537 (1991)
Li, L. & Paczynski, B., *ApJ*, **507**, L59 (1998)
Li, Z., & Chevalier, R.A., *ApJ*, **551**, 940 (2001)
Lichti, G.G., Georgii, R., von Kienlin, A. et al. , *in Proc. of the 5th Compton Symp.*, AIP Conf. Proc. 510, 722 (2000)

Lloyd-Ronning, N.M., & Ramirez-Ruiz, E., *ApJ*, **576**, 101 (2002)
MacFadyen, A.I., & Woosley, S.E., *ApJ*, **524**, 262 (1999)
Malesani, D., Tagliaferri, G., Chincarini, G., et al. , *ApJL*, **609**, L5 (2004)
Mannucci, F., Basile, F., Poggianti, B.M., et al. , MNRAS, **326**, 745 (2001)
Mannucci, F., Masetti, N., Pian, E., et al. , *GCN*, **1309** (2002)
Mannucci, F., Maiolino, R., Cresci, G., et al. , *A&A*, **401**, 519 (2003)
Maraston C., *MNRAS*, **300**, 872 (1998)
Masetti, N., Palazzi, E., Pian, E., et al. , *A&A*, **374**, 382 (2001)
Masetti, N., Palazzi, E., Pian, E., et al. , *A&A*, **404**, L465 (2003)
Mazets, E. et al., it Astrophys. Space Sci., **80**, 119 (1981)
McGaugh, S.S., *ApJ*, **380**, 140 (1991)
Meegan, C. A., Fishman, G. J., Wilson, R. B., et al. , *Nature*, **355**, 143 (1992)
Mereghetti, S., Götz D., Borkowski, J. et al. , *in Proc. of the 5th INTEGRAL Workshop*, ESA SP 552, 599 (2004)
Mereghetti, S., Götz D., von Kienlin, A. et al. , *ApJ*, **624**, L105 (2005)
Metzger, M.R., Djorgovski, S.G., Kulkarni, S.R., et al. , *Nature*, **387**, 879 (1997a)
Metzger, M.R., Kulkarni, S.R., Djorgovski, S.G., et al. , *IAU Circ*, 6588 (1997b)
Meszaros, P., & Rees, M.J., *ApJ*, **418**, L59 (1993)
Mirabal, N., & Halpern, J.P., *GCN*, **2273** (2003)
Mirabal, N., Halpern, J. P. Chornock, R, *ApJ*, **595**, 935 (2003)
Monet, D.B.A., Canzian, B., Dahn, C., et al. , VizieR Online Data Catalog, 1252 (1998)
Mukherjee, S. Feigelson, E. D., Jogesh Babu, G., et al. , *ApJ*, **508**, 314 (1998)
Nakar, E., & Piran, T., *NewAstr*, **8**, 141 (2003)
Narayan, R., Paczynski, B., & Piran, T., *ApJ*, **395**, L83 (1992)
Nemiroff, R.J., *Gamma-Ray Bursts, Proceedings of the 2nd Workshop Huntsville*, Edited by G.J. Fishman, AIP Conference Proceedings Vol. 307, p.730 (1994)
Nishiyama, S., Baba, D., Nagata, T., *GCN*, **2195** (2003)
Nomoto, K., Maeda, K., Mazzali, P.A., et al. , in *Stellar Collapse*, ed. C.L. Fryer, Astrophysics and Space Science, Kluwer (2003)
Norris, J., Cline, T., Desai, U., & Teegarden, B., *Nature*, **308**, 434 (1984)
Norris, J., Scargle, J., & Bonnell, J., *B.A.A.S.*, **32(3)**, 1244 (2000)
Paciesas, W. S., Meegan, C. A., Pendleton, G. N. et al. , *ApJS*, **122**, 465 (1999)
Paczynski, B. & Rhoads, J.E., *ApJ*, **418**, L5 (1993)
Paczynski, B., *ApJ*, **494**, L45 (1998)
Pagel, B.E.J., Edmunds, M.G., Blackwell, D.E., et al. , *MNRAS*, **255**, 325 (1999)
Panaitescu, A. & Kumar, P., *ApJ*, **554**, 667 (2001)
Pallavicini, R., Golub, L., Rosner, R., et al. , *ApJ*, **248**, 279 (1981)
Park, H.S., Porrata, R.A., Williams, G.G, et al. , *A&AS*, **138**, 577 (1999)
Pendleton, G. N., Hakkila, J. & Meegan, C. A., *in Proc. of the 4th Huntsville Symp.*, AIP Conf. Proc. 428, 899 (1998)
Perna, R., & Loeb, A., *ApJ*, **509**, L85 (1998)
Pickles, A.J., *PASP*, **110**, 863 (1998)
Piro, L., Frail, D.A., Gorosabel, J., et al. , *ApJ*, **577**, 680 (2002)

Podsiadlowski, P., Mazzali, P.A., Nomoto, K., Lazzati, D., Cappellaro, E., *ApJ*, **607**, L17 (2004)
Preece, R.D., Briggs, M.A., Mallozzi, R.S., et al. , *ApJS*, **126**, 19 (2000)
Price, P.A., Berger, E., Reichart, D.E., et al. , *ApJ*, **572**, L51 (2002)
Price, P.A., Jensen, B.L., Jargensen, U.G., et al. , *GCN*, **3612** (2005a) Price, P.A., Roth, K., & Fox, D.W., *GCN*, **3605** (2005b)
Prochaska, J.X., Bloom J.S., Chen, H-W., et al. , *ApJ*, **611**, 200 (2004)
Prochaska, J.X., Cooper, M., Newman, J., et al. , *GCN*, **3390**, (2005a)
Prochaska, J.X., Bloom, J.S., Chen, H.-W., et al. , *GCN*, **3700**, (2005b) Ramaprakash, A. N., Kulkarni, S.R., Frail, D.A., et al. , *Nature*, **393**, 43 (1998)
Rau, A., von Kienlin, A., Lichti, G.G., Hurley, K. & Beck M., *GCN*, **2568** (2004)
Rau, A., Greiner, J., Klose, S., et al. , *A&A*, **427**, 815 (2004b)
Rees, M.J. & Meszaros, P., *MNRAS*, **258**, 41 (1992)
Rees, M.J. & Meszaros, P., *ApJL*, **430**, 93 (1994)
Reichart, D.E., Lamb, D.Q., Metzger, M.R., et al. , *ApJ* **517**, 692 (1999)
Reichart, D.E., Lamb, D.Q., Fenimore, E.E. et al. , *ApJ*, **552**, 57 (2001)
Reid, I.N., Hawley, S.L., & Gizis, J.E., *AJ*, **110**, 1838 (1995)
Rhoads, J.E., *ApJ*, **487**, L1 (1997)
Rhoads, J., *ApJ*, **525**, 943 (1999)
Rhoads, J.E. & Fruchter, A.S., *ApJ*, **546**, 117 (2001)
Rhoads, J., *ApJ*, **591**, 1097 (2003)
Rol, E., Wijers, R.A.M.J., Vreeswijk, P.M, et al. , *ApJ*, **544**, 707 (2000)
Rol, E., Wijers, R.A.M.J., Kouveliotou, C., Kaper, L., & Kaneko, Y., *ApJ*, **624**, 868 (2005)
Rosa-Gonzalez, D., Terlevich, E. & Terlevich, R., *MNRAS*, **332**, 283 (2002)
Ruffer, M. & Janka, H.-T., *A&A*, **338**, 535 (1998)
Rutledge, R.E., & Fox, D.B., *MNRAS*, **350**, 1288 (2004)
Ryde, F., Borgonovo, L., Larsson, S., Lund, N., von Kienlin, A. & Lichti, G.G., *A&A*, **411**, L331 (2003)
Rykoff, E., Aharonian, F., Akerlof, C.W., et al. , *ApJ*, **631**, 1032 (2005)
Sakamoto, T., Lamb, D.Q., Graziani, C., et al. , *ApJ*, **602**, 875 (2004)
Sakamoto, T., Lamb, D.Q., Kawai, N., et al. , *ApJ*, **629**, 311 (2005)
Sari, R., Piran, T., & Narayan, R., *ApJ*, **497**, L17 (1998)
Sari, R., *ApJ*, **524**, L43 (1999)
Schaefer, B.E., Gerardy, C.L., Höflich, P., *ApJ*, **588**, 387 (2003)
Schlegel, D.J., Finkbeiner D.P., & Davis, M., *ApJ*, **500**, 525 (1998)
Schmidt, M., *ApJ*, **151**, 393 (1968)
Segreto, A., IN-IB-IASF/Pa-RP-030/02 (2002)
Soderberg, A.M., et al. , AAS Meeting 203, 132.07 (2003)
Soderberg, A.M., Kulkarni, S.R., Berger, E., et al. , *ApJ*, **606**, 994 (2004)
Soderberg, A.M., Cameron, P.B., & Frail, D.A., *GCN*, **3684** (2005a)
Soderberg, A.M., Kulkarni, S.R., Fox, D.B., et al. , *ApJ*, **627**, 877 (2005b)
Sollerman, J., Östlin G., J.P.U. Fynbo, et al. , astro-ph/0506686 (2005)
Sokolov, V.V., Fathkhullin, T.A., Castro-Tirado, A.J., et al. , *A&A*, **372**, 438 (2001)

Stanek, K.Z., Matheson, T., Garnavich, P. M., et al. , *ApJ*, **591**, L17 (2003)
Strong, I.B., Klebesadel, R.W. & Olsen, R.A., *ApJ*, **188**, L1 (1974)
Tanvir, N.R., Barnard, V.E., Blain, A.W., et al. , *MNRAS*, **253**, 1073 (2004)
Taylor, G.B., Bloom, J.S., Frail, D.A., et al. , *ApJ*, **537**, L17 (2000)
Taylor, G.B., Frail, D.A., & Kulkarni, S.R., *GCN*, **1136** (2001)
Torii, K., *GCN*, **2253** (2003)
Totani, T., & Panaitescu, A., *ApJ*, **576**, 120 (2002)
Ubertini, P., Lebrun, F., Di Cocco, G. et al. , *A&A*, **411**, L131 (2003)
Uemura , M., Ishioka, R., Kato, T. & Yamaoka, H., *GCN*, **2252** (2003)
Valentini, G., Alleva, G., Brocato, E., & Palazzi, E., *GCN*, **2258** (2003
van Dokkum, P.G., & Bloom, J.S., *GCN*, **2380** (2003)
Vanden Berk, D.E., Lee, B.C., Wilhite, B.C., et al. , *ApJ*, **576**, 673 (2002)
van Paradijs, J., Groot, P.J., Galama, T., et al. , *Nature*, **386**, 686 (1997)
van Paradijs, J., Kouveliotou, C., & Wijers, R.A.M.J., *ARA&A*, **38**, 379 (2000)
Vedrenne, G., Roques, J.-P., Schönfelder, V. et al. , *A&A*, **411**, L63 (2003)
Verbunt, F., Bunk, W.H., Ritter, H., Pfeffermann, E., *A&A*, **327**, 602 (1997)
Vestrand, W.T., Borozdin, K., Casperson, D.J, *AN*, **325**, 549 (2004)
Villasenor, J., Butler, N., Crew, G., et al. , *GCN*, **2261** (2003)
Voges, W., Aschenbach, B., Boller, T., et al. , *IAU Circ.*, **7432** (2000)
Vreeswijk, P.M., Ellison, S.L., Ledoux, C., et al. , *A&A*, **419**, 927 (2004)
Vreeswijk, P.M., Rol, E., Kouveliotou, C., et al. , *GCN*, **492** (1999)
Waxman, E., *Lect.Notes Phys.*, **598**, 393, (2003)
Wigger, C., Hajdas, W., Arzner, K., Güdel, M., & Zehnder, A., *ApJ*, **613**, 1088 (2004)
Wiijers, R.A.M.J., Vreeswijk, P.M., Galama, T.J., et al. , *ApJ*, **523**, L33 (1999)
Winkler, C., Courvoisier, T.J.-L., Di Cocco, G. et al. , *A&A*, **411**, L1 (2003)
Woosley, S.E., *ApJ*, **405**, 273 (1993)
Woosley, S.E., Zhang, W. & Heger, A., in *Gamma-Ray Burst and Afterglow Astronomy 2001*, AIP Conf. Proc., Volume 662, p.185 (2002)
Yamazaki, R., Ioka, K., & Nakamura, T., *ApJ*, **571**, L31 (2002)
Zeh, A., Klose, S., & Hartmann, D.H., *ApJ*, **609**, 952 (2004)
Zeh, A., Klose, S., Kann, D.A., *ApJ* submitted, astro-ph/0509299 (2005)
Zhang, B. & Meszaros, P., *International Journal of Modern Physics*, **19**, 2385 (2004)

List of Publications

Refereed Journals

Rau, A.; Greiner, J.; Schwartz, R.; *Constraining the GRB Collimation with a Survey for Orphan Afterglows*; A&A, in press (2006)

Marcinkowski, R.; Denis, M.; Bulik, T.; Goldoni, P.; Laurent P.; **Rau, A.**; *GRB 030406 - an extremely hard burst outside of the INTEGRAL field of view*; A&A, submitted (2005)

Küpcü Yoldas, A.; Salvato, M.; Greiner, J.; Pierini, D.; Pian, E.; **Rau, A.**; *The young star-forming sub-luminous host-galaxy of GRB 011121*; A&A, submitted (2005)

Rau, A.; Salvato, M.; Greiner, J.; *The host of GRB/XRF 030528 - an actively star forming galaxy at z=0.782*; A&A, 444, 425 (2005)

Rau, A.; Kienlin, A. von; Hurley, K., Lichti, G.G.; *The 1st INTEGRAL SPI-ACS Gamma-ray burst catalogue*; A&A, 438, 1175 (2005)

Mereghetti, S.; Götz, D.; von Kienlin, A.; **Rau, A.**; Lichti, G.; Weidenspointner, G.; Jean, P.; *The first giant flare from SGR 1806-20: observations with the INTEGRAL SPI anti-coincidence shield*; ApJ, 624, (2005) L105

Hurley, K.; Boggs, S. E.; Smith, D. M.; Duncan, R. C.; Lin, R.; Zoglauer, A.; Krucker, S.; Hurford, G.; Hudson, H.; Wigger, C.; Hajdas, W.; Thompson, C.; Mitrofanov, I.; Sanin, A.; Boynton, W.; Fellows, C.; von Kienlin, A.; Lichti, G.; **Rau, A.**; Cline, T.; *A tremendous flare from SGR 1806-20 with implications for short-duration gamma-ray bursts*; Nature 434, (2005) 1098

Rau, A.; Greiner, J.; Klose, S.; Salvato, M.; Castro Cern, J. M.; Hartmann, D. H.; Fruchter, A.; Levan, A.; Tanvir, N. R.; Gorosabel, J.; Hjorth, J.; Zeh, A.; Küpcü Yoldas, A.; Beaulieu, J. P.; Donatowicz, J.; Vinter, C.; Castro-Tirado, A. J.; Fynbo, J. P. U.; Kann, D. A.; Kouveliotou, C.; Masetti, N.; Mller, P.; Palazzi, E.; Pian, E.; Rhoads, J.; Wijers, R. A. M. J.; van den Heuvel, E. P. J.; *Discovery of the near-IR afterglow and of the host of GRB 030528*; A&A 427 (2004), 815

Klose, S.; Greiner, J.; **Rau, A.**; Henden, A. A.; Hartmann, D. H.; Zeh, A.; Ries, C.; Masetti, N.; Malesani, D.; Guenther, E.; Gorosabel, J.; Stecklum, B.; Antonelli, L. A.; Brinkworth, C.; Cern, J. M. Castro; Castro-Tirado, A. J.; Covino, S.; Fruchter, A.; Fynbo, J. P. U.; Ghisellini, G.; Hjorth, J.; Hudec, R.; Jelnek, M.; Kaper, L.; Kouveliotou, C.; Lindsay, K.; Maiorano, E.; Mannucci, F.; Nysewander, M.; Palazzi, E.; Pedersen, K.; Pian, E.; Reichart, D. E.; Rhoads, J.; Rol, E.; Smail, I.; Tanvir, N. R.; de Ugarte Postigo, A.; Vreeswijk, P. M.; Wijers, R. A. M. J.; van den Heuvel, E. P. J.; *Probing a Gamma-ray burst progenitor at a redshift of z = 2: a comprehensive observing campaign of the afterglow of GRB 030226*; AJ 128 (2004), 1942

Greiner, J.; Klose, S.; Reinsch, K.; Martin Schmid, H.; Sari, R.; Hartmann, D.H.; Kouveliotou, C.; **Rau, A.**; Palazzi, E.; Straubmeier, C.; Stecklum, B.; Zharikov, S.; Tovmassian, G.; Bärnbantner, O.; Ries, C.; Jehin, E.; Henden, A.; Kaas, A.A.; Grav, T.; Hjorth, J.; Pedersen, H.; Wijers, R.A.M.J.; Kaufer, A.; Park, H-S.; Williams, G.; Reimer, O.; *Evolution of the polarization of the optical afterglow of the Gamma-ray burst GRB030329*; Nature 426 (2003), 157

Kienlin, A. v.; Beckmann, V.; Covino, S.; Götz, D.; Lichti, G. G.; Malesani, D.; Mereghetti, S.; Molinari, E.; **Rau, A.**; Shrader, C. R.; Sturner, S. J.; Zerbi F.; *INTEGRAL results on GRB 030320: A long gamma-ray burst detected at the edge of the field of view*; A&A 411 (2003), 321

Kienlin, A. v.; Beckmann, V.; **Rau, A.**; Arend, N.; Bennett, K.; McBreen, B.; Connell, P.; Deluit, S.; Hanlon, L.; Hurley, K.; Kippen, M.; Lichti, G. G.; Moran, L.; Preece, R.; Roques, J.-P.; Schönfelder, V.; Skinner, G.; Strong, A.; Williams, R.; *INTEGRAL spectrometer SPI's GRB detection capabilities. GRBs detected inside SPI's FoV and with the anticoincidence system ACS*; A&A 411 (2003), 299

Rau, A.; Greiner, J.; McCollough, M. L.; *The 590 day long-term periodicity of the microquasar GRS 1915+105*; ApJ 590 (2003), L37

Rau, A.; Greiner, J.; *Comptonization and reflection of X-ray radiation and the X-ray-radio correlation in the χ-states of GRS 1915+105*; A&A 397 (2003), 711

Greiner, J.; Tovmassian, G.; Orio, M.; Lehmann, H.; Chavushyan, V.; **Rau, A.**; Schwarz, R.; Casalegno, R.; Scholz, R.-D.; *BZ Camelopardalis during its 1999/2000 optical low state*; A&A 376 (2002), 1031

Greiner, J.; **Rau, A.**; *The X-ray spectrum of LSI+61°303*; A&A 375 (2001), 145

Conference Proceedings

Rau, A.; Kienlin, A. v.; Hurley, K.; Lichti, G.G.; *The sample of INTEGRAL SPI-ACS Gamm-*

ray bursts; 4^{th} Workshop on Gamma-Ray Bursts in the Afterglow Era, Rome; (2005)

Rau, A.; Greiner, J.; *A survey for GRB orphan afterglows*; 4^{th} Workshop on Gamma-Ray Bursts in the Afterglow Era, Rome; (2005)

Marcinkowski, R.; Laurent, F.; Denis, M.; Goldoni, P.; Bulik, T.; **Rau, A.**; *Gamma-ray burst detection and localization capabilities of the IBIS Telescope Compton Mode*; 4^{th} Workshop on Gamma-Ray Bursts in the Afterglow Era, Rome; (2005)

Rau, A.; Kienlin, A. v.; Hurley, H.; Lichti, G.G.; *The sample of Gamma-ray bursts observed with SPI-ACS*; 5^{th} INTEGRAL Workshop on The INTEGRAL Universe, Edited by V. Schönfelder, G. Lichti, C. Winkler, ESA Publication Division; SP-552, pp. 607-613 (2004)

Hurley, K.; **Rau, A.**; Kienlin, A. v.; Lichti, G.; *INTEGRAL joines the 3^{rd} Interplanetary Network*; 5^{th} INTEGRAL Workshop on The INTEGRAL Universe, Edited by V. Schönfelder, G. Lichti, C. Winkler, ESA Publication Division; SP-552, pp. 645-648 (2004)

Kienlin, A. v.; **Rau, A.**; Beckmann, V.; Deluit, S.; *Gamma-ray bursts observed with the spectrometer SPI onboard INTEGRAL*; Gamma-Ray Bursts: 30 Years of Discovery: Gamma-Ray Burst Symposium., Edited by E. E. Fenimore and M. Galassi. Melville, NY, American Institute of Physics; AIP Conference Proceedings Volume 727, pp. 622-625 (2004)

Klose, S.; Greiner, J.; Zeh, A.; **Rau, A.**; Henden, A. A.; Hartmann, D. H.; Masetti, N.; Castro-Tirado, A. J.; Hjorth, J.; Pian, E.; Tanvir, N. R.; Wijers, R. A. M. J.; van den Heuvel, E.; *The optical afterglow of GRB 030226*; Gamma-Ray Bursts: 30 Years of Discovery: Gamma-Ray Burst Symposium, Edited by E. E. Fenimore and M. Galassi. Melville, NY, American Institute of Physics; AIP Conference Proceedings Volume 727, pp. 483-486 (2004)

Rau, A.; Greiner, J.; Klose, S.; Castro Cern, J.; Fruchter, A.; Küpcü Yoldas, A.; Gorosabel, J.; Levan, A.; Rhoads, J.; Tanvir, N.; *Discovery of the faint near-IR afterglow of GRB 030528*; Gamma-Ray Bursts: 30 Years of Discovery: Gamma-Ray Burst Symposium, Edited by E. E. Fenimore and M. Galassi. Melville, NY, American Institute of Physics; AIP Conference Proceedings Volume 727, pp. 439-442 (2004)

Greiner, J.; Klose, S.; Reinsch, K.; Schmid, H. M.; Sari, R.; Hartmann, D. H.; Kouveliotou, C.; **Rau, A.**; Palazzi, E.; Straubmeier, C.; Stecklum, B.; Zharikov, S.; Tovmassian, G.; Bärnbantner, O.; Ries, C.; Jehin, E.; Henden, A.; Kaas, A. A.; Grav, T.; Hjorth, J.; Pedersen, H.; Wijers, R. A. M. J.; Kaufer, A.; Park, H.-S.; Williams, G.; Reimer, O.; *The polarization evolution of the optical afterglow of GRB 030329*; Gamma-Ray Bursts: 30 Years of Discovery: Gamma-Ray Burst Symposium, Edited by E. E. Fenimore and M. Galassi. Melville, NY, American Institute of Physics; AIP Conference Proceedings Volume 727, pp. 269-273 (2004)

Staude, A.; Schwope, A. D.; Hedelt, P.; **Rau, A.**; Schwarz, R.; *Tomography of AM Her and QQ Vul*; Magnetic Cataclysmic Variables, IAU Colloquium 190, Edited by S. Vrielmann and M. Cropper. ASP Conference Proceedings Volume 315, pp.251 (2004)

Schwarz, R.; Schwope, A. D.; Staude, A.; Urrutia, T.; **Rau, A.**; Hasinger, G.; *RX J0524+42: A New Asynchronous Magnetic CV*; Magnetic Cataclysmic Variables, IAU Colloquium 190, Edited by S. Vrielmann and M. Cropper. ASP Conference Proceedings Volume 315, pp.230 (2004)

Deluit, S.; Kienlin, A. v.; Lichti, G.; **Rau, A.**; *Gamma-Ray Bursts Studies with the Anti-Coincidence Shield of INTEGRAL/SPI*; SF2A-2003: Semaine de l'Astrophysique Franaise, meeting held in Bordeaux, Edited by F. Combes, D. Barret, T. Contini, and L. Pagani; EdP-Sciences, Conference Series pp. 469 (2003)

Staude, A.; Schwarz, R.; Schwope, A.; **Rau, A.**; *Photometry with the Potsdam 70cm-telescope*; The Physics of Cataclysmic Variables and Related Objects, Edited by Edited by B. T. Gänsicke, K. Beuermann, and K. Reinsch, San Francisco, Astronomical Society of the Pacific; ASP Conference Proceedings Volume 261, pp. 680 (2002)

Schwarz, R.; Hedelt, P.; **Rau, A.**; Staude, A.; Schwope, A. D.; *Tomography of AM Herculis*; The Physics of Cataclysmic Variables and Related Objects Edited by Edited by B. T. Gänsicke, K. Beuermann, and K. Reinsch, San Francisco, Astronomical Society of the Pacific; ASP Conference Proceedings Volume 261, pp. 167 (2002)

Rau, A.; Greiner, J.; *Comptonization, the X-ray-radio-correlation and the long-term periodicity in the χ-state of GRS 1915+105*; New Views on Microquasars, the Fourth Microquasars Workshop, Corsica, Edited by Ph. Durouchoux, Y. Fuchs, and J. Rodriguez, Center for Space Physics: Kolkata; pp. 202 (2002)

Rau, A.; Greiner, J.; *Broadband X-ray spectroscopy of GRS 1915+105*; Microquasars, Proc. of the 3rd Microquasars Workshop, Edited by A.J. Castro-Tirado, J. Greiner & J.M. Paredes; Astrophysics and Space Science Supplement, Volume 276, pp. 225 (2001)

Circulars (not listed $>$ 100 IPN triangulations and SGR notifications)

Rau, A.; von Kienlin, A.; Lichti, G.; Hurley, K.; Beck, M.; *INTEGRAL-SPI/ACS GRB data: timing correction*; GRB Coordinates Network, Circular 2568 (2004)

Greiner, J.; **Rau, A.**; Klose, S.; *GRB 030528: tentative NIR counterpart*; GRB Coordinates Network, Circular 2271 (2003)

Rau, A.; Schönfelder, V.; Kienlin, A. V.; Lichti, G. G.; Arend, N.; Roques, J.-P.; Borkowski, J.; Walter, R.; Produit, N.; Hurley, K.; *GRB021113, SPI ACS observation*; GRB Coordinates Network, Circular 1703 (2002)

Miscellaneous

Greiner, J.; **Rau, A.**; *Gewaltige Explosionen im All*; Sterne und Weltraum Special: Lebendige Galaxis (2004), p.78

Rau, A.; *Reflexion und Comptonisierung der Röntgenstrahlung sowie Akkretionsscheiben-Jet-Instabilitäten in GRS 1915+105*; Master Thesis (german version) / Diplomarbeit; Universität Potsdam (2001)

Acknowledgments

So, now that the main work for the thesis is done, it is time to thank all those people who supported me in which ever way throughout my (young) scientific career and especially here at the MPE in Garching. Thank you all!

Where to start if not with my dear advisor Dr. Jochen Greiner, who gave me the opportunity to perform my PhD at the MPE, supported me on many travels, taught me among many other things all the nasty details of proposal deadlines and opened my view to the large scales of astrophysical research. Thank you very much for all and good luck with GROND, Jochen! I am also very grateful to my Co-Advisor Dr. Andreas von Kienlin and my Thesis-Committee member Dr. Gieselher Lichti, who were an important help, especially for my work on the INTEGRAL SPI-ACS GRB sample and with whom I had many lively discussions. In this context I would also like to thank Kevin Hurley for the great collaboration which connected SPI-ACS to the Interplanetary Network. I like to acknowledge as well all the other collaborators with which I had many fruitful and educating discussions over the last years, among others Dieter H. Hartmann, Sandra Savaglio, Silvio Klose, Robert Schwarz, Jurek Borkowski, Matthias Beck.

Now, it is also a good moment to express my gratitude to the International Max-Planck Research School on Astrophysics in which I participated and to the many course lectures during the years. You provided me with detailed and less detailed informations on all the variety of research topics outside my high-energy vision. I am grateful also for the support of my Director Prof. Günther Hasinger, who first recommended me the IMPRS and supported me in several ways during the time of my PhD.

A very special thank you is dedicated to Mara Salvato who turned from an Italian teacher to a neighbor and very good and close friend and collaborator. Thank you for all! I'm especially grateful for the many discussions and mirrors we had during our daily freeway journeys and all the evenings and weekends we spend together. Just a great time!

I thank Daniele Pierini, not only for teaching me the crucial parts of the Italian language but also for his discussions on galaxies, dust and its properties. I would also like to thank all the members of the MPE gamma-ray group for the nice and enjoyable time I shared with you. A special thanks goes out to my PhD fellow Aybüke Küpcü Yoldas whom I could 'stress' during all that time. Good luck with your thesis!

A very special thank you goes out to Ingo EED Kommenda for his dedication to something which I love and which is important to me and the many great atmospheric evenings we shared with Sikko, Uwe, Marco, Jenny and all the others. We won't fail you, Janrenia! Another special "thank you" is dedicated to the former Garching Gatherers and the dreaded

SWAD E-.T.W. Inept for many enjoyable hours and challenging duels. You kept me skilled. Last, but of course not least, I would like to thank my family for all their support during my studies and the time at the MPE. That’s all because of you!